ISSN 8755-6839

SCIENCE OF TSUNAMI HAZARDS

Journal of Tsunami Society International

Volume 41 Number 4 2022

TSUNAMI SOCIETY INTERNATIONAL, 1325 South 33rd Avenue, Hollywood, Florida 33021, USA.

SCIENCE OF TSUNAMI HAZARDS is a CERTIFIED OPEN ACCESS Journal included in the prestigious international academic journal database DOAJ.
SCIENCE OF TSUNAMI HAZARDS is also preserved, archived and disseminated by the National Library, The Hague, NETHERLANDS, the Library of Congress, Washington D.C., USA, the Electronic Library of Los Alamos, National Laboratory, New Mexico, USA, the EBSCO Publishing databases and ELSEVIER Publishing in Amsterdam. The vast dissemination gives the journal additional global exposure andreadership in 90% of the academic institutions worldwide, including nation-wide access to databases inmore than 70 countries.

OBJECTIVE: Tsunami Society International publishes this interdisciplinary journal to increase and disseminate knowledge about tsunamis and their hazards.

Submit manuscripts of research papers, notes or letters to the Editor. If a research paper is accepted for publication the author(s) must submit a scan-ready manuscript, a Doc, TeX or a PDF file in the journal format. Issues of the journal are published electronically in PDF format. There is a minimal publication fee for authors who are members of Tsunami Society International for three years and slightly higher for non-members.Tsunami Society International members are notified by e-mail when a new issue is available. Permission to use figures, tables and briefexcerpts from this journal in scientific and educational works is granted provided that the source is acknowledged. Recent and all past journal issues are available at: http://www.TsunamiSociety.org CD-ROMs of pastvolumes may be purchased by contacting Tsunami Society International at postmaster@tsunamisociety.org Issues of the journal from 1982 thru 2005 are also available in PDF format at the U.S. Los Alamos National Laboratory Library http://epubs.lanl.gov/tsunami/

ISSN 8755-6839

SCIENCE OF **TSUNAMI HAZARDS**

Journal of Tsunami Society International

Volume 41 Number 4 2022

GLOBAL TREND OF MEGATHRUST RESEARCH IN THE LAST TEN YEARS

Hasan Nuurul Hidaayatullaah[1], Nadi Suprapto[1,*]

[1] *Universitas Negeri Surabaya, Surabaya, **INDONESIA***

*Email: nadisuprapto@unesa.ac.id

ABSTRACT

Megathrusts have been the subject of more research recently. Therefore efforts are needed to understand the patterns, novelties, research trends, and potential future research areas connected to megathrusts. This study aims to analyze research trends, document types, source documents, most prolific authors, most cited documents globally, most contributing countries and affiliations, top subject areas and keywords, and visualization mapping of megathrust research trends over ten years. This bibliometric study and review of the literature use metadata from the Scopus database and a mapping application created with the help of the based program of bibliometrics and VOSViewer. The bibliometric results show that the trend of megathrust research over the last ten years is relatively stagnant, with most types of documents being articles and document sources published in journals, one of the journals that contributes the most is the Journal of Geophysical Research: Solid Earth. The top prolific author is Lay, T. The most cited document globally is by Hayes G. P. The top affiliates and countries that researched megathrust the most were Nanyang Technological University and the USA. The top subject areas and keywords in megathrust research in the last ten are Earth and Planetary Sciences and Earthquake. The mapping of visualization of megathrust research trends over the past ten years, seven clusters focus on active faults, crustal earthquakes, geology, geomorphology, amplitude, crustal deformation, seismic, and kinematics. Meanwhile, the opportunity and potential for future researchers to conduct megathrust research are keywords that are still few found, such as mitigation, aftershock, and ground motion.

Keywords: *Megathrust, Bibliometric, Review, Bibliometric and VOSViewer*

1. INTRODUCTION

Lately, natural disasters, especially earthquakes, often occur and cause significant damage and impact on life. There have been 17 largest earthquakes recorded in history, 15 megathrust earthquakes (Atakan, 2015; Mallick et al., 2021; Ye et al., 2016). Megathrust is a big earthquake occurring in a subduction zone or megathrust zone with a magnitude of Mw 8.0 - 9.0 (Kirkpatrick et al., 2020; Michel et al., 2019). Megathrust is also one of the causes of large-scale earthquakes that have occurred throughout the world and can also be one of the causes of severe tsunamis that have been experienced by several countries in the world, such as Indonesia, to be precise in Aceh and Japan sometimes ago (Hutchings & Mooney, 2021; Melnick et al., 2017; Mitogawa & Nishimura, 2020).

The megathrust zone or in Indonesia known as the Sunda strait subdivision zone (Sunda megathrust), is one of the most active zones in the world. These zones are responsible for large earthquakes and tsunamis worldwide (Bilek & Lay, 2018; Gao & Wang, 2017; Khaledzadeh & Ghods, 2022). The Megathrust Zone is divided into three major zones: Andaman Megathrust, Sumatra Megathrust, and Java Megathrust (Bilek & Lay, 2018; Cerchiari et al., 2020). The zone is extensive, has an area or range of more than 5,500 km starting from the north of Myanmar, to the southwest in the Sumatra region, then can continue to the south of Java and Bali, and ends in Australia (Inca & Nikorn, 2019; Silpa & Earnest, 2020; Widiyantoro et al., 2020).

Research on megathrust is fundamental to study, one of which is literacy and awareness among the public about the importance of mitigation efforts against the megathrust disaster (Mardiatno et al., 2017; Sari & Soesilo, 2020). Publication of research on megathrust continues to increase every year, although the increase is not so fast. Therefore, efforts are needed to know and understand the status and trends of a research topic. Bibliometric studies can be a solution to understanding research trends, novelties, and related studies (Hidaayatullaah et al., 2021; Suprapto et al., 2021; 2022). Bibliometric analysis is also a popular and rigorous method for exploring and analyzing large amounts of scientific data through the metadata of Scopus, Web of Science, Google Scholar, etc. (Echchakoui, 2020; Prahani et al., 2022; Suprapto et al., 2021).

Many authors have researched megathrust worldwide, for example, Ulrich et al. (2022) entitled Stress, rigidity, and sediment strength control megathrust earthquake and tsunami dynamics. Acuña et al. (2022) researched how good a paleoseismic record of megathrust earthquakes is for probabilistic forecasting. Chile's super-interseismic phase of the megathrust earthquake cycle (Melnick et al., 2017). Cascadia megathrust earthquake rupture model constrained by geodetic fault locking (Li & Liu, 2021). Research by Widyantoro et al. (2020) is implications for megathrust earthquakes and tsunamis from seismic gaps south of Java, Indonesia. However, research on megathrust trends through bibliometric analysis has never been done. Therefore, this study will conduct a bibliometric analysis of the global trends of megathrust research in the last ten years.

This research is a bibliometric and literature review study on megathrust in the last ten years using metadata from the Scopus database. The application used to map the data uses bibliometric and VOSviewer. This study aims to determine the pattern, novelty, research trends, and future research opportunities regarding megathrust. Thus, the questions posed in this study are as follows:

a) What has been the trend of publications, document types, and document sources in megathrust research over the last ten years?

b) Who are the top authors' production and the most globally cited document in megathrust research?
c) Where are the most productive affiliates and countries in megathrust research?
d) What are the subject areas and keywords in megathrust research trends?
e) What is the trend of visualization mapping in megathrust research?

2. RESEARCH METHOD

This descriptive study uses bibliometric analysis (Donthu et al., 2021; Hidaayatullaah et al., 2021; Suprapto et al., 2022). The bibliometric analysis aims to evaluate the research performance and publications of individuals and institutions and to reveal a study topic's structure and dynamics (Goyal & Kumar, 2021; Guo et al., 2019; Nurhasan et al., 2022). The Scopus database (www.scopus.com) is the metadata used in this study. The Scopus database is used because it is one of the largest academic databases globally, providing abstracts and indexing with full-text links (Hidaayatullaah et al., 2021; Polat et al., 2022; Purnell, 2022; Zakhiyah et al., 2021). The research procedure is depicted in Figure 1.

Figure 1. Steps of bibliometric study (Donthu et al., 2021; Prahani et al., 2022; Suprapto et al., 2021)

Data was collected on August 23, 2022, with 1433 documents generated in the search range of the last ten years (2013 to 2022). After that, the data is downloaded in .ris and .csv formats. Next, the data were processed using the program bibliometrics and VOSViewer to detail the data transcripts and visualize the bibliometric mapping. For the final stage, the data were analyzed descriptively to answer the research objectives, namely: (1) analyzing the trend of publications, types, and sources of megathrust research for the last ten years; (2) Top authors production over time and most cited documents globally; (3) Top affiliates and productive countries conducting megathrust research; (4) Subjects and keywords in megathrust research trends; and (5) Trends in visualization mapping in megathrust research.

3. RESULTS AND DISCUSSION

3.1 Megathrust research distribution by year, document types, and document sources

The distribution of publications and average research citations on megathrust over the last ten years (2013 to August 2022) is presented in Figure 2. It can be seen that the development of megathrust research is relatively stagnant in the range of 100-200 documents each year. Meanwhile, the mean total citations per article each year regarding research on megathrust has decreased.

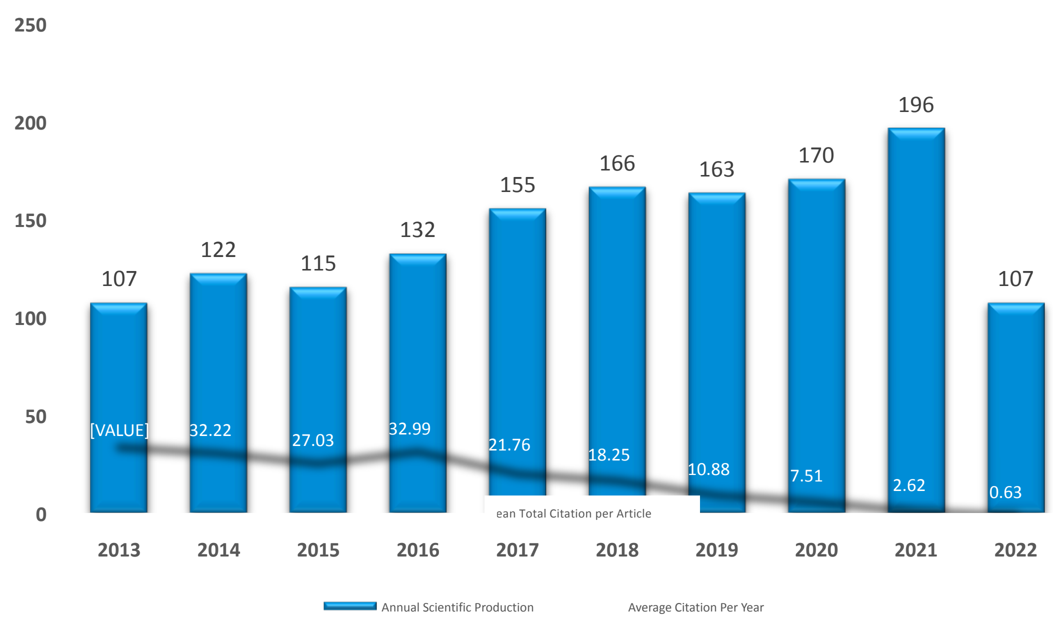

Figure 2. Annual scientific production and mean total citation per article in megathrust research

Figure 3 shows the types and sources of documents regarding megathrust research over the last ten years. Based on the search results from the Scopus database, a total of 1433 documents were obtained from 2013 to August 2022. Most types of documents from the search results of megathrust research are documents from articles, as much as 85.1% (1219 documents). In addition, the most sources of documents published in journals are 1309 documents. Meanwhile, other sources are found in the conference proceedings of 89 documents, 19 document book series, 15 books, and 1 item trade journal. Most documents about megathrust are published in journals by researchers because journals have higher quality and are in high demand compared to other sources.

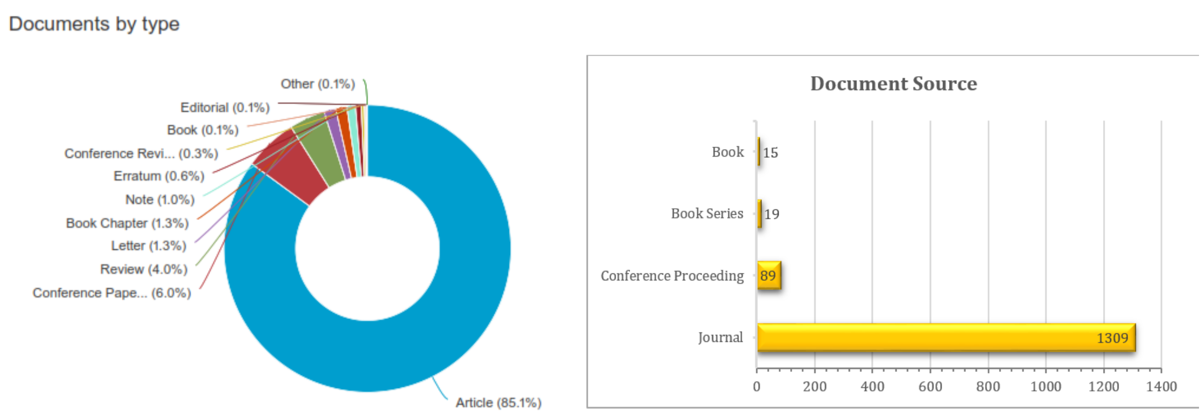

Figure 3. The document by type and source of megathrust research

The top 10 most relevant sources regarding megathrust research are presented in Figure 4. It can be seen that the journal that has contributed a lot over the last ten years to megathrust research is "The Journal of Geophysical Research: Solid Earth," which has 189 documents. Journal of Geophysical Research: Solid Earth is a Q1 journal (SJR: 1.77) from the United States with a subject area and category, namely earth and planetary sciences, geochemistry and petrology, geophysics, space, and planetary Science. The second journal source is occupied by the journal "Geophysical Research Letters" from the United States, with 139 documents. Geophysical Research Letters is a Q1 journal (SJR: 1.86) with a subject area and category, namely earth and planetary (miscellaneous) and geophysics. On average, journals in the third to tenth place contributed <100 documents over the last ten years. The graph in Figure 5 shows the distribution of documents per year by source from 4 journals.

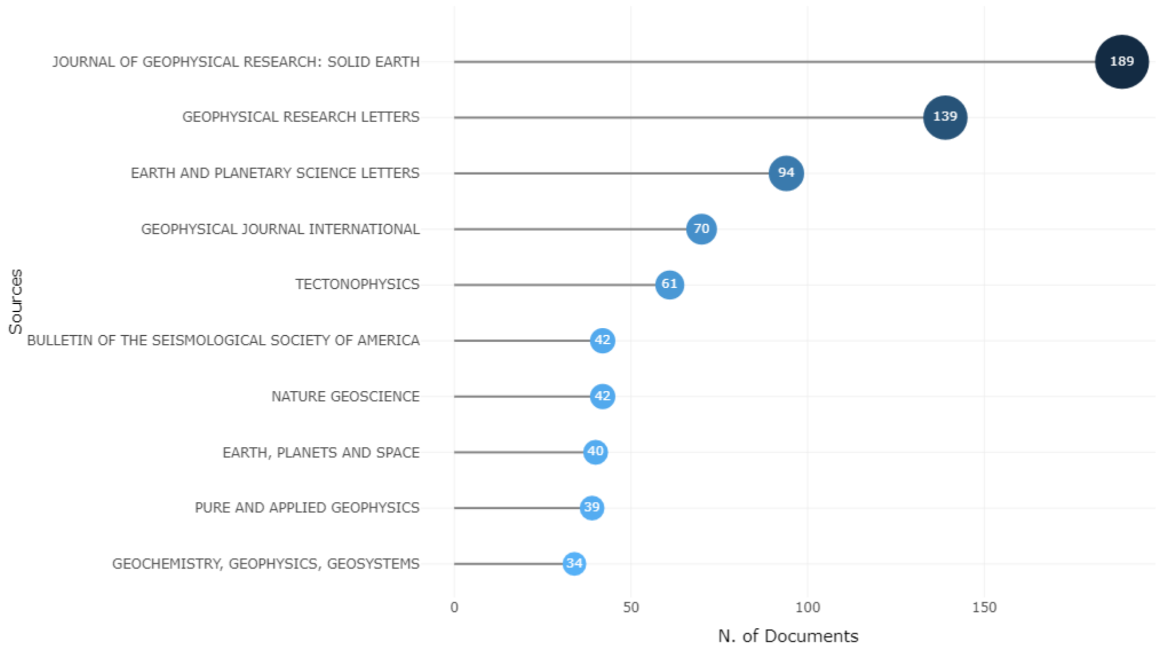

Figure 4. Top 10 most relevant sources of megathrust research

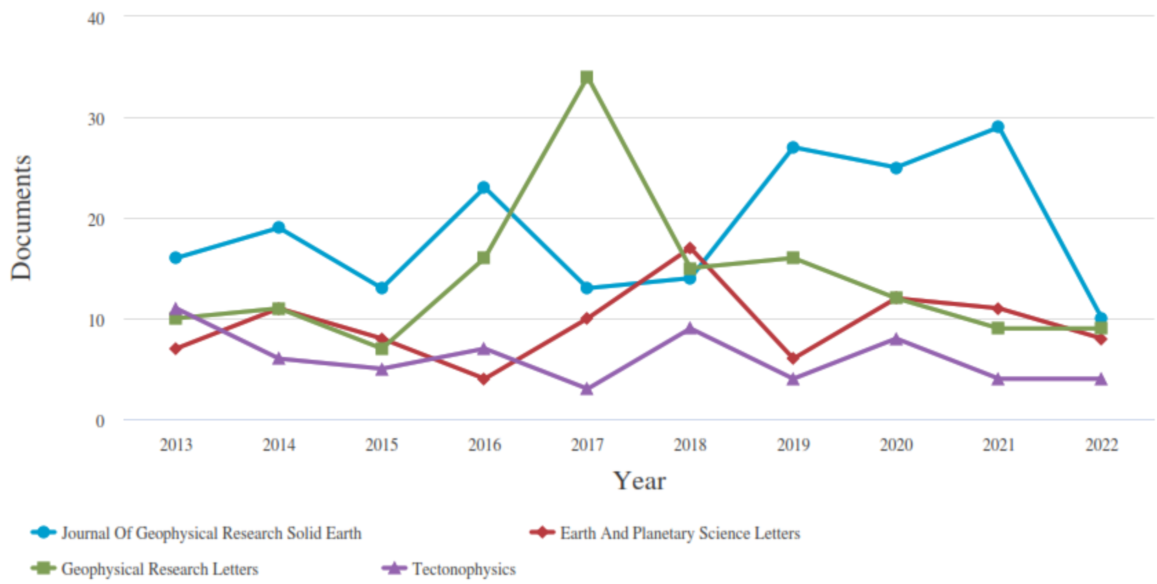

Figure 5. Documents per year by source

3.2 Top Authors' Production and The Most Global Cited Document

The top 10 authors who have been productive in the last ten years conducting megathrust research are presented in Figure 6. It is seen that the top author is occupied by Lay, T., with 39 published documents. Furthermore, Wang, K. is the second author who contributed 35 documents, and the third position is Kodaira, S., with 28 published documents. Authors ranked fourth to tenth and contributed fewer than 25 documents over the past ten years on megathrust research. Figure 6 on the right shows a network visualization co-authorship conducting research on megathrust over the past ten years. It can be seen that writers with larger circles and thicker networks are very productive writers who do megathrust research and collaborate more with other writers. These authors include Lay, T., with 13 links and 72 total link strengths. Wang, K. has 21 links and 57 link strengths, and Kodaira, S. has 15 links and 65 links strengths.

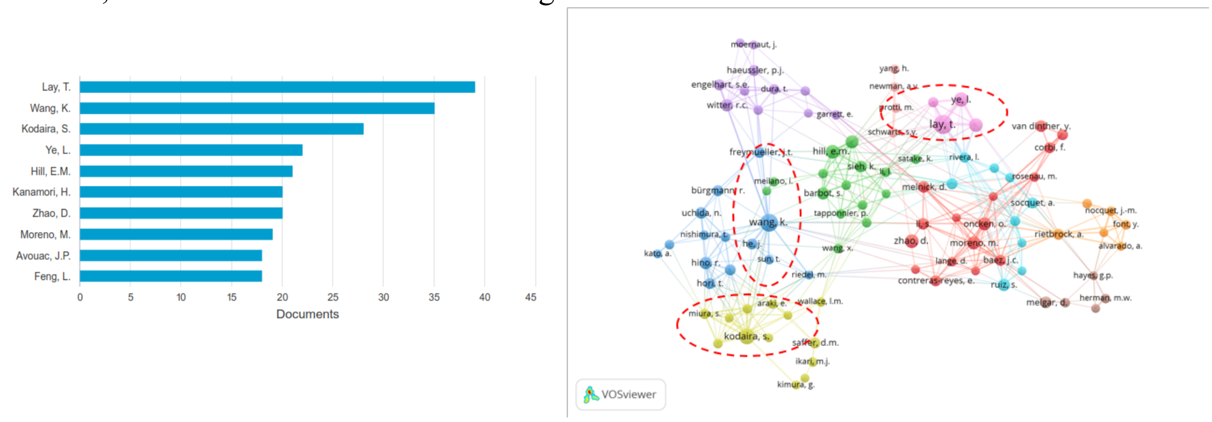

Figure 6. Documents by author and network visualization co-authorship

Table 1 shows the top 10 most global cited documents regarding megathrust research over the last ten years. It can be seen that the first top paper with total citations of 402 and total citations per year of 80.40 is a paper written by Hayes, G. P. (2018) with the title "Slab2, a comprehensive subduction zone geometry model," published in the journal Science. The second top paper is written by Obara, K. (2016) and the top author on megathrust research, with the paper titled "Connecting slow earthquakes to huge earthquakes" with 308 citations and 44.00 total citations per year. The third widely cited paper globally on megathrust research over the past decade is entitled "Slip pulse and resonance of the Kathmandu basin during the 2015 Gorkha earthquake, Nepal," written by Galetzka, J. (2015) with 289 total citations and 36.13 total citations per year. Elliott JR writes the fourth top document. (2016) published in the journal nature geoscience with 262 total citations over the last ten years. The fifth top document was written by Ito Y. (2013) and published in the journal Tectonophysics obtaining 241 total citations over the last ten years. Likewise, for the following document, the top documents quoted globally in megathrust research are in the fifth to tenth order, namely obtaining <200 total citations for the last ten years.

Table 1. 10 Top most global cited document

Paper	DOI	Total Citations	TC per Year
Hayes GP, 2018, Science	https://doi.org/10.1126/science.aat4723	402	80.40
Obara K, 2016, Science	https://doi.org/10.1126/science.aaf1512	308	44.00
Galetzka J, 2015, Science	https://doi.org/10.1126/science.aac6383	289	36.13
Elliott JR, 2016, Nat Geosci	https://doi.org/10.1038/ngeo2623	262	37.43
Ito Y, 2013,	https://doi.org/10.1016/j.tecto.2012.08.022	241	24.10

Paper	DOI	Total Citations	TC per Year
Tectonophysics			
Wang K, 2014, Tectonophysics	https://doi.org/10.1016/j.tecto.2013.11.024	189	21.00
Ujiie K, 2013, Science	https://doi.org/10.1126/science.1243485	188	18.80
Araki E, 2017, Science	https://doi.org/10.1126/science.aan3120	170	28.33
Bollinger L, 2014, J Geophys Res Solid Earth	https://doi.org/10.1002/2014JB010970	169	18.78
Saffer DM, 2015, Nat Geosci	https://doi.org/10.1038/ngeo2490	163	20.38

3.3 Most Relevant Affiliations and Country Scientific Production

Figure 7 shows the top 5 most relevant megathrust research affiliates over the last ten years. It can be seen that the top rank is Nanyang Technological University, with a total of 185 articles over the last ten years. Then the second affiliation is Tohoku University (159 articles), Universidad De Chile (148 articles), University of California (143 articles), and University of Tokyo (108 articles). Meanwhile, the top 10 country contributions in megathrust research over the last ten years are shown in Figure 8. The top countries that contributed the most to megathrust research were the USA, with 1758 documents. Japan, with 1231 documents, is in second place, and France, with 520 documents in third. They were followed by Germany, Chile, China, and Canada, with documents produced during the last ten years, less than 500.

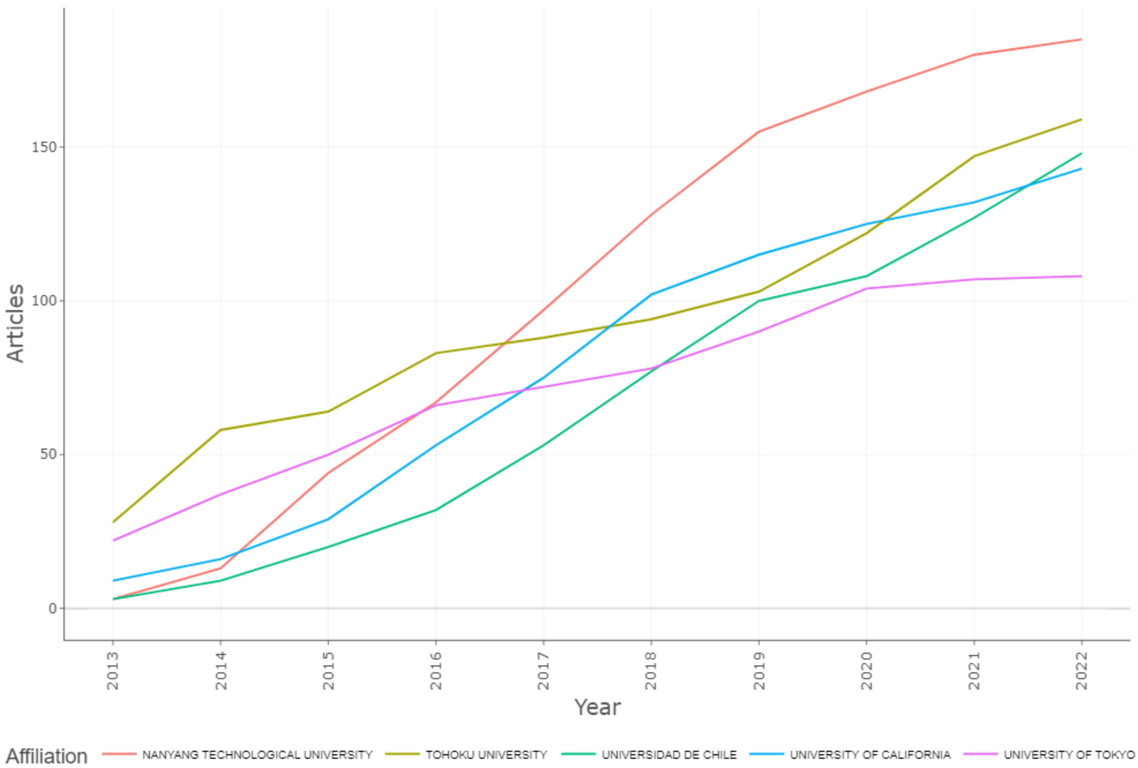

Figure 7. Affiliations' production over time in megathrust research

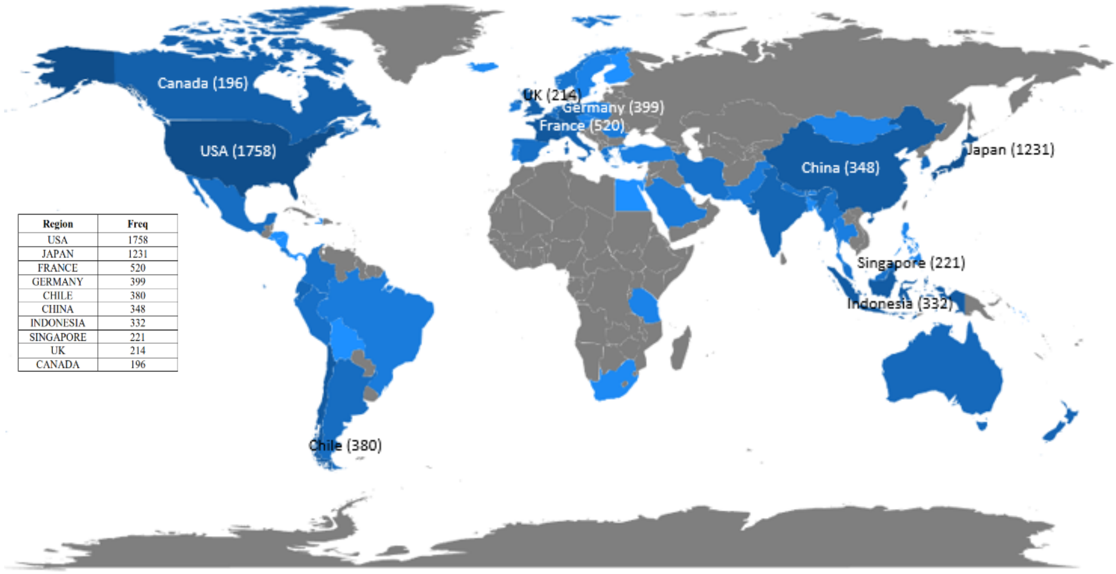

Figure 8. Top 10 Country scientific production in megathrust research

3.4 Top Subject Area and Keyword Tren in Megathrust Research

Table 2 shows megathrust research's top 10 subject areas over the last ten years. Earth and Planetary Sciences (1210), Environmental Science (106), and Engineering (101) are in the top 3 because they are highly relevant to megathrust. Other top subject areas are Physics and Astronomy (75), Multidisciplinary (70), Social Sciences (58), Agricultural and Biological Sciences (42), Arts and Humanities (29), Computer Science (27), and Biochemistry, Genetics, and Molecular Biology (24).

Table 2. The top subject era in megathrust research

Subject Area	Frequency
Earth and Planetary Sciences	1210
Environmental Science	106
Engineering	101
Physics and Astronomy	75
Multidisciplinary	70
Social Sciences	58
Agricultural and Biological Sciences	42
Arts and Humanities	29
Computer Science	27
Biochemistry, Genetics, and Molecular Biology	24

The most frequent words or keyword trends in megathrust research can be seen in Figure 9. The most common terms in megathrust research are earthquakes, marked by extensive writing. The emergence of the term earthquakes in the megathrust study is 610 occurrences. The second term that often appears is subduction zone (499), followed by earthquake rupture (392), megathrust earthquakes (342), earthquake event (325), earthquake magnitude (266), pacific ocean (262), deformation (244), Japan (220), seismicity (215) and the emergence of several other terms relevant to research on the megathrust.

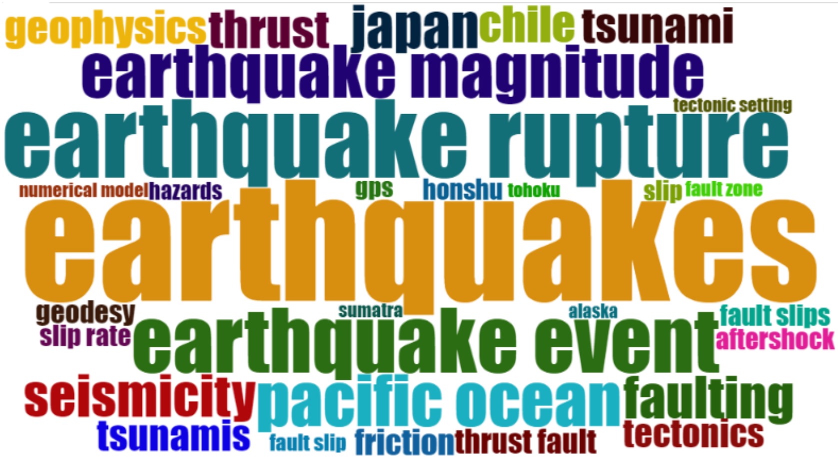

Figure 9. Top most frequent words in megathrust research

3.5 Mapping Visualization of Trends in Megathrust Research

Figure 10 maps megathrust research trends over the past ten years to find research updates. The mapping results show seven keyword clusters related to the Magahtrust research. The first cluster of red nodes (n=63) focuses on asperity, earthquake cycles, earthquake epicenter, earthquake trigger, fluid pressure, etc. The second cluster of green nodes (n=54) focuses on active faults, crustal earthquakes, disasters, earthquake damage, earthquake effects, seismic response, etc. The third cluster of dark blue nodes (n=49) focuses on geology, geomorphology, geophysics, lithology, seismology, stratigraphy, etc. The four yellow nodes (n=42) cluster focuses on the accretionary prism, amplitude, geometry, heterogeneity, megathrust, etc. The fifth cluster of superior nodes (n=40) focuses on crustal deformation, displacement, earthquake mechanism, geodynamics, etc. The cluster of six light blue nodes (n=29) focuses on aftershock, algorithm, data inversion, seismic source, etc. The seventh cluster of orange nodes (n=4) focuses on articles, priority journals, earthquakes, and kinematics.

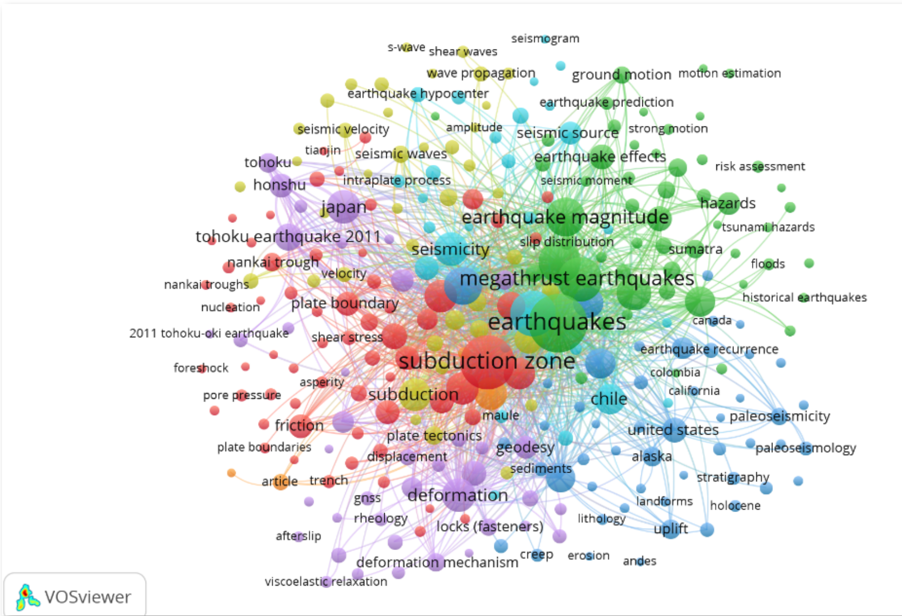

Figure 10. Network visualization of keyword co-occurrence on all megathrust research

Looking at the association between keywords in smaller circles or farther out from the primary term is one technique to identify novelty based on mapping findings. (Hidaayatullaah et al., 2021; Suprapto et al., 2022: Polat et al., 2022). For example, megathrust research related to subduction zones and earthquakes has been widely studied in the last ten years because many keywords are marked with large circles. Meanwhile, many researchers have not researched aftershocks related to megathrust because the keywords found are relatively few. Other examples include megathrust analysis related to rheology, teleseismic waves, ground motion, seismic reflection, etc. this is an opportunity and potential for research on megathrust now and in the future.

Figure 11 shows examples of more specific keyword mapping results regarding megathrust occurrence, areas that have experienced megathrust disasters, and megathrust modeling or analysis. Figure 11a-11b represents the top research trends on megathrust over the last ten years. It can be seen that megathrust has a very close relationship with the keywords subduction zone and thrust fault. Megathrust refers to a substantial thrust fault, typically formed at the plate interface along a subduction zone, such as the Sunda megathrust (Bilek & Lay, 2018; Nelson et al., 2021; Tal et al., 2020).

Figure 11c-11d is a country that has experienced a megathrust disaster. The largest megathrust earthquake recorded with magnitude Mw 9.4-9.6 centered off the coast of Chile along the Peru-Chile trench (Ruiz & Madariaga, 2018; Sippl et al., 2021). Indonesia, precisely in the province of Aceh, Sumatra, has also experienced a natural disaster that brought sorrow to one world, namely the megathrust disaster that caused a massive tsunami with an earthquake magnitude of Mw 9.1-9.3 (Ibrahim et al., 2022; Rubin et al., 2017).

Figure 11e-11f is an analysis of megathrust modeling and is an opportunity for future researchers to research megathrust because the keywords generated are still few or have small circles. Aftershock analyzes aftershocks or small earthquakes after the mainshock (Sladen & Trevisan, 2018; Soto et al., 2019). Ground motion is modeling that can determine the magnitude of the earthquake hazard in bedrock at a site and determine the earthquake's source that has the most dominant impact on a site (Hong et al., 2021).

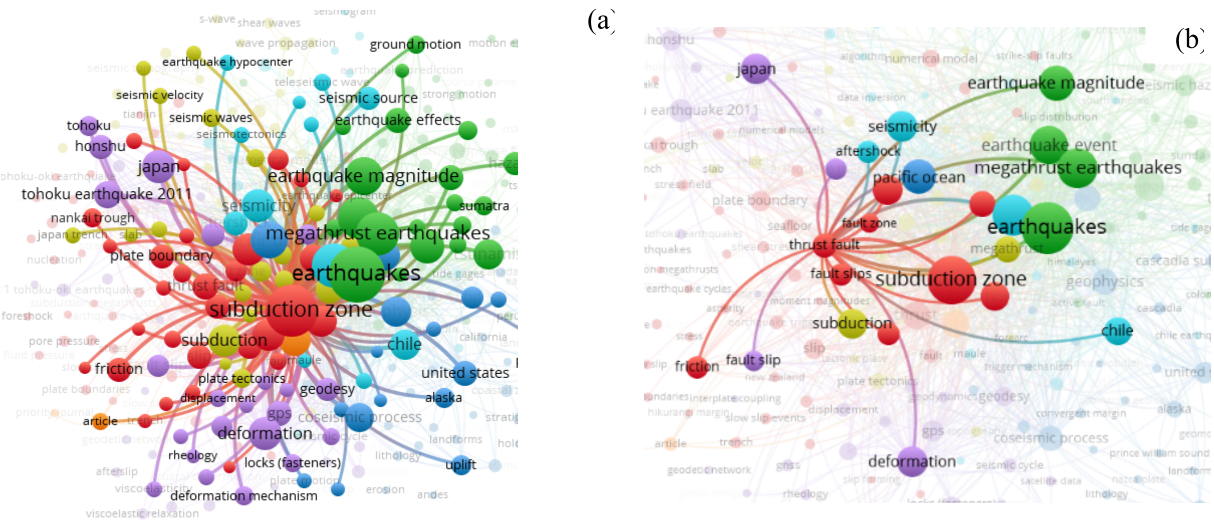

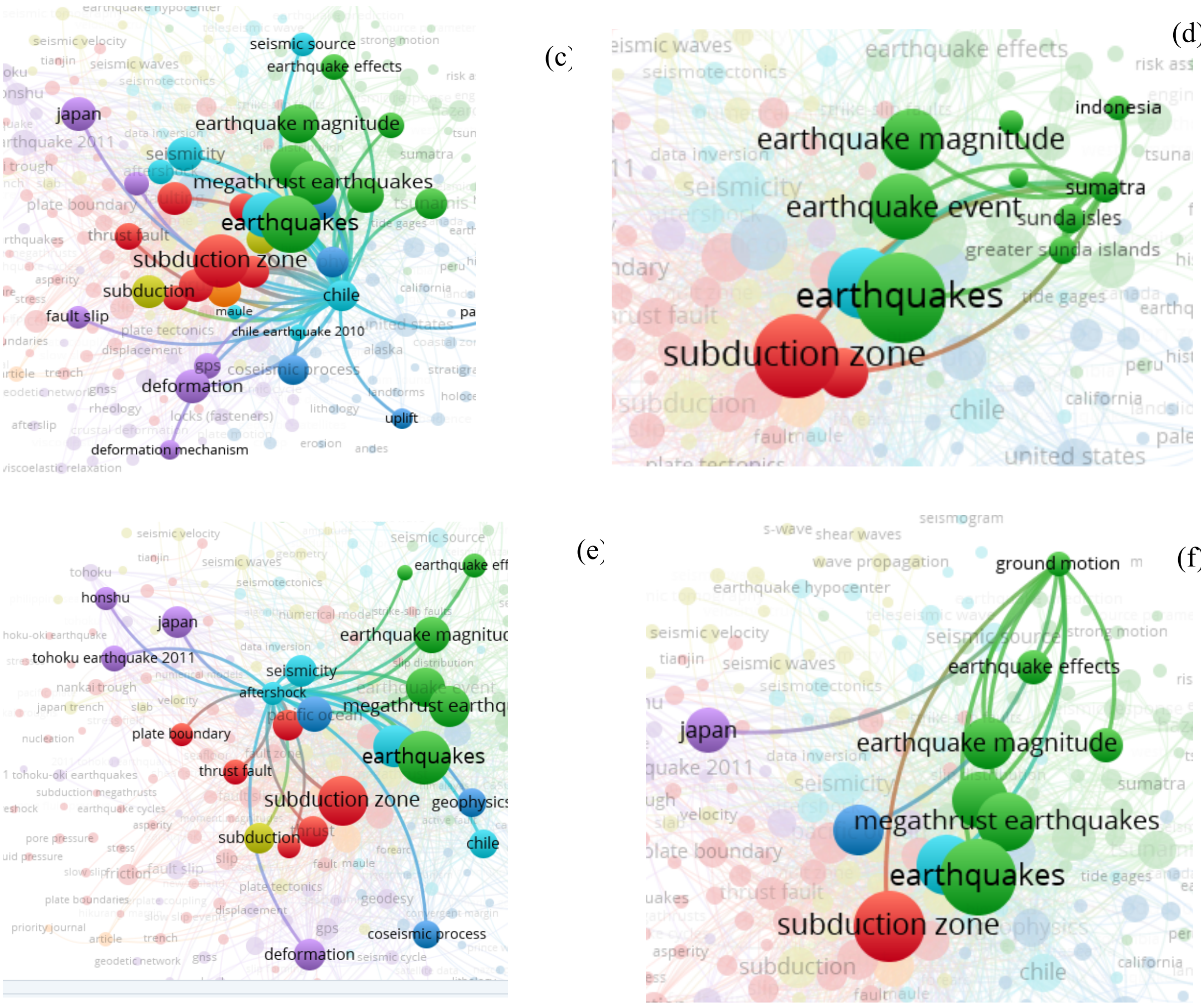

Figure 11. Some examples of the results of mapping specific keywords on topics from (a) subduction zone; (b) thrust fault; (c) Chile; (d) Sumatra; (e) aftershock; dan (f) ground motion

4. CONCLUSIONS

This study is the first to assess publications of megathrust research over the previous ten years and analyze global trends. There are the following five conclusions from this research:

a) The development of research on megathrust during the last ten years has been relatively stagnant every year, with most documents being articles (1219) and most document sources being published in journals (1309). The most contributing journal is the Journal of Geophysical Research: Solid Earth (189)
b) The top writer who is productive over time doing megathrust research is Lay, T. (39), with collaboration between other writers has 13 links and 72 total link strength. Meanwhile, the first top paper cited the most in the last ten years was written by Hayes, G. P., 2018, with 402 total citations.
c) Most of the affiliates that researched megathrust were Nanyang Technological University, Tohoku University, Universidad De Chile, the University of California, and the University of Tokyo. Meanwhile, the USA, Japan, France, Germany, and Chile are the most productive countries in researching megathrust.

d) The top subject areas of megathrust research are Earth and Planetary Sciences, Environmental Science, and Engineering. At the same time, the top keywords for megathrust research that are often used are Earthquake, Subduction Zone, and Earthquake Rupture.
e) The visualization mapping of megathrust research trends over the last ten years shows 7 clusters focusing on active faults, crustal earthquakes, geology, geomorphology, amplitude, crustal deformation, seismic, and kinematics. Meanwhile, the opportunity and potential for future researchers to conduct megathrust research are keywords that are still few found, such as mitigation, aftershock, and ground motion keywords.

The study aims to identify some instances of novelty in megathrust research to serve as a reference for future megathrust researchers. This research can also find the most relevant issues about megathrust, the most contributing countries and affiliations, types of documents, and top global citations. It can pinpoint the critical areas of scientific inquiry over a given period. As a result, it also helps to prevent the next trend in this field of study from emerging.

5. REFERENCES

Atakan, K. (2015). On the origin of megathrust earthquakes. *In Geotechnical, Geological and Earthquake Engineering*, 39. https://doi.org/10.1007/978-3-319-16964-4_19

Bilek, S. L., & Lay, T. (2018). Subduction zone megathrust earthquakes. *Geosphere*, 14(4), 1468–1500. https://doi.org/10.1130/GES01608.1

Cerchiari, A., Remitti, F., Mittempergher, S., Festa, A., Lugli, F., & Cipriani, A. (2020). Cyclical variations of fluid sources and stress state in a shallow megathrust-zone mélange. *Journal of the Geological Society*, 177(3), 647–659. https://doi.org/10.1144/jgs2019-072

Donthu, N., Kumar, S., Mukherjee, D., Pandey, N., & Lim, W. M. (2021). How to conduct a bibliometric analysis: An overview and guidelines. *Journal of Business Research*, 133, 285–296. https://doi.org/10.1016/j.jbusres.2021.04.070

Echchakoui, S. (2020). Why and how to merge Scopus and Web of Science during bibliometric analysis: the case of sales force literature from 1912 to 2019. *Journal of Marketing Analytics*, 8(3). https://doi.org/10.1057/s41270-020-00081-9

Elliott, J. R., Jolivet, R., Gonzalez, P. J., Avouac, J. P., Hollingsworth, J., Searle, M. P., & Stevens, V. L. (2016). Himalayan megathrust geometry and relation to topography revealed by the Gorkha earthquake. *Nature Geoscience* 2016 9:2, 9(2), 174–180. https://doi.org/10.1038/ngeo2623

Galetzka, J., Melgar, D., Genrich, J. F., Geng, J., Owen, S., Lindsey, E. O., Xu, X., Bock, Y., Avouac, J. P., Adhikari, L. B., Upreti, B. N., Pratt-Sitaula, B., Bhattarai, T. N., Sitaula, B. P., Moore, A., Hudnut, K. W., Szeliga, W., Normandeau, J., Fend, M., … Maharjan, N. (2015). Slip pulse and resonance of the Kathmandu basin during the 2015 Gorkha earthquake, Nepal. *Science*, 349(6252), 1091–1095. https://doi.org/10.1126/SCIENCE.AAC6383/SUPPL_FILE/PAPV2.PDF

Gao, X., & Wang, K. (2017). Rheological separation of the megathrust seismogenic zone and episodic tremor and slip. *Nature*, 543(7645), 416–419. https://doi.org/10.1038/nature21389

Goyal, K., & Kumar, S. (2021). Financial literacy: A systematic review and bibliometric analysis. *In International Journal of Consumer Studies*, 45(1). https://doi.org/10.1111/ijcs.12605

Guo, Y. M., Huang, Z. L., Guo, J., Li, H., Guo, X. R., & Nkeli, M. J. (2019). Bibliometric analysis on smart cities research. *Sustainability (Switzerland)*, 11(13), 1–18. https://doi.org/10.3390/su11133606

Hayes, G. P., Moore, G. L., Portner, D. E., Hearne, M., Flamme, H., Furtney, M., & Smoczyk, G. M. (2018). Slab2, a comprehensive subduction zone geometry model. *Science*, 362(6410), 58–61. https://doi.org/10.1126/SCIENCE.AAT4723/SUPPL_FILE/AAT4723-HAYES-SM.PDF

Hidaayatullaah, H. N., Suprapto, N., Hariyono, E., Prahani, B. K., & Wulandari, D. (2021). Research trends on ethnoscience based learning through bibliometric analysis: Contributed to physics learning. *Journal of Physics: Conference Series*, 2110(012026), 1–8. https://doi.org/10.1088/1742-6596/2110/1/012026

Hong, T. K., Kim, I., Park, S., & Kil, D. (2021). Elastogravity Waves and Dynamic Ground Motions in the Korean Peninsula Generated by the March 11, 2011 MW9.0 Tohoku-Oki Megathrust Earthquake. *Journal of Geophysical Research: Solid Earth*, 126(2). https://doi.org/10.1029/2020JB020628

Hutchings, S. J., & Mooney, W. D. (2021). The seismicity of Indonesia and tectonic implications. *Geochemistry, Geophysics, Geosystems*, 22(9), 1–41. https://doi.org/10.1029/2021GC009812

Ibrahim, Syamsidik, Azmeri, Hasan, M., & Tursina. (2022). Investigating characteristics of tsunami hazards for west coast of Aceh Besar district, Indonesia. *E3S Web of Conferences*, 340. https://doi.org/10.1051/e3sconf/202234001005

Inca, L. R., & Nikorn, S. (2019). The location-allocation decision under the dynamic increment of demand for selecting the local distribution centers to face sumatra megathrust: Study case of Padang City. *International Journal on Advanced Science, Engineering and Information Technology*, 9(1), 293–299. https://doi.org/10.18517/ijaseit.9.1.8030

Ito, Y., Hino, R., Kido, M., Fujimoto, H., Osada, Y., Inazu, D., Ohta, Y., Iinuma, T., Ohzono, M., Miura, S., Mishina, M., Suzuki, K., Tsuji, T., & Ashi, J. (2013). Episodic slow slip events in the Japan subduction zone before the 2011 Tohoku-Oki earthquake. *Tectonophysics*, 600, 14–26. https://doi.org/10.1016/J.TECTO.2012.08.022

Khaledzadeh, M., & Ghods, A. (2022). Estimation of size of megathrust zone in the Makran subduction system by thermal modelling. *Geophysical Journal International*, 228(3), 1530–1540. https://doi.org/10.1093/gji/ggab417

Kirkpatrick, J. D., Edwards, J. H., Verdecchia, A., Kluesner, J. W., Harrington, R. M., & Silver, E. A. (2020). Subduction megathrust heterogeneity characterized from 3D seismic data. *Nature Geoscience*, 13(5), 369–374. https://doi.org/10.1038/s41561-020-0562-9

Li, D., & Liu, Y. (2021). Cascadia megathrust earthquake rupture model constrained by geodetic fault locking. Philosophical Transactions of the Royal Society A: Mathematical, Physical and Engineering Sciences, 379(2196). https://doi.org/10.1098/rsta.2020.0135

Mallick, R., Meltzner, A. J., Tsang, L. L. H., Lindsey, E. O., Feng, L., & Hill, E. M. (2021). Long-lived shallow slow-slip events on the Sunda megathrust. *Nature Geoscience*, 14(5), 327–333. https://doi.org/10.1038/s41561-021-00727-y

Mardiatno, D., Malawani, M. N., Annisa, D. N., & Wacano, D. (2017). Review on tsunami risk reduction in Indonesia based on coastal and settlement typology. *Indonesian Journal of Geography*, 49(2), 186–194. https://doi.org/10.22146/ijg.28406

Melnick, D., Moreno, M., Quinteros, J., Baez, J. C., Deng, Z., Li, S., & Oncken, O. (2017). The super-interseismic phase of the megathrust earthquake cycle in Chile. *Geophysical Research Letters*, 44(2), 784–791. https://doi.org/10.1002/2016GL071845

Michel, S., Gualandi, A., & Avouac, J. P. (2019). Interseismic Coupling and Slow Slip Events on the Cascadia Megathrust. Pure and Applied Geophysics, 176(9), 3867–3891. https://doi.org/10.1007/s00024-018-1991-x

Mitogawa, T., & Nishimura, T. (2020). Coulomb stress change on inland faults during megathrust earthquake cycle in southwest Japan. Earth, Planets and Space, 72(1), 1–10. https://doi.org/10.1186/s40623-020-01174-6

Nelson, A. R., DuRoss, C. B., Witter, R. C., Kelsey, H. M., Engelhart, S. E., Mahan, S. A., Gray, H. J., Hawkes, A. D., Horton, B. P., & Padgett, J. S. (2021). A maximum rupture model for the central and southern Cascadia subduction zone—reassessing ages for coastal evidence of megathrust earthquakes and tsunamis. Quaternary Science Reviews, 261, 1–19. https://doi.org/10.1016/j.quascirev.2021.106922

Nurhasan, N., Prahani, B. K., Suprapto, N., Setiawan, B., Deta, U. A., & Al Ardha, M. A. (2022). Sports Research Trends in the Last 10 Years: Information to Librarians, Researchers, and Policy Makers. *TEM Journal*, 11(1). https://doi.org/10.18421/TEM111-36

Obara, K., & Kato, A. (2016). Connecting slow earthquakes to huge earthquakes. *Science*, 353(6296), 253–257. https://doi.org/10.1126/SCIENCE.AAF1512

Polat, Z. A., Alkan, M., Paulsson, J., Paasch, J. M., & Kalogianni, E. (2022). Global scientific production on LADM-based research: A bibliometric analysis from 2012 to 2020. *Land Use Policy*, 112, 1–9. https://doi.org/10.1016/j.landusepol.2021.105847

Prahani, B. K., Nisa', K., Jatmiko, B., Suprapto, N., Amelia, T., & Candrawati, E. (2022). The comparison of the top 100 cited publications of augmented reality and virtual reality for the last thirty years. *International Journal of Online and Biomedical Engineering*, 18(6), 13–29. https://doi.org/10.3991/ijoe.v18i06.30069

Purnell, P. J. (2022). The prevalence and impact of university affiliation discrepancies between four bibliographic databases—Scopus, Web of Science, Dimensions, and Microsoft Academic. *Quantitative Science Studies*, 3(1). https://doi.org/10.1162/qss_a_00175

Rubin, C. M., Horton, B. P., Sieh, K., Pilarczyk, J. E., Daly, P., Ismail, N., & Parnell, A. C. (2017). Highly variable recurrence of tsunamis in the 7,400 years before the 2004 Indian Ocean tsunami. *Nature Communications*, 8, 1–12. https://doi.org/10.1038/ncomms16019

Ruiz, S., & Madariaga, R. (2018). Historical and recent large megathrust earthquakes in Chile. *In Tectonophysics*, 733, 37–56 https://doi.org/10.1016/j.tecto.2018.01.015

Sari, D. A. P., & Soesilo, T. E. B. (2020). Measuring community resilience to the tsunami disaster (Study of Sukarame Village, Carita District, Pandeglang Regency). *IOP Conference Series: Earth and Environmental Science*, 448(012092), 1–10. https://doi.org/10.1088/1755-1315/448/1/012092

Silpa, K., & Earnest, A. (2020). A note on stress rotations due to the 2004 M w 9.2 Sumatra–Andaman megathrust earthquake. *Journal of Earth System Science*, 129(1). https://doi.org/10.1007/s12040-020-01446-5

Sippl, C., Moreno, M., & Benavente, R. (2021). Microseismicity appears to outline highly coupled regions on the central Chile megathrust. *Journal of Geophysical Research: Solid Earth*, 126(11). https://doi.org/10.1029/2021JB022252

Sladen, A., & Trevisan, J. (2018). Shallow megathrust earthquake ruptures betrayed by their outer-trench aftershocks signature. *Earth and Planetary Science Letters*, 483, 105–113. https://doi.org/10.1016/j.epsl.2017.12.006

Soto, H., Sippl, C., Schurr, B., Kummerow, J., Asch, G., Tilmann, F., Comte, D., Ruiz, S., & Oncken, O. (2019). Probing the Northern Chile megathrust with seismicity: The 2014 M8.1 Iquique Earthquake Sequence. *Journal of Geophysical Research: Solid Earth*, 124(12). https://doi.org/10.1029/2019JB017794

Suprapto, N., Bestiantono, D.S., Ku, C.-H., Zamroni, A., & Hariyono, E. (2022). Research trends on liquefaction in 2011-2021: A review and bibliometric analysis. *Science of Tsunami Hazards*, 41(3), 264-285

Suprapto, N., Kholiq, A., Prahani, B. K., & Deta, U. A. (2021). Research on physics of photography: A bibliometric study (2000-2020). *Journal of Physics: Conference Series*, 2110(012017). https://doi.org/10.1088/1742-6596/2110/1/012017

Suprapto, N., Prahani, B., & Deta, U. A. (2021). Research trend on ethnoscience through bibliometric analysis (2011-2020) and the contribution of Indonesia. *Library Philosophy and Practice (e-Journal)*, 5599, 1–17. https://digitalcommons.unl.edu/libphilprac/5599

Suprapto, N., Yanti, V. K., & Hariyono, E. (2022). Global research on tsunami education and tsunami mitigation: A bibliometric analysis. *Science of Tsunami Hazards*, 41(2), 130–148.

Tal, Y., Rubino, V., Rosakis, A. J., & Lapusta, N. (2020). Illuminating the physics of dynamic friction through laboratory earthquakes on thrust faults. *Proceedings of the National Academy of Sciences of the United States of America*, 117(35). https://doi.org/10.1073/pnas.2004590117

Widiyantoro, S., Gunawan, E., Muhari, A., Rawlinson, N., Mori, J., Hanifa, N. R., Susilo, S., Supendi, P., Shiddiqi, H. A., Nugraha, A. D., & Putra, H. E. (2020). Implications for megathrust earthquakes and tsunamis from seismic gaps south of Java Indonesia. Scientific Reports, 10(1), 1–11. https://doi.org/10.1038/s41598-020-72142-z

Ye, L., Lay, T., Kanamori, H., & Rivera, L. (2016). Rupture characteristics of major and great (Mw ≥ 7.0) megathrust earthquakes from 1990 to 2015: 2. Depth dependence. *Journal of Geophysical Research: Solid Earth*, 121(2), 845–863. https://doi.org/10.1002/2015JB012427

Zakhiyah, I., Suprapto, N., & Setyarsih, W. (2021). Prezi mind mapping media in physics learning: A bibliometric analysis. *Journal of Physics: Conference Series*, 2110(012015). https://doi.org/10.1088/1742-6596/2110/1/012015

ISSN 8755-6839

SCIENCE OF TSUNAMI HAZARDS

Journal of Tsunami Society International

Volume 41 Number 4 2022

NUMERICAL MODELING OF A TSUNAMI OF LANDSLIDE ORIGIN IN THE KURIL BASIN

R.Kh. Mazova, A.A. Kurkin, D.A. Okunev

Nizhny Novgorod State Technical University n.a. R.E. Alekseev, Nizhny Novgorod, Russia. e-mail: raissamazova@yandex.ru

The work is devoted to the study of landslide-induced tsunami in the area of the Sea of Okhotsk on the western slope of the Kuril Basin. Landslide areas, up to 2 km in size, are located on the North Hokkaido marginal plateau and near the Patience Ridge. Possible strong tsunamis generated by landslide processes in the Kuril depression, which represent a potential hazard for the eastern coast of the island, are considered. Sakhalin Island, where there is currently an intensive development of infrastructure related to the development of oil and gas fields. To assess the risks, it is necessary to carry out numerical simulation of possible catastrophic landslide processes in the Kuril Basin and tsunamis generated by these processes. In this work, such modeling was carried out on the basis of a solid-block segmental model of a landslide body.

Key words: *Sea of Okhotsk, Kuril basin, landslide slope, solid block segmental model of landslide body, numerical modeling.*

1. INTRODUCTION

The tsunami problem is especially relevant for the Russian Far East. There are many studies on the tsunami hazard of the Sea of Okhotsk and the Kuril-Kamchatka region, both for seismic events and for landslides (see, for example, [1-7]). The waves formed by landslides often have a shorter period and length compared to the waves that appeared as a result of an earthquake, and diminish rather quickly. However, their destructive power is comparative with that of seismic tsunami. Large waves caused by landslides have been observed quite often in recent decades. So, for example, on June 17, 2017, a landslide descended into the Karrats Fjord (Greenland), which caused a tsunami more than 90 meters high, although the magnitude of the earthquake was M ~ 4 [8]. A well-known tsunamigenic underwater landslide Storegga along the continental slope on the coast of Norway, which was about 290 km wide and extended for more than 800 km. The maximum height of tsunami waves reached 10–12 m, and in the Shetland Islands it exceeded 20 m [4]. On December 22, 2018, a tsunami occurred in the Sunda Strait, in the southwestern part of Indonesia, which was presumably caused by a landslide (from the slope of the Anak-Krakatau volcano) in an area of 64 hectares [9]. Widespread landslides were noted in the southern part of the eastern slope of Sakhalin Island (western slope of the Kuril basin) [3].

Under computation of tsunami waves caused by landslides, the main point is the choice of a model for describing the behavior of a landslide in numerical simulation. Currently, there are a number of models, the main of which are the model of solid block [10-13], and the model of a viscous or viscoelastic fluid [14-17], etc. In the model of solid block, the motion of a landslide is described within the framework of the rigid body dynamics, and for generation of surface water waves, shallow water equations are used. An underwater landslide is modeled by a rectangular block that moves with a constant speed on the bottom or sea slope. At the beginning of the landslide movement, in the general case, a dipole wave is generated — an elevation of water (crest) at the front edge of the landslide and a dip in the water level (trough) at its back. The relationship between landslide and water was based on the assumption of an impermeable solid bottom interacting with water for a certain period of time. A landslide usually consists of disconsolidated sediments that travel downslope and accumulate in a new location. The process of interaction of disconsolidated deposits does not always imply volume conservation.

In a number of cases, when landslide materials, such as lava, river sediments, or snow, behave approximately in the same way as a plastic Bingham fluid, an underwater plastic landslide is studied using the viscoelastic fluid approximation (see, for example, [14, 15]). In this model, the nonlinear equations of shallow water are used both for the movement of a landslide and for the generation of surface water waves. The variety of models of wave generation on the water surface by an underwater landslide leads to a difference in its parameters, which, of course, affects the characteristics of the waves generated on the coast (see, e.g., [13, 18-22]). Recently, several new models of landslide processes have been developed [23-25]. In contrast to these models, there is an elastic-plastic model of a landslide [26], which takes into account both the morphology of the landslide body and the mechanical characteristics of the sliding body components during the sliding process. At the same time, part of the sedimentary material is shifted from the upper part of the landslide body down the slope. When the elastic-plastic sedimentary layer slips, it generates a surface water wave, which is formed until the landslide stops, and then propagates over the water area [27, 28].

The complexity of the modeling problem is associated with the localization of an underwater landslide, as well as with its initial displacement. In addition, it is important how complex the geometry of the underwater part of the slope along which the landslide moves is. During the underwater localization of a landslide, a long wave is formed on the surface of the water during the sliding process. As is known, at the beginning of a landslide movement, in the general case, a dipole wave is generated — an elevation of water (crest) at the front edge of the landslide and a dip in the water level (trough) at its back. As a result, the surface wave splits into two waves. The first train is moving towards the open sea, and the second one, consisting of two low waves and a crest, is moving towards the coastline.

As known, on Sakhalin Island, there are enterprises for the extraction and processing of oil, there are numerous settlements. With any significant earthquake or landslide process in the nearby zone, followed by a tsunami to the coast of Sakhalin Island, huge loss of human and material are possible. A wide distribution of landslides was noted in the southern part of the eastern slope of Sakhalin Island (western slope of the Kuril basin),

2. PROBLEM STATEMENT

This paper considers the landslide process on the western slope of the Kuril Basin. As noted in [3], the material was obtained in five marine expeditions in 2004-2015 during the survey of the Kuril basin. On the western slope of the Kuril basin, based on the data of bathymetric and seismic surveys, areas of possible landslide processes were identified. Using the data of these studies, the work considered the western slope of the Kuril Basin and the western part of the basin itself. The data of [3] made it possible to identify sections of the slope that may be subject to destruction. A map of landslide hazard from landslides in the Kuril Basin is shown in fig. 1. The red dots mark the localizations of the largest landslide slopes, the arrows indicate the landslide centers considered in [3].

In this paper, we consider the distribution of maximum tsunami wave heights along the eastern coast of Sakhalin Island, which, with possible landslide processes on the western slope of the Kuril Basin, will be most susceptible to such waves. To do this, the paper considers several options for the implementation of the landslide process in the Kuril basin. The shelf area is occupied by the South Sakhalin sedimentary basin, which consists of the Aniva and Patience troughs. A graphical illustration of the profiles of the main landslide slopes taken from [3] is shown in Fig. 2. Two hypothetical centers of landslides were chosen in the work, located under the numbers 1 and 4 presented in Fig. 2 [3]. The landslide movement is modeled as the movement of a rigid body, divided into a number of blocks-segments, and the landslide process was modeled by the dynamic vertical displacement of segment blocks along the landslide slope, simulating the sliding of the landslide mass. The kinematics of the movement of blocks is determined by the schematic behavior of the landslide movement, corresponding to a typical implementation of the calculation within the framework of the elastic-plastic model — sliding of the upper part of the landslide layer with a simultaneous increase in the thickness of the lower part of the slope (see, e.g., [28]). To implement this simulation, the landslide body is represented by 4 segmental blocks located along the slope. This process, can be roughly approximated by the displacement of the upper segment blocks first downwards, with the simultaneous displacement of the lower blocks upwards. To model various landslide processes for each scenario, their own options for shifting the blocks into which the landslide is divided are proposed. Data are presented for each option in Tables 1 and 2 (see below). In this case, the two upper blocks sequentially move down, with the simultaneous sequential movement of the two lower blocks upwards (see Tables below). Figure 3 shows the computational domain used for numerical simulation: 44.5° — 55°N (N), 141.7°-149°E (E). Since the computation of the tsunami hazard of the eastern part of Sakhalin is of particular importance, due to its population and the presence of dense infrastructure along the coasts, in the area of populated areas such as the cities of Poronaysk, Makarov, Dolinsk, Korsakov and Nogliki, virtual tide gauges were set up to record possible maximum wave heights on the calculated 5-meter isobath.

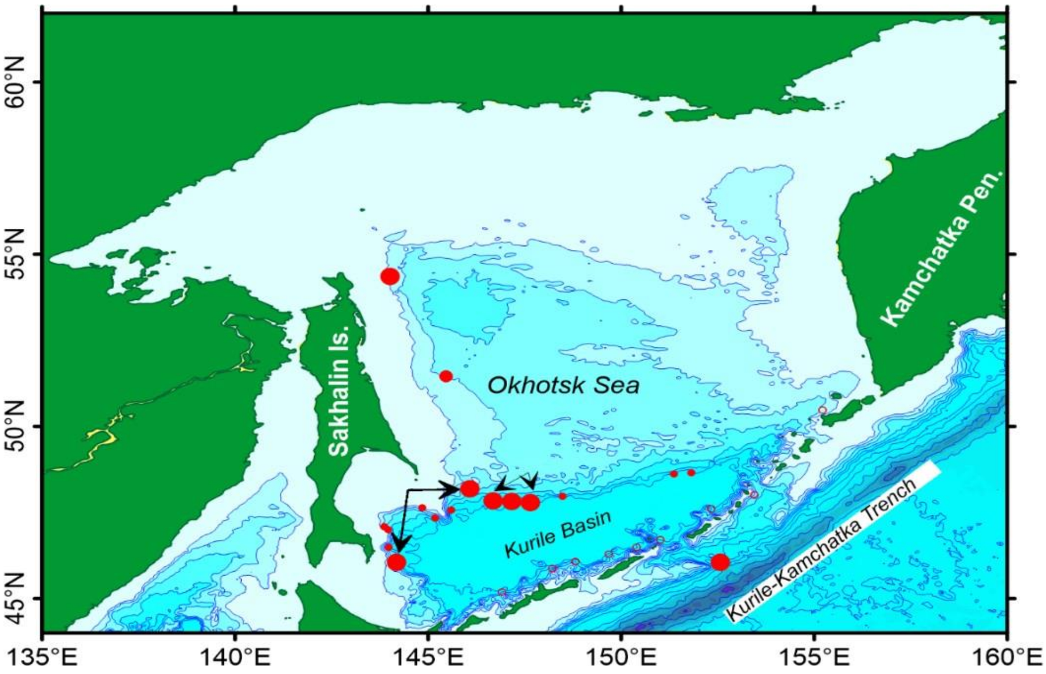

Fig. 1. Map of landslide hazard from landslides in the Kuril basin [3].

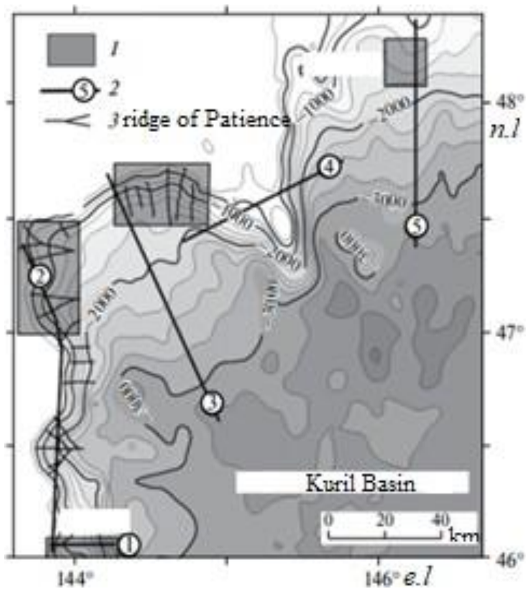

a)

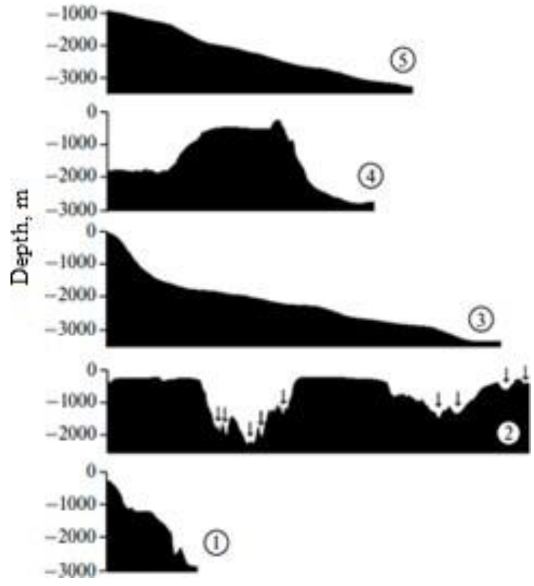

b)

Fig. 2. a) Bathymetric map of the study area. Circles with numbers indicate the areas of landslide localization; b) Bathymetric profiles illustrating landslide slopes in the study area [3].

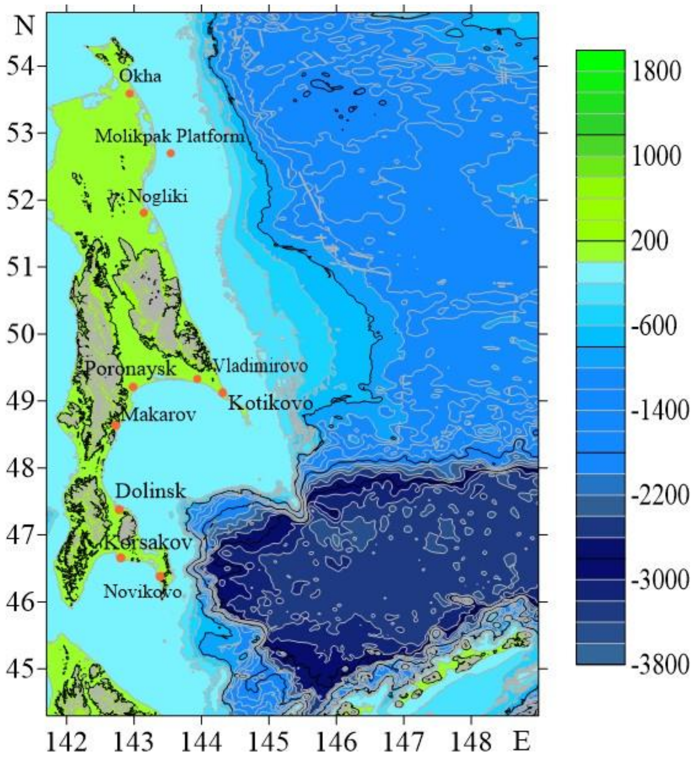

Fig. 3. Computed water area for modeling the landslide process in the Kuril basin

For a more detailed analysis of the generation of the tsunami source obtained during the movement of an underwater landslide, larger-scale areas of the water area shown in Fig.4 were considered. Fig. 4 shows the possible localization of landslide sources modeled by segment blocks for cases (1) and (4) depicted in Fig. 2b.

Thus, two landslide centers were considered in the Kuril depression: near the eastern part (Cape Patience) and near the southeastern part of Sakhalin Island (Cape Aniva). To simulate possible landslide processes, we will assume that the landslide precedes a virtual earthquake with a magnitude of M ~ 7.

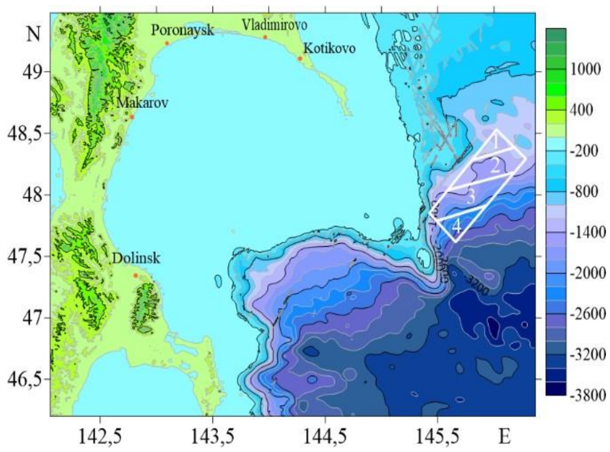

a)

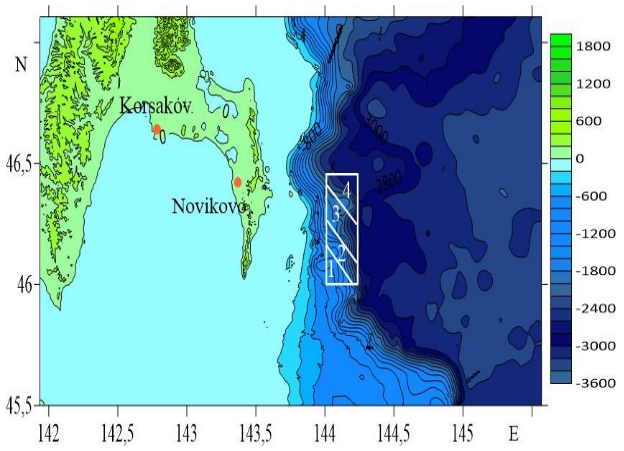

b)

Fig.4.a) Design water area for the first landslide (Scenario 1);

b) Estimated water area for the second landslide (Scenario 2).

3. MATHEMATICAL STATEMENT OF THE PROBLEM

To calculate the generation and propagation of long waves on the water surface caused by the movement of an underwater landslide, a system of nonlinear shallow water equations (1) is used. Numerical simulation was carried out using an upgraded software package based on a scheme with high algorithmic versatility proposed in [29]. To describe the generation and propagation of a wave caused by the movements of segmental solid blocks in the landslide source, a nonlinear system of shallow water equations in a two-dimensional formulation [27, 28, 30] was used

$$\begin{cases} \dfrac{\partial u}{\partial t}+u\dfrac{\partial u}{\partial x}+v\dfrac{\partial u}{\partial y}=-g\dfrac{\partial \eta}{\partial x} \\ \dfrac{\partial v}{\partial t}+u\dfrac{\partial v}{\partial x}+v\dfrac{\partial v}{\partial y}=-g\dfrac{\partial \eta}{\partial y} \\ \dfrac{\partial \eta}{\partial t}+\dfrac{\partial}{\partial x}[(\eta+H-B)\,u]+\dfrac{\partial}{\partial y}[(\eta+H-B)\,v]=\dfrac{\partial B}{\partial t} \end{cases} \quad (1)$$

where η is the displacement of the water surface, H is the depth of the basin, u and v are the components of the horizontal wave velocity. The evolution of the function B (x, y, t) in these equations was determined by the kinematic motion of the block segments. The beginning of the landslide movement, modeled by the movement of segmental blocks along the underwater slope. At the same time, it was assumed that there is a clear boundary between the liquid and the landslide body — the density of water is considered constant, the density of the landslide is also constant. At the last sea point at a depth of 5 m, the condition of total reflection is set (vertical a wall that makes it possible to fix the maximum and minimum values of the wave level shift at this depth.

3. Numerical modeling of a tsunami in the Sea of Okhotsk from a landslide source on the southwestern slope of the Kuril Basin.

3.1. Scenario 1.

Numerical simulation of a tsunami in the Sea of Okhotsk from a landslide source on the western slope of the Kuril Basin (Scenario 1). When considering Scenario 1, a hypothetical block-segment landslide source was modeled with a center at the point 48.27°N, 146.04°E [3]. The coordinates of the block segments, the displacement values of the blocks and their movement dynamics are given in Table 1.

Table 1. Kinematics of movement of segmental blocks in a landslide source (Scenario 1)

	Block 1	Block 2	Block 3	Block 4
x1	145.8212	145.5943	145.4266	145.4938
y1	48.2992	48.0435	47.8527	47.7859
x2	146.0229	145.8212	145.5943	145.9307
y2	48.5290	48.2992	48.0435	47.9098
x3	146.1558	146.1589	146.1793	145.6637
y3	48.4133	48.3805	48.1785	47.6203
x4	146.1589	146.1793	145.9307	145.6557
y4	48.3805	48.1785	47.9098	47.6203
Start time of movement (s)	0	20	30	40
Total time of movement (s)	30	20	30	30
Final time of movement (s)	30	40	60	70
Height (m)	-3	-2	2	3

The complete computational area with the localization of the landslide source for the implementation of Scenario 1 is shown in Fig. 5.

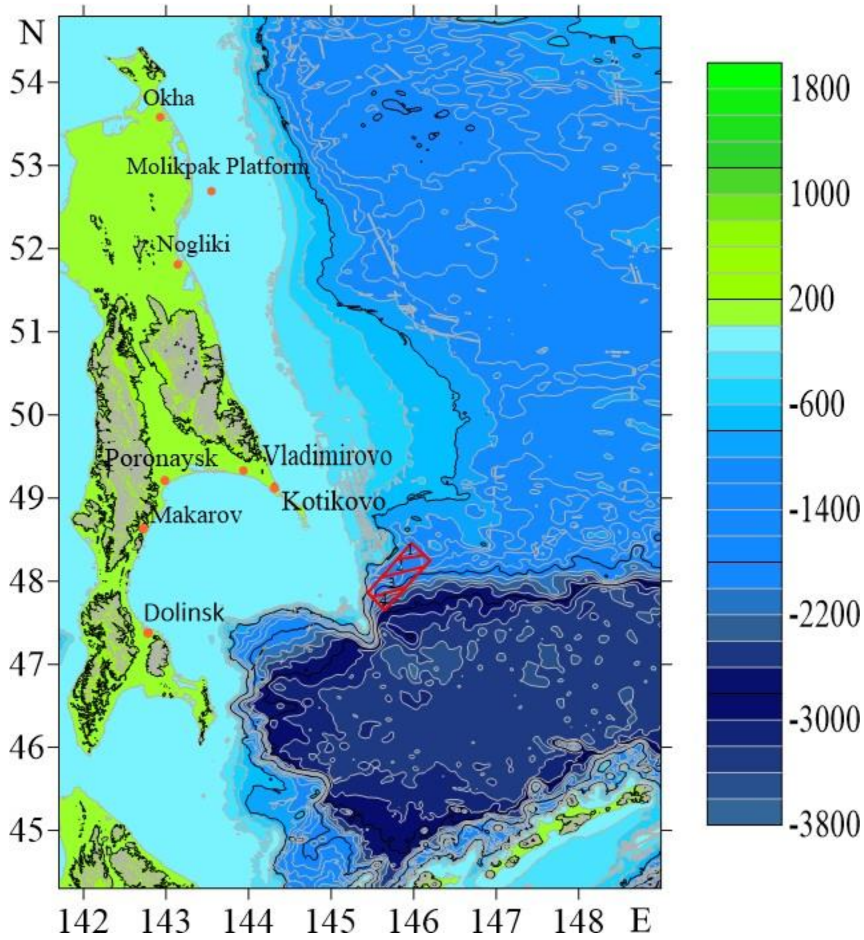

Fig. 5. Computed water area with the localization of the landslide source for Scenario 1

Figure 6 shows the results of numerical simulation of the generation of a tsunami source by a four-segment landslide source. It is clearly seen that when the first two segments move down the slope, the wave surface moves down (Fig. 6a, b), but simultaneously with this process, segments 3 and 4 rise, which corresponds to the upward displacement of the wave surface above these segments (Fig. 6b,c,d). Figure 6e,f shows the first moments of wave propagation from the tsunami source.

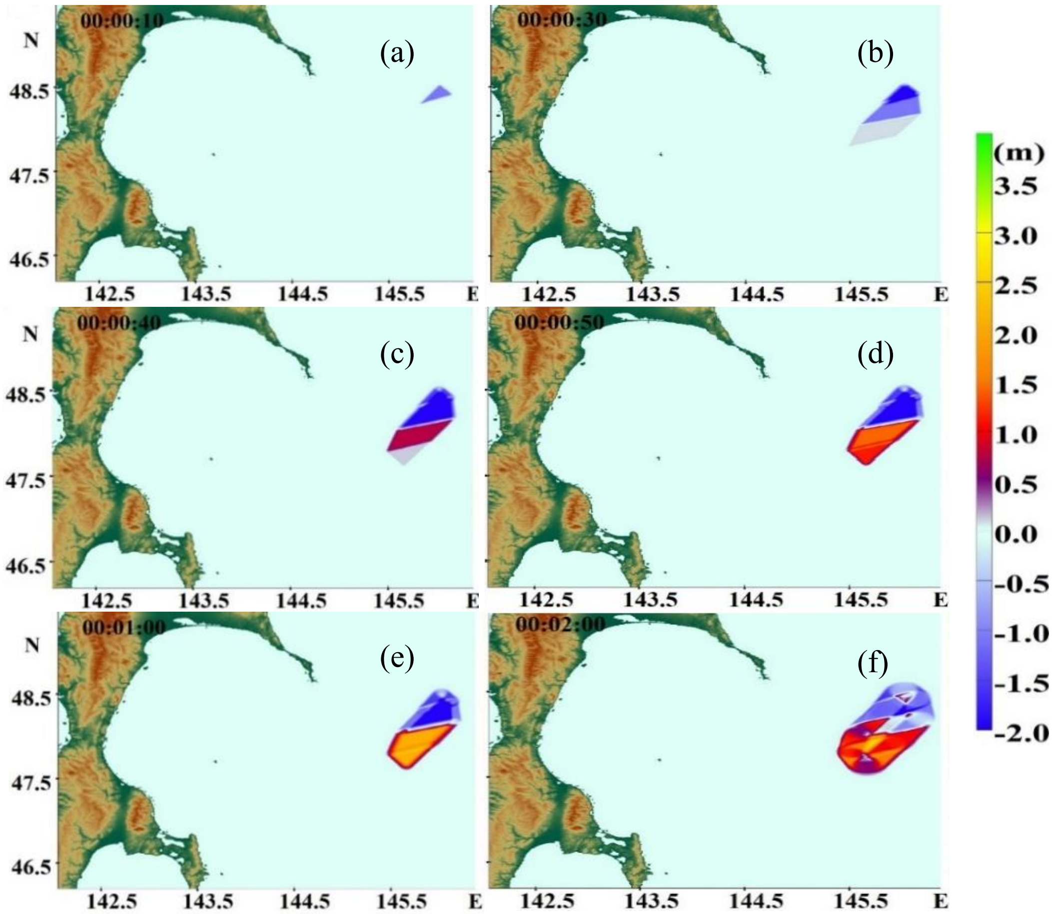

Fig. 6. Generation of a tsunami source in numerical simulation of a landslide process under Scenario 1

Figure 7 shows the further propagation of tsunami waves in a part of the Sea of Okhotsk (Fig. 7a-c) towards the Kuril Islands and Sakhalin Island. Displacement wave fields were obtained along Terpenya Bay and the eastern coast of Sakhalin Island. So, at t = 40 minutes (Fig. 8d), one can see how the wave front reached Cape Patience, Cape Aniva and began to spread in the Gulf of Patience. Figure f 7 shows how the wave moves towards the coast of the Gulf of Patience with a height ranging from 0.5 to 1.5 meters. Figure f 7 clearly shows how the wave front propagates along the east coast, towards the city of Okha. East

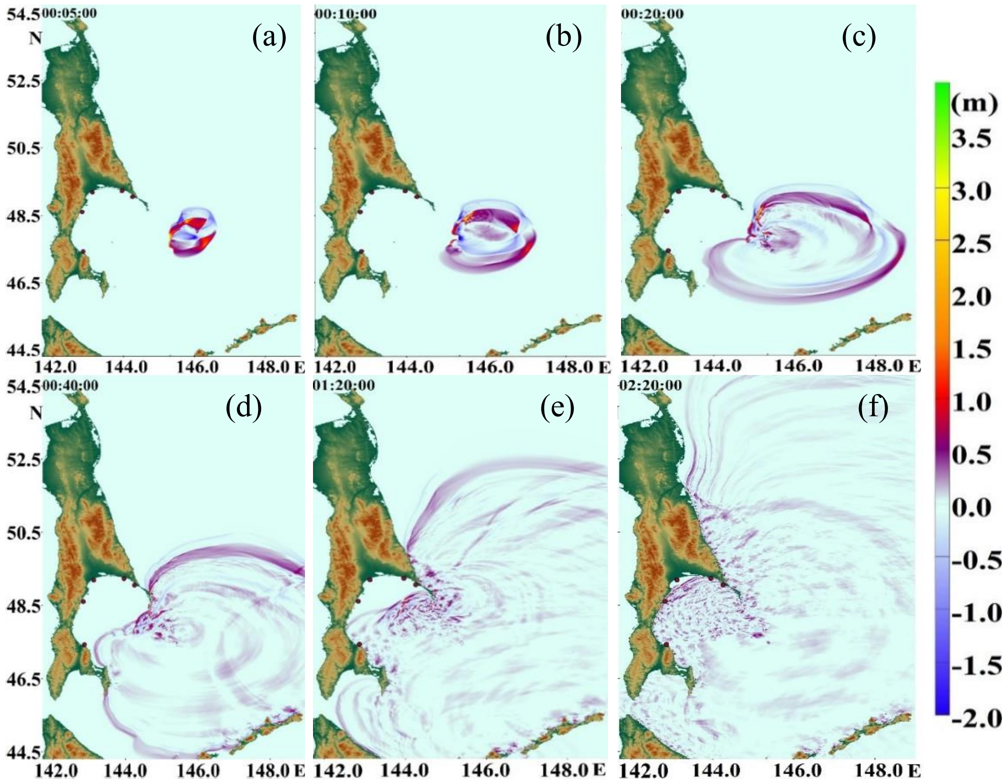

Fig. 7. Propagation of wave fronts in the Sea of Okhotsk (Scenario 1)

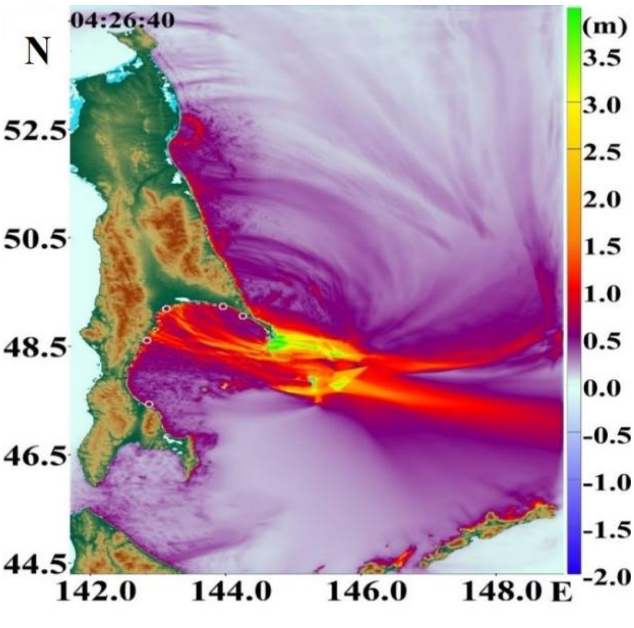

Fig. 8. Distribution of wave heights over the estimated water area during implementation Scenario 1

Figure 8 shows the distribution of heights over the computed water area under the implementation of Scenario 1 (Fig. 5). Almost along the entire coast, wave heights are observed in the range from 1-1.5 m. However, there are local areas with high heights, which is well observed in Fig. 9, which shows a 2D histogram of the distribution of maximum wave heights along the southeastern part of the coast of Sakhalin Island . It is clearly seen that the peak of heights falls on Cape Patience (144.8 E) and reaches 14 meters

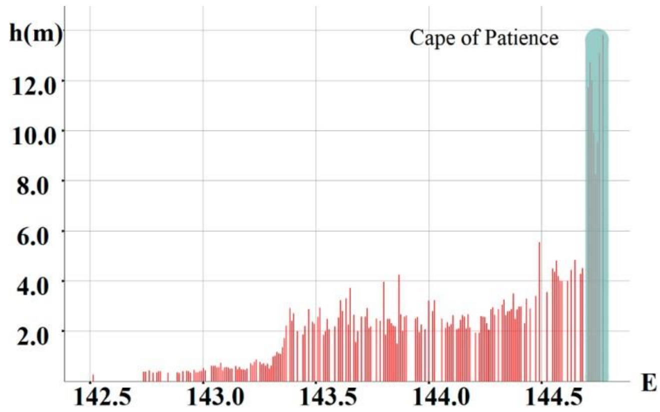

Fig. 9. Height Distribution Histogram (Scenario 1)

Figure 10 shows 3D histograms of the distribution of maximum wave heights along the eastern coast of Sakhalin Island on a 5-meter isobath. It can be seen that for this problem statement, the maximum wave heights reach 14 meters, while the average values do not exceed 1.5-3 meters.

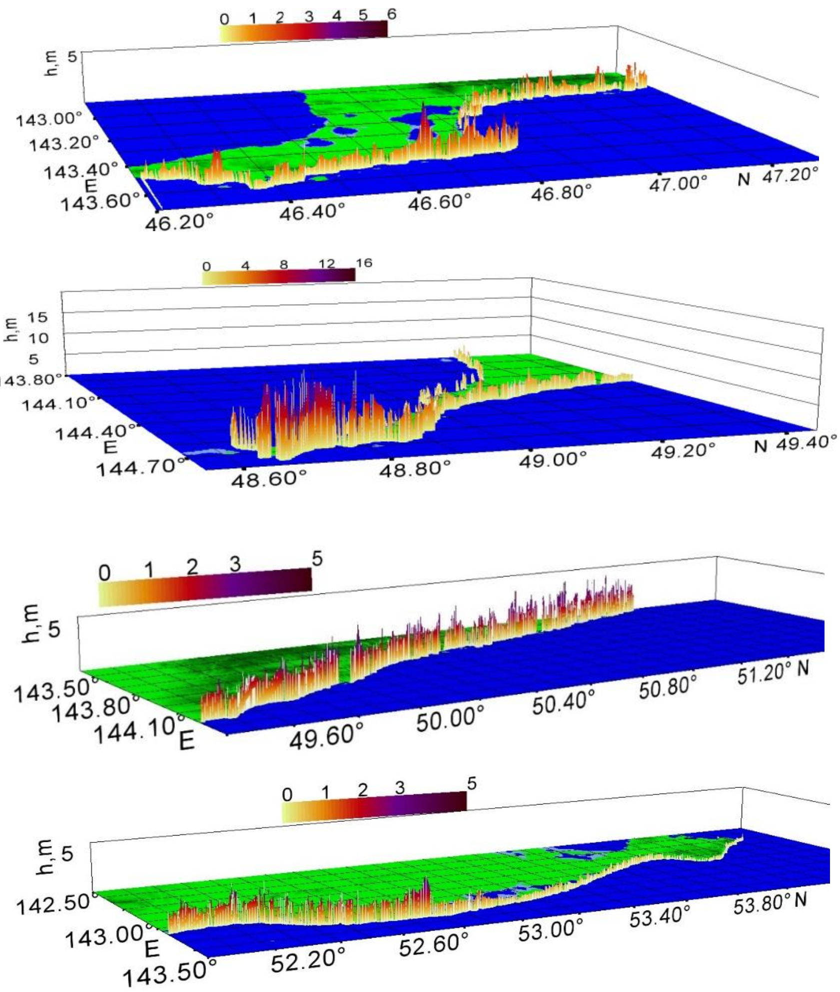

Fig. 10. 3D histograms of wave heights in some parts of the coast of about. Sakhalin under Scenario 1: a) coastal area near Cape Aniva and the cities of Dolinsk and Makarov; b) a section of the coast near the points of Kotikovo and Vladimirovo, as well as Cape Terpenya; c-d) sections of the northeastern coast of Sakhalin Island.

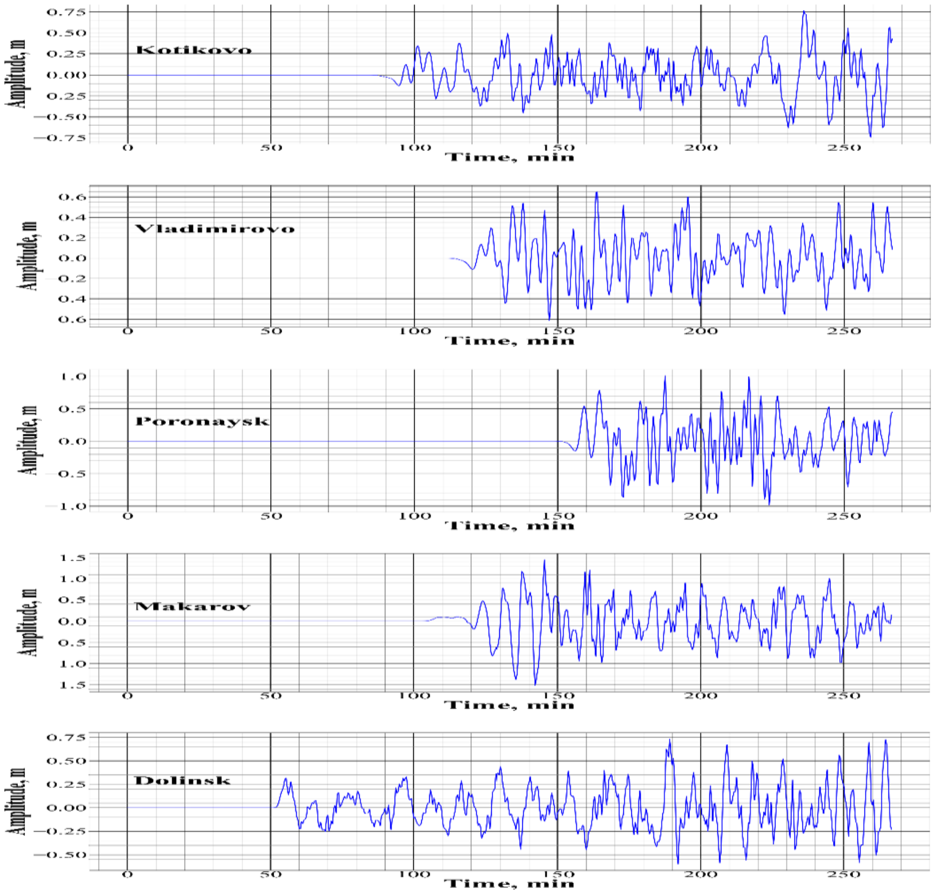

Fig. 11. The records from virtual tide gauges off the coast of Terpenya Bay (Sakhalin Island)

Figure 11 shows the data of records of virtual tide gauges set up in five points (Fig. 11, points 1-5). It is clearly seen on the tide-gauge records that the phase of the wave approach to the shore remains the same as in the first calculation at three points: Kotikovo, Vladimirovo and Poronaysk, the arrival of the first wave was accompanied by a slight rundown, where the vertical displacement was up to 0.2 m. At such points as Dolinsk and Makarov, the first wave was an elevation wave in the region from 0.25 to 0.5 m. You can also see that a train of waves approaches each point where virtual tide gauges are located, and the first positive wave nowhere was the maximum. The maximum wave height was recorded in the area of Makarov, when the fourth wave approached, with a height of more than 1 m. According to the tide-gauge records, the scatter of the maximum and minimum sea level heights is clearly visible, which is 2.96: from +1.45 to-1.51m.

3.2. Scenario 2.

To implement the Scenario 2, a hypothetical variant of a block-segment landslide source was modeled in the Kuril basin, near the Aniva cape, consisting of 4 segments (Fig. 12, see also Fig. 4 (b))]. The coordinates of the block segments, the displacement values of the blocks, and their dynamics of movement are given in Table 2. Figure 13 shows 6 times of generation of the tsunami source by the landslide source.

Thus, the formation of a tsunami source is clearly visible: at a) t = 10 sec, the downward movement of the first segment gives a decrease in the still water level by 3 m; b) t = 30 sec the second segment moves down by 2 m, and the third segment starts moving up by 2 m; c) t = 40 sec the fourth segment begins to move, which gives a vertical displacement of the wave surface by 3 m. The time of formation of the tsunami source is 1 minute 10 seconds. Figure 13e shows the formed wave front at time $t = 2$ minutes.

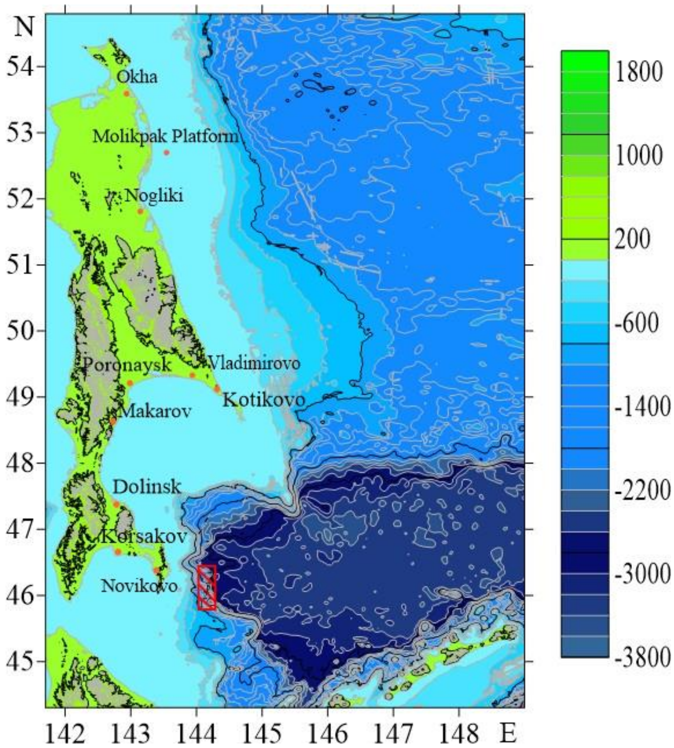

Fig. 12. Computation water area with the localization of the landslide source for Scenario 2

Table 2. Kinematics of movement of segmental blocks in a landslide Source (Scenario 2)

	Block 1	Block 2	Block 3	Block 4
x1	144.0324	144.0312	144.0111	144.0105
y1	45.7919	45.9696	46.1607	46.3472
x2	144.0312	144.0111	144.0105	144.0111
y2	45.9696	46.1607	46.3472	46.4092
x3	144.2567	144.2379	144.2377	144.2375
y3	45.7908	45.9398	46.1417	46.4079
x4	144.2157	144.2567	144.2379	144.2377
y4	45.7771	45.7908	45.9398	46.1417
Start time of movement (s)	0	20	30	40
Total time of movement (s)	30	20	30	30
Final time of movement (s)	30	40	60	70
Height (m)	-3	-2	2	3

Figure 14 shows the results of numerical simulation of tsunami wave propagation in a part of the Sea of Okhotsk. The wave from the source begins to propagate towards the Kuril Islands, Hokkaido Island and Sakhalin Island. Figure 14,b shows that when t = 10 min the wave reached Cape Aniva. Further, the wave front continued to propagate towards Aniva Bay and Cape Kostroma with wave heights in the range of 0.5 to 1.5 meters (Fig. 14c,d). At t = 1 hour 20 minutes (Fig. 14,f), the tsunami wave reached the entire coast of Aniva Bay. In Fig. 14,e, the wave propagates along the eastern coast of Sakhalin Island. As can be seen in Figure 15 and Figure 16, the average wave height is 1-2 meters, while Cape Aniva has a maximum wave height of 11.5 meters. It is clearly seen that some of the large waves reached Cape Kostroma. Figure 17 shows 3D histograms that confirm the conclusion about the average wave range of 1-2 meters, excluding Cape Aniva. Figures 17a and 17c show histograms of wave heights along Cape Aniva, where a wave peak is visible in the interval (46.2-46.4 N), the value of which reaches 12 meters. In Fig. 17d, in the range (142.4-142.8 E), the Korsakov and Novikovo points are located, where the average wave value does not exceed 1 meter. Also, in the range from (142 - 142.2 E) a tsunami wave comes to Cape Kostroma with a height of about 4-6 meters. The histogram in Fig. 17b shows the Gulf of Patience, where the average range of tsunami waves is 0.2 – 0.6 meters.

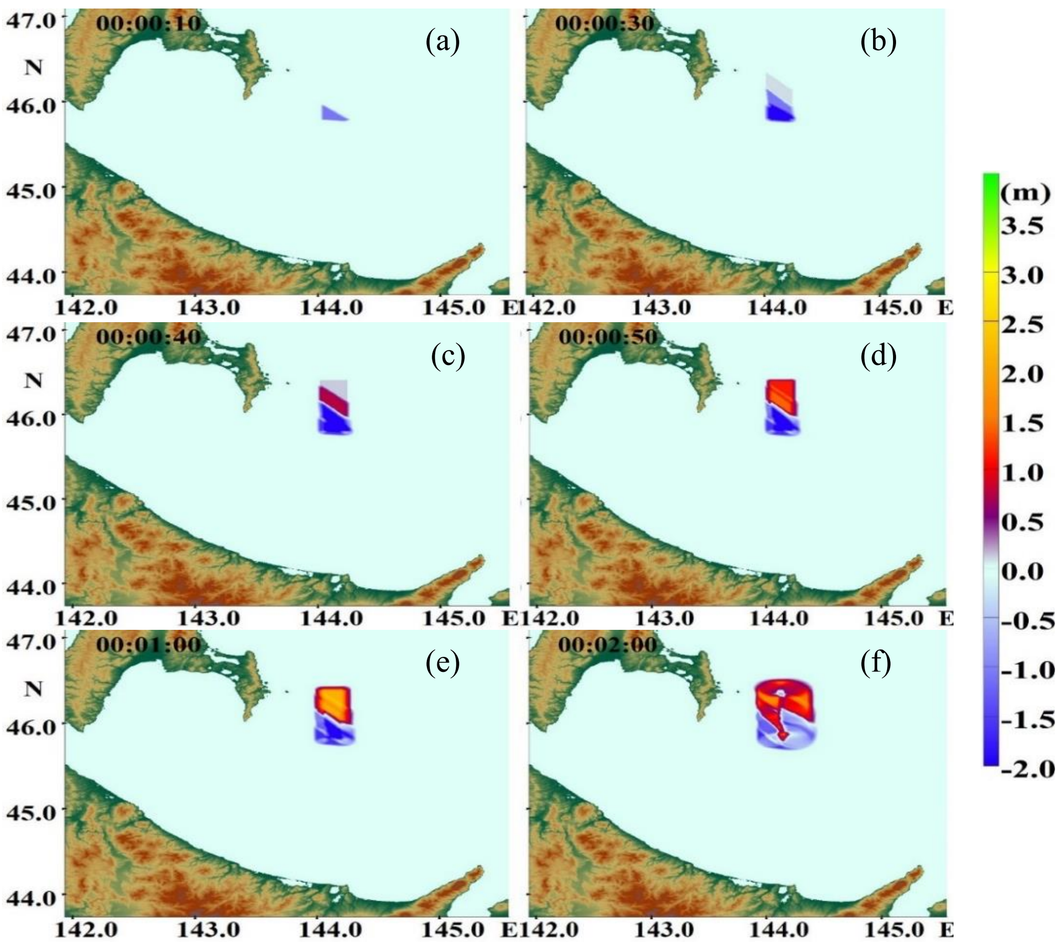

Fig.13. Generation of a tsunami source in numerical simulation of a landslide process under Scenario 2

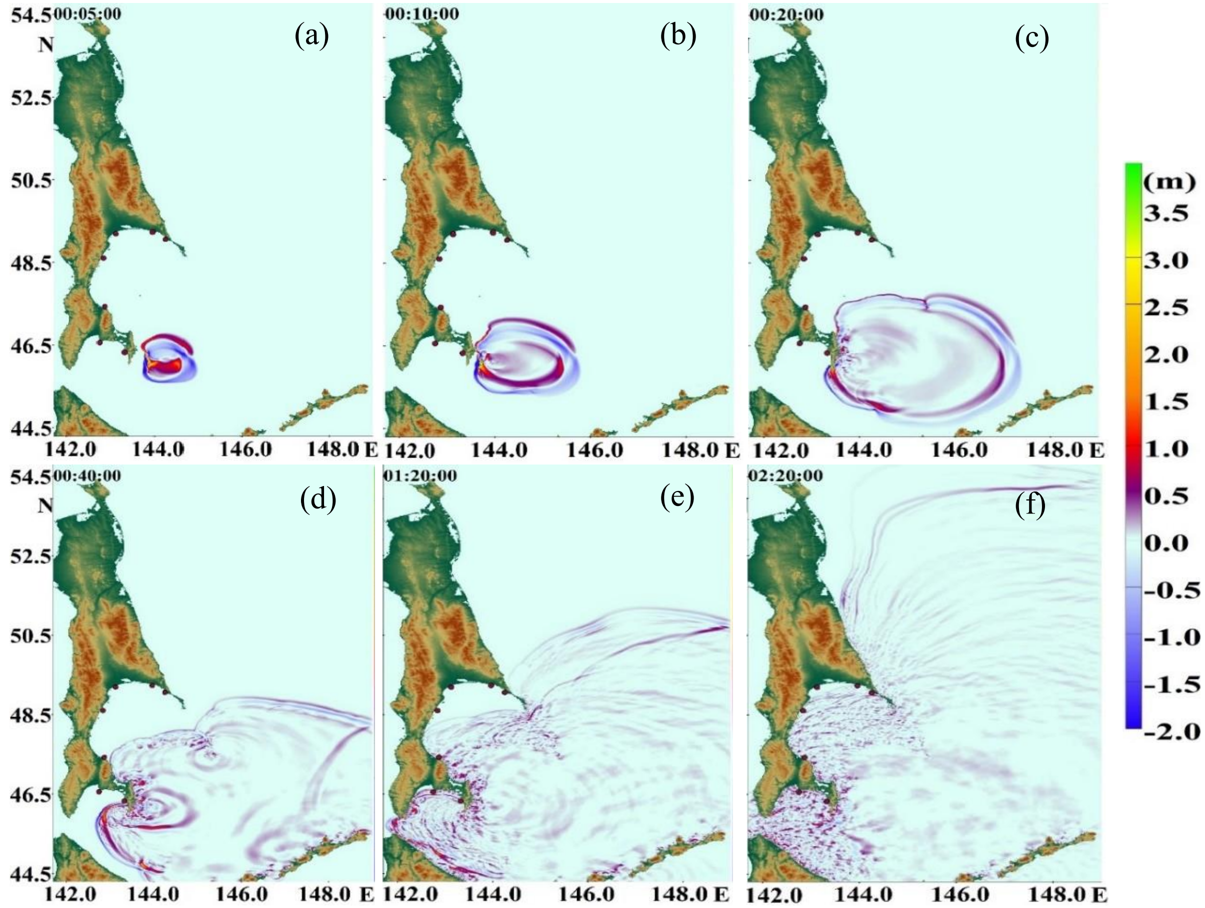

Fig.14. Propagation of wave fronts in the Sea of Okhotsk (Scenario 2)

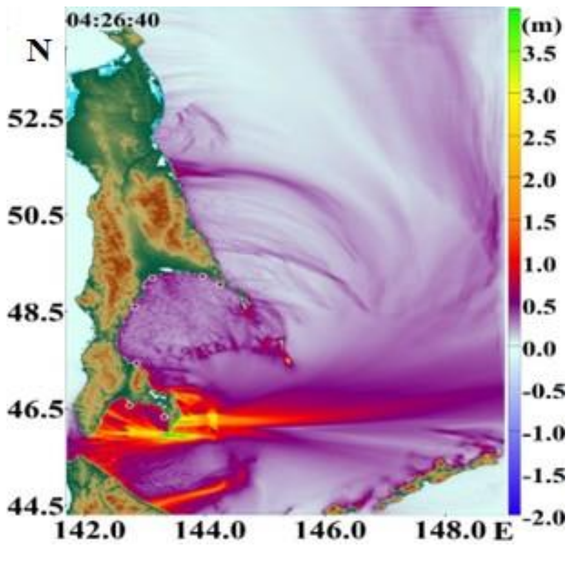

Fig. 15. Distribution of wave heights over the estimated water area during implementation Scenario 2

For a more detailed analysis of the computation, virtual tide gauges were set in points (1-7), the tide gauges from which are shown in Fig.18.

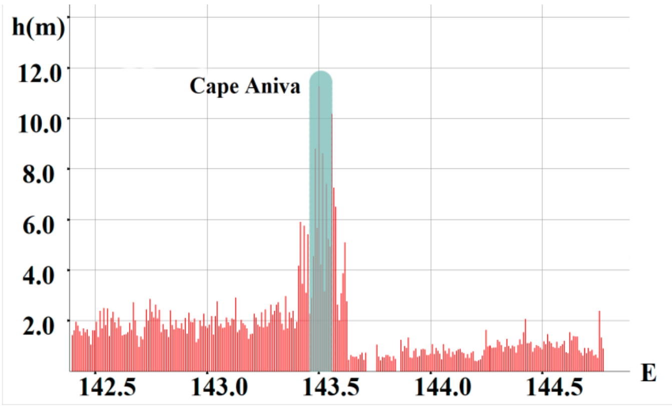

Fig.16. Height Distribution Histogram (Scenario 2)

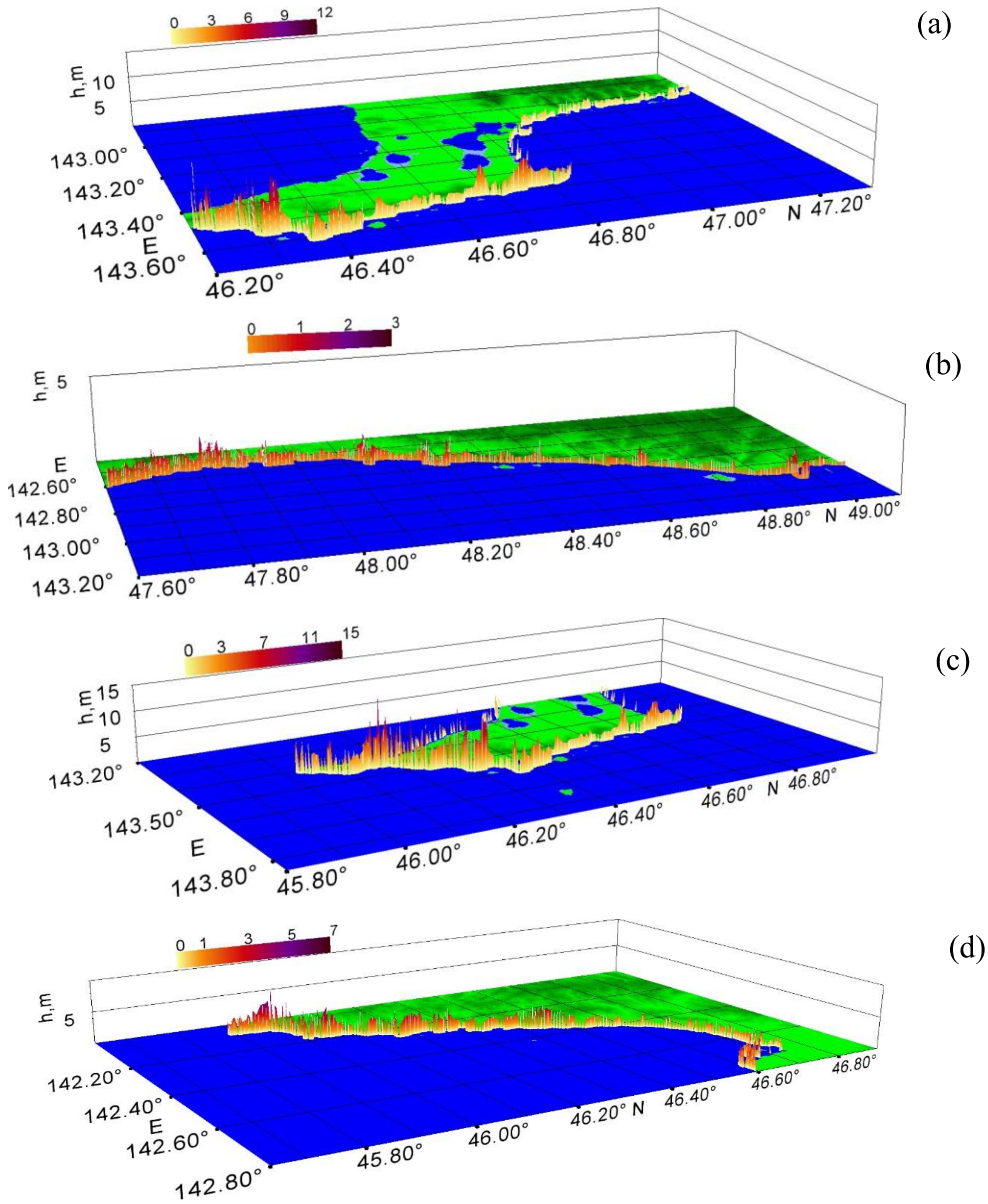

Fig. 17. 3D histograms of maximum wave heights along the coast of Sakhalin during the implementation of the landslide process (Scenario 2): a) a section of the coast near the cities of Dolinsk and Makarov; b) a strip of the coast of the Gulf of Patience; (c) a stretch of coast near Cape Aniva; d) Aniva Bay coast zone, near the town of Korsakov.

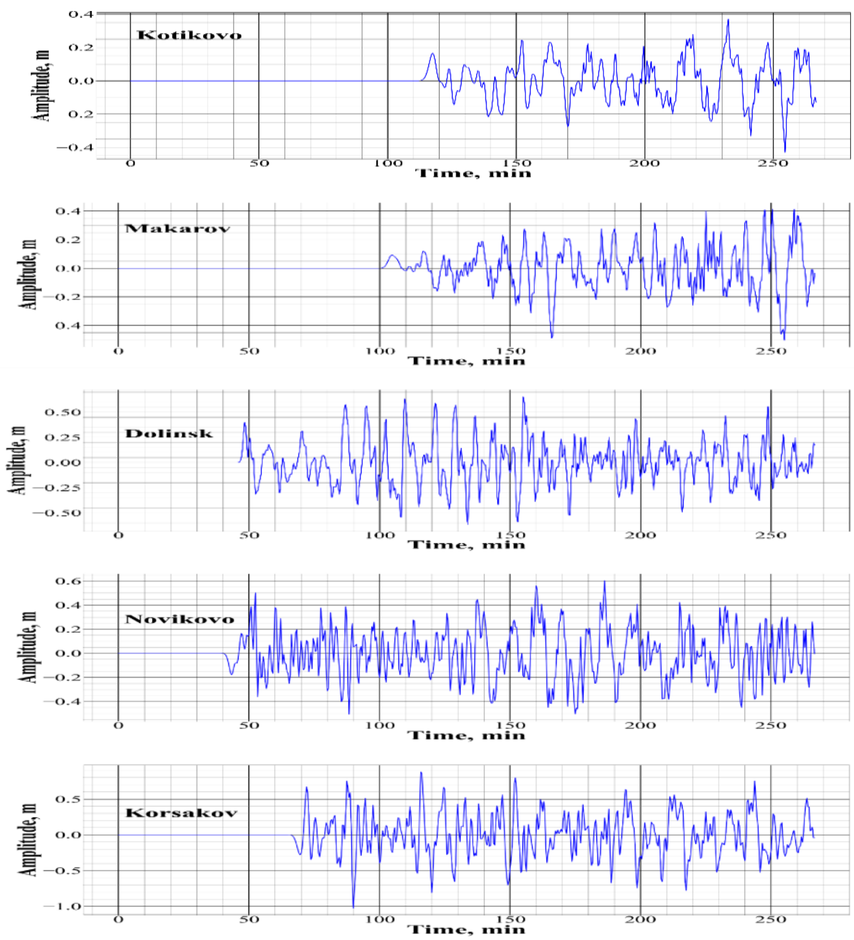

Fig.18. Tide-gauge records of the coast of Aniva Bay (Sakhalin Island, Scenario 2)

According to the data of tide-gauge records, it can be seen that at such points as Kotikovo, Vladimirovo, Poronaysk and Dolinsk, the wave arrived with a positive phase, i.e., the tsunami began with a wave runup onto the shore, in the range from 0.1 to 0.2 meters. In the points of Korsakovo and Novikovo, adjacent to the source, a low tide of up to 0.3 meters is observed, followed by the arrival of a wave up to 0.5 meters high, and this first wave is not the highest at these points. Also, according to the data from tide-gauge records, one can see the spread of wave heights, which is 1.9 m: from + 0.88 to-1.025 meters.

4. CONCLUSIONS

The work considered landslide processes in the Kuril Basin on the western slope in the Sea of Okhotsk. In the computation, data from the work of Baranov V.V. et al. [3] on the western slope of the Kuril Basin in the Sea of Okhotsk were used. The considered landslide processes were modeled on the basis of studies of international marine expeditions of the Russian Academy of Sciences. Four scenarios were considered, two landslide processes, two of which are presented in this article. Two scenarios for localizing a landslide opposite Cape Patience and two scenarios for localizing a landslide opposite Cape Aniva were considered. Landslide processes were modeled within the framework of a solid-block segmental model of a landslide source. During the movement of the landslide, a tsunami source and tsunami wave fronts were generated, the propagation of which was considered in part of the Sea of Okhotsk, along the. Sakhalin Island. It should be noted that at the points of Cape Aniva and Cape Patience, peaks in wave height are observed, which is possibly associated with resonance phenomena. Compared to the computations in [6], where the landslide process was considered, with the center at the point 51.5°N; 145.4°E, the data differ. For example, in the study [6], the waves that reached the coast of Sakhalin Island in the area of the village of Nogliki had an average height of 3 to 6 meters, moreover. The height peak was reached at the Molikpak platform and was equal to 16 m. In our computations, the average wave heights in this section are from 1 to 3 m, and the peak falls on Cape Patience and reaches 14 m. However, it should be noted that the localization of landslide masses in both cases is significantly different. The landslide in [6] is located to the north of the landslide localized in the Kuril Basin (Scenario 1), which well explains the lower average heights in our computation.

Acknowledgements

The authors acknowledge the funding of this study provided by grant of President of the Russian Federation for the state support of Leading Scientific Schools of the Russian Federation (Grant No. NSH-70.2022.1.5).

REFERENCES

1. Soloviev S.L., Go Ch.N. Catalog of tsunamis on the West Pacific coast. – M.: Nauka, 1974. 310 p.
2. Shchetnikov N.A. Tsunami on the coast of Sakhalin and the Kuril Islands from tide-gauge data 1952-1968. – Vladivostok: Far Eastern Branch of the Academy of Sciences of the USSR, 1990 24 p.
3. Baranov B.V., Prokudin V.G., Dzhin Ya.-K., Dozorova K.A., Rukavishnikova D.D.. Underwater landslides on the western slope of the Kuril Basin of the Sea of Okhotsk // Oceanologia. 2018. V. 58. No. 3. P. 452–462.
4. www. sakhmeteo.ru
5. Zaitsev A.I., Kostenko I.S., Kurkin A.A., Pelinovsky E.N. Tsunami on Sakhalin Island: Observations and Numerical Modeling. - Nizhny Novgorod: Nizhny Novgorod. State Tech. Univ. n.a. R.E. Alekseev, 2016. 122 p.
6. Ivanova A.A., Kulikova E.A., Fine I.V., Baranov B.V.. Generation of a Tsunami from the Submarine Landslide Near the East Coast of Sakhalin Island // Moscow University Physics Bulletin. 2018. V. 73. No. 2. P. 234–239.
7. Lobkovsky L.I., Mazova R.Kh., Kataeva L.Yu., Baranov B.V. Generation and propagation of catastrophic tsunamis in the Sea of Okhotsk. Possible scenarios // Doklady RAS. 2006. V. 410. No. 4. P. 528–531.
8. Schiermeier Q. Huge Landslide triggered rare Greenland mega-tsunami // Nature. 2017. https://doi.org/10.1038/nature..22374
9. Heidarzadeh M., Ishibe T., Sandanbata O., Muhari A., Wijanarto A.B. Numerical modeling of the subaerial landslide source of the 22 December 2018 Anak Krakatoa volcanic tsunami, Indonesia // Ocean Eng. 2020. V. 195. Art. No. 106733.
10. Iwasaki S.-I., Furumoto A., Honza E. Can be a submarine landslide be considered as a tsunami source? // Science of Tsunami Hazards. 1996. V. 14. P. 89-100.
11. Iwasaki S.-I. The wave forms and directivity of a tsunami generated by an earthquake and landslide // Science of Tsunami Hazards. 1997. V. 15. P. 23-40.

12. Pelinovsky E., Poplavsky A. Simplified model of tsunami generation by submarine landslides // Physics and Chemistry of the Earth. 1996. V. 21. P. 13-17.
13. Didenkulova I., Nikolkina I., Pelinovsky E., Zahibo N. Tsunami waves generated by submarine landslides of variable volume: analytical solutions for a basin of variable depth // Nat. Hazards Earth Syst. Sci. 2010. V. 10. No. 11. P. 2407–2419.
14. Jiang L., LeBlond P.H. Numerical modeling of an underwater Bingham plastic mudslide and the waves which it generates // J. Geophys. Res. 1993. V.98. No. C6. P.10.303-10.317.
15. Jiang L., LeBlond P.H. Three-dimensional modeling of tsunami generation due to a submarine mudslide // J. Phys. Oceanogr. 1994. V.24. No. 3. P.559-572
16. Fine I.V., Rabinovich A.B., Thomson R.E., Kulikov E.A. Numerical modeling of tsunami generation by submarine and subaerial landslides // In: Submarine Landslides and Tsunamis (Eds.: A.C. Yalciner, E.N. Pelinovsky, E. Okal, C.E. Synolakis), NATO Science Series, IV. Earth & Environmental Sciences, Kluwer Acad. Publ. 2003. V. 21. P. 69-88.
17. Fine I.V., Rabinovich A.B., Bornhold B.D., Thomson R.E., Kulikov E.A. The Grand Banks landslide-generated tsunami of November 18 1929: preliminary analysis and numerical modeling // Marine Geology. 2005. V. 215. P. 45-57.
18. Ostapenko V.V. Numerical modeling of wave currents caused by a coastal landslide // Appl. Math. 1999. V. 40. No. 4. P. 109–117.
19. Fedotova Z. I., Chubarov L. B., Shokin Yu. I. Simulation of surface waves generated by landslides // Comp. Technology. 2004. V. 9. No. 6. P. 89–96.
20 Marchuk An.G. Numerical modeling of the resonant tsunami generation by the submarine landslide // Bull. Nov. Comp. Center , Math. Model. in Geoph. 2008. V. 12. P. 45–54.
21. Khakimyazov G.S., Shokina N.Yu. Numerical modeling of surface waves arising from the movement of an underwater landslide on an uneven bottom // Comp. Technology. 2010. V. 15. No. 1. P. 105–119.
22. Chernyshov A.D. On the conditions of snow avalanches and ground landslides // Izv. RAS. MTT. 2013. No. 3. P. 135-143.
23. De Blasio F.V., Elverhoi A., Issler D., Harbitz C.B., Bryn P., Lien R. Flow models of natural debris flows originating from overconsolidated clay material // Marine Geol. 2004. V. 213. P. 439-455.
24. Liu W, He S. A two-layer model for simulating landslide dam over mobile river beds // Landslides. 2016. V. 13. P. 565-576.
25 Ma G, Kirby J.T., Shi F. Numerical simulations of tsunami waves generated by deformable submarine landslides // Ocean Modeling. 2013. V. 69. P. 146-165.
26. Garagash I.A., Chemenda A. Numerical modeling of submarine landsliding triggered by seismic and tectonic processes // In: Proc. of 2nd Taiwan-France Symposium on Natural Hazards Mitigation: Methods and Applications, Villfranchesur-Mer (SE France), 2003.
27. Papadopoulos G.A., Lobkovsky L.I., Mazova R.Kh., Garagash I.A., Karastathis V., Kataeva L.Yu., Kaz'min V.G. Numerical Modeling of Sediment Mass Sliding and Tsunami Generation: the Case of 7 February 1963, in Corinth Gulf, Greece // Marine Geodesy. 2007. V. 30. P. 335-344.
28. Lobkovsky L., Mazova R., Remizov I. et al. Local tsunami run-up depending on initial localization of the landslide body at submarine slope // Landslides. 2021. V. 18. P. 897–907.
29. Marchuk A.G., Chubarov L.B., Shokin Yu.I. Numerical modeling of tsunami waves. – Novosibirsk: Nauka, 1983. 160 p.
30. Voltsinger N.E., Klevanny K.A., Pelinovsky E.N. Long-wave dynamics of the coastal zone. – Leningrad: Gidrometeoizdat, 272 p.

ISSN 8755-6839

SCIENCE OF TSUNAMI HAZARDS

Journal of Tsunami Society International

Volume 41 Number 4 2022

RUPTURE KINEMATIC PROCESS OF THE MW 5.9 SERAM EARTHQUAKE IMAGED BY BACK-PROJECTION TECHNIQUE FOLLOWED BY THE TSUNAMI

Muhammad Nurul Fahmi*, Arie Realita, and Madlazim

Physics Department, Faculty of Mathematics and Natural Sciences, Universitas Negeri Surabaya, Surabaya 60231, Indonesia

*muhammadfahmi@unesa.ac.id

ABSTRACT

The 16 June 2021 Seram earthquake occurred at a moderate magnitude of Mw 5.9 along the Banda Arc close to Seram Island, followed by a tsunami with a runup height of 0.51 m. A detailed kinematic study of the earthquake helps us better understand the tectonic environment of the secondary faults and the causes of an unexpected tsunamis after earthquakes, particularly on the island. In this study, we image the rupture processes of this earthquake using a Multiple Signal Classification Back-Projection (MUSIC-BP) method. This method used P-seismic waveforms from teleseismic data recorded by seismic stations across the Australian continent (AU arrays). These waveforms were filtered in the range of 0.5-1.0 Hz to remove unwanted phases. Our results show that the rupture moves bilaterally to southwest and northeast at a relatively slow speed of 1.47 km/s. In this earthquake, the rupture propagated ~35 km away from the epicenter and had a total duration of ~30 s. The maximum peak of the energy released is estimated to be ~15 km from the epicenter. The rupture directivity agrees well with the spatial distribution of aftershock events and the reported focal mechanism solution. According to the result of the rupture kinematics parameter, the tsunami was not caused directly by the earthquake. However, the direction of tsunami propagation is the same as that of earthquake rupture propagation. Furthermore, the results of this study reveal that the seismogenic fault under Seram Island has an SSW-NNE fault orientation.

Keywords: *Seram earthquake, Rupture processes, MUSIC-BP, AU arrays, tsunami*

1. INTRODUCTION

Eastern Indonesia is a region with a high level of seismicity because this region has complex tectonic environments caused by the interaction of the Pacific, Sunda, and Australian plates. The Banda Arc is where earthquakes occur most frequently, consisting of an inner volcanic arc, outer arc island, and trough (Hamilton, 1979; Spakman and Hall, 2010). In the outer Banda arc, there are several islands where earthquakes frequently occur: Seram, Haruku, Saparua, and Ambon islands. All islands adjacent to the Seram Trench's northern part always experience moderate to large earthquakes (Irsyam etal., 2020). Most recently, an earthquake occurred on 16 June 2019, located at the top of the Banda Arc on Seram Island, which resulted in a tsunami, and it is still unclear what caused it.

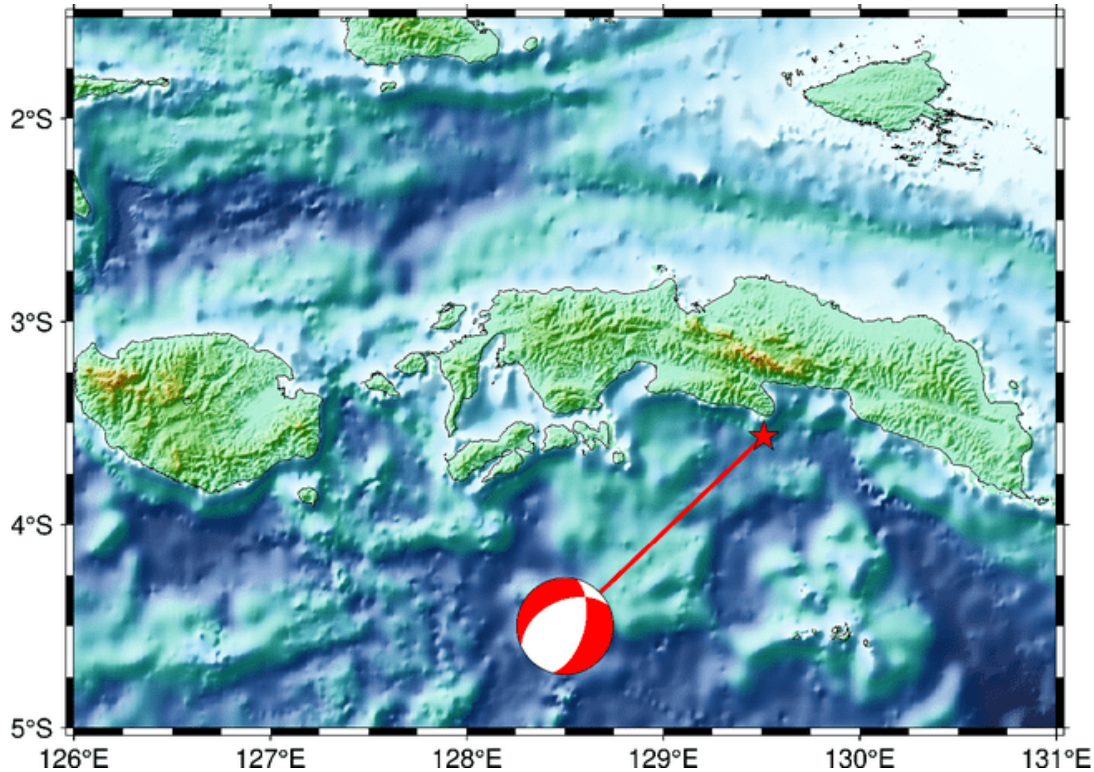

Figure 1. *Location of the 16 June 2021 M_w 5.9 Seram Earthquake.*

On 16 June 2021 at 04:43:07 UTC, a moderate shallow earthquake occurred near Seram Island, triggering an unexpected tsunami(Figure 1). This was confirmed by the National Center for Environment Information (NOAA) (https://www.ngdc.noaa.gov/hazard/tsu_db.shtml) which reported that this earthquake caused a small tsunami with a runup height of 0.5 m. In general, moderate earthquakes infrequently generate large tsunami waves. Even if it could generate a tsunami, the runup would be unnoticeable and the amplitude would be only a few centimeters. Mainly this earthquake is located at the top of Banda Arc and the epicenter of this earthquake at 3.56^{o} S, 129.51^{o} E, with a depth of 9.95 km. The moment tensor of Global-Centroid-Moment-Tensor (Global CMT, 2022; Ekström et al., 2012) provides a focal mechanism indicating a normal fault mechanism, where the nodal plane 1 (NP1) with strike1 = 245^{o}, dip1 = 46^{o}, rake1 = -50°; and nodal plane 2 (NP2) with strike1 = 14°, dip1 = 57°, rake1 = -124°. In addition, Global CMT positioned the centroid of the mainshock at a depth of 14.3 km. This moderate earthquake occurs in an area with complex geological conditions and can cause unexpectedly large tsunamis. Thus, rupture imaging is a solution to determine the kinematics of earthquake rupture and causes of unexpected tsunamis.

The kinematics rupture process of the earthquake can be known based on recording high-frequency (HF) seismic waveforms from the analysis using the Back-Projection (BP) method. This method uses an array signal processing technique to analyze the seismic waves recorded on dense seismic networks (Ishii et al., 2005; Krüger and Ohrnberger. 2015; Ishii et al., 2007). Thus, it can image the position of the rupture propagation and obtain a spatiotemporal distribution image of the earthquake source. The BP method produces robust resolution at each time frame since it only utilizes array processing and ignores fault geometry or Greens function assumptions. The BP method has been successfully applied to recent studies of large earthquakes worldwide (Kiser et al., 2011; Meng et al., 2011; Meng et al., 2012; Yao et al., 2012; Fan and Shearer, 2015; Liu et al., 2017; Wong et al., 2018; Bao et al., 2019; Xie and Meng, 2020; Kehoe and Kiser. 2020; Kiser and Kehoe, 2021; Madlazim et al., 2021; Sultan et al., 2022). Thus, this method is excellent and accurate for revealing earthquake rupture kinematics.

One of the accurate and high-resolution back-projection methods is the Multiple Signal Classification Back-Projection (MUSIC-BP) method developed by (Meng et al., 2011, Meng et al., 2016). The first thing to use the MUSIC-BP method is to evaluate the covariance matrix of the waveform in each sliding time window and sampling frequency. The steering vector which consists of travel time shift at each station is calculated for each candidate source node. The direction of arrival corresponding to the most probable source location is then determined by the maximum amplitude of the MUSIC pseudospectrum, which is defined as the inversion of the steering vector projection to the subspace noise (Schmidt, 1986). In a previous study, Bao et al. (2019) revealed the direction of rupture propagation and persistent supershear rupture speed from the 2018 Palu earthquake using the MUSIC-BP method. In addition, Madlazim et al. (2021) used the same method to determine the direction of propagation and low-velocity rupture that caused the tsunami in the Aegean Sea.

In this study, we adopted the multitaper back-projection (MUSIC BP) method (Meng et al., 2011, Meng et al., 2016) to investigate the rupture kinematics for the Seram earthquake. The position of the seismic source of an earthquake is determined by time shifts and a collection of waveforms (stacked waveforms) recorded at the teleseismic distance to the grid from the potential source location as a function of time (Ishii et al., 2005; Krüger and Ohrnberger, 2005). Based on this information, parameters of rupture kinematics (rupture direction, speed, and length) dan direction of tsunami propagation can be estimated. We also compared our result with a relevant previous study.

2. METHOD

The back-projection method can be utilized with any seismic station network and any seismic phase, while P waves recorded at teleseismic distances are most commonly used for most earthquakes due to little interference with other seismic phases. The method is most commonly applied to seismic arrays with dense station spacing and a small overall aperture. Because the wave pathways from the source to the receivers are comparable in these circumstances, the recorded waveforms are coherent across the array. The waveform coherence improves the stacking process and quickly removes artefacts from the source image. While using a single array yields reliable results, the small aperture limits spatial and temporal resolution. Increased distribution of seismic stations can result in better resolution, although care must be given to minimize source image artefacts caused by incoherent data. Visual assessment of the data or a measure of similarity between waveform segments is frequently used (for example, correlation values). While picking data based on waveform features can be beneficial, this method ignores the sources of artefacts in back-projection results.

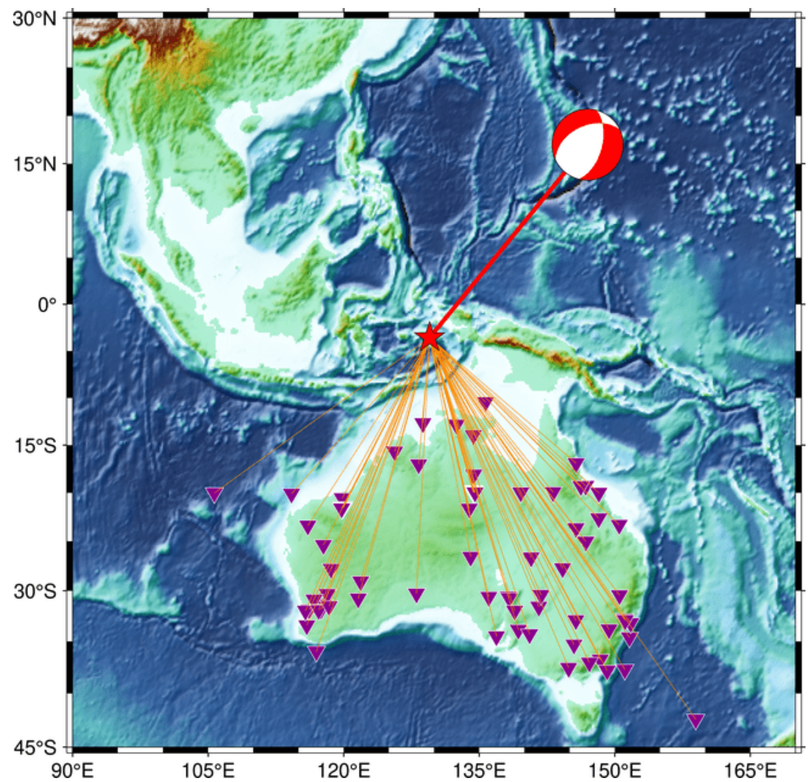

***Figure 2**. AU array location that recorded P-seismic waveforms from Seram earthquake.*

In this study, Multiple Signal Classification Back-Projection (Meng et al., 2011; Bao et al., 2019), an array processing approach, was used. P-seismic waveform from a wide distribution of Australian teleseismic stations (AU array) was used to describe the rupture properties of the Seram earthquake on 16 June 2021 (Figure 2). The epicenter distance from the AU array is about 50^{o} for better rupture imaging results. The initial step for rupture process imaging using MUSIC-BP is 60 seconds first time window from the arrival of the P-seismic waveform as this method's input process. Nevertheless, the amplitude of the P-seismic waveform is affected by the radiation pattern (noise). Back projection rupture imaging with MUSIC prioritizes tracking the most coherent phases within the time window. Furthermore, alignment is performed on the first arrivals of the P-seismic waveform so that the lateral velocity variations for each waveform become coherent (Goldstein and Archuleta 1987). After the alignment, the high-frequency P-seismic waveforms are filtered at a range of 0.5 to 1 Hz, as this is the highest band where coherent arrival initials must be closely aligned. This step applies an empirical travel time correction to the data, ensuring that the P-seismic waveforms arrive at the same time as predicted by the one-dimensional Earth model (IASP91) (Kennett and Engdahl, 1991). This step additionally corrects waveform polarities and normalizes P-seismic waveform amplitudes such that the initial waveforms have the same polarity. This technique is better than previous methods, such as the beamforming technique (Rost and Thomas, 2002) and this method not only produces a rupture imaging model for large earthquakes but can also be used for moderate earthquakes (Jian, 2021; Meng et al., 2020).

3. RESULTS AND DISCUSSION

MUSIC-BP analysis was applied to the Seram earthquake to determine the kinematic rupture process, where the rupture kinematics consisted of the parameters of rupture, namely rupture directivity, rupture length, rupture duration, and rupture speed. The back-projection results are integrated with the AU arrays to reconstruct the imaging rupture results from this earthquake. The P-seismic waveforms recorded by the AU arrays are filtered in the frequency range of 0.5-1.0 Hz. The filter range selection is based on the fact that teleseismic waveforms accommodate much noise and then a higher frequency is needed to obtain acceptable seismic waveforms [29].

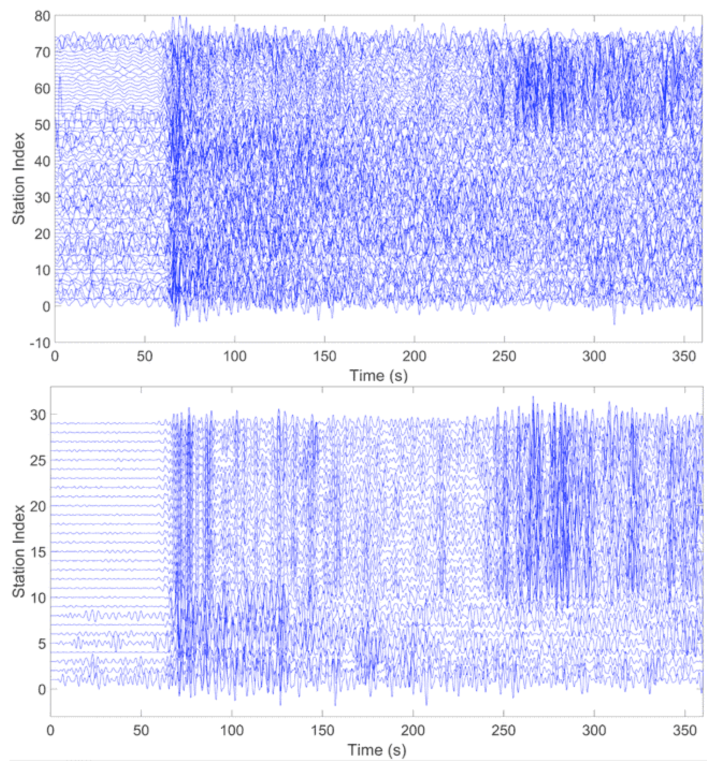

Figure 3. *Seismogram of AU array. a) unfiltered seismogram and b) filetered coherent seismogram.*

Figure 2a demonstrates an unfiltered seismogram (raw data) and Figure 2b describes a filtered coherent seismogram. The filtered coherent seismogram is used as the initial process for imaging rupture processes (Ishii et al., 2007; Meng et al., 2018; Zeng et al., 2019). The smoother and more coherent the filtered seismogram provides better results for rupture imaging. It can be seen that the filtered seismogram of each station in the AU array has the same initial phase and lower noise (compared to unfiltered seismograms), which can reduce the uncertainty of rupture imaging results. Thus, the initial step of MUSIC-BP processing obtained good results and can be used to determine the kinematic rupture process of the Seram earthquake.

The rupture imaging results from the filtered coherent seismogram processed using the MUSIC-BP method can be seen in Figure 4. Processing using the AU array on the Seram earthquake can produce better imaging because almost all stations on the Australian continent work well. AU array distance is relatively closer than other arrays, so it has acceptable seismograms, so the seismogram data set is used as acceptable input for MUSIC-BP.

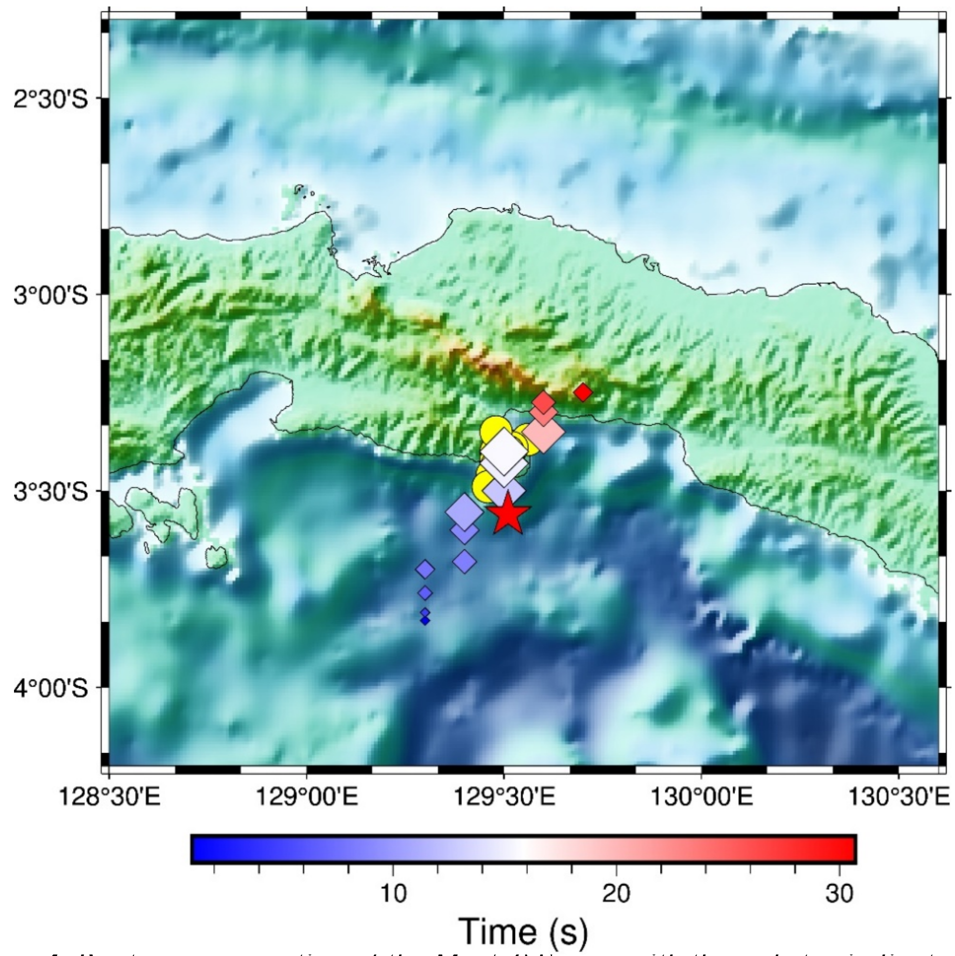

***Figure 4**. Rupture propagation of the Mw 5.9 Seram with the red star indicates the epicenter, the orange circle is the distribution of aftershocks and the gradation coloured diamond demonstrated rupture propagation.*

It is clear that the rupture imaging results for this earthquake (Figure 4) have a bilateral distribution of shear rupture, where the direction of rupture propagation is towards the southwest and northeast (gradation colored diamond). This is confirmed by the presence of aftershocks (orange circle) along the rupture trajectory. The majority of aftershock has a magnitude between 4 and 5 with shallow depth. The well-located aftershocks are associated with the direction of rupture propagation (Yukutake and Iio, 2017) because the presence of aftershocks is caused by changes in coseismic stress in the fault segmentation around the earthquake epicenter [33, 34]. In addition, the direction of rupture propagation can be used to determine active faults in the study area. If the rupture directivity in this study is correlated with the results of the Global CMT focal mechanism solution, then the actual fault plane is indicated to have a strike angle of 245^o. Thus, the activated fault plane of the Mw 5.9 Seram earthquake is NP 1 with a fault plane orientation consisting of strike1 = 245^o, dip1 = 46^o, and rake1 = -50^o with a normal fault type. Note that the orientation parameter of the fault plane at NP 1 shows that the dip parameter has a low angle value. Based on previous research conducted by (Cummins et al., 2020) stated that the characteristics of earthquakes that occur in the Banda Sea area (covering the bottom of Seram Island) have a low dip angle value termed as the Low-Angle Normal Fault (LANF) which can cause a tsunami due to earthquake-triggered slumping. This finding reveals that there is an activated fault in the area under the island of Seram, which often causes earthquakes with shallow depths. This also indicates that this island has a shallow tectonic structure with potential earthquake and tsunami hazards.

Rupture directivity is the result of the rupturing movement of the earthquake source. Rupture movement has a certain speed that is correlated with the energy released from the earthquake source, where the rupture speed and earthquake energy are positively correlated (Noda et al., 2011; Weng and Ampuero, 2020). The previous paragraph only describes the orientation of the rupture propagation of the earthquake but does not explain the rupture's length, duration, speed and energy when it propagates. Here, we plot the relationship between rupture length (spatial parameter) and rupture propagation duration (temporal parameter) with respect to the relative amplitude (Figure 5).

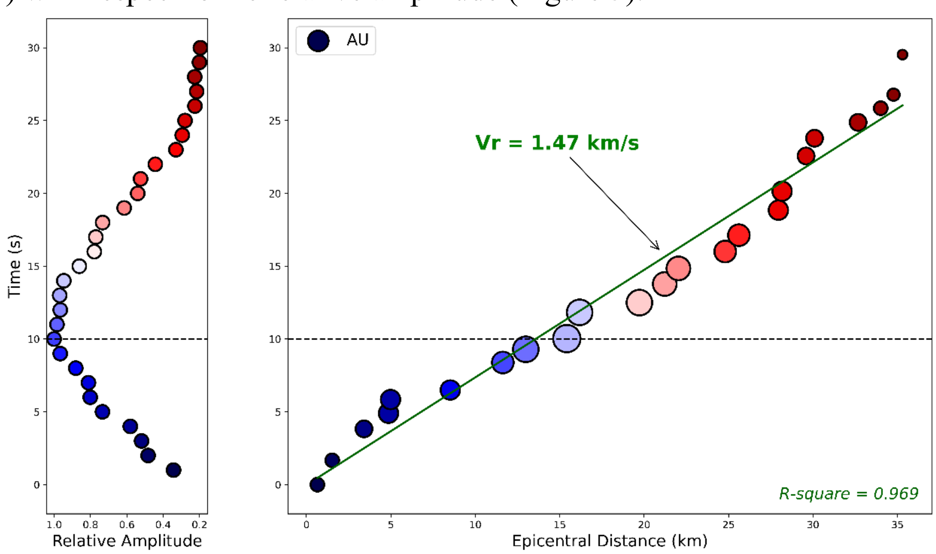

Figure 5. *The spatio-temporal variations of rupture kinematic*

The top panel describes the time-varying normalised amplitude of the bilaterally moving rupture in the southwest and northeast directions. During this time, the peak of seismic energy is released from the earthquake source in the first 15 seconds (black dashed line). This correlates with the visualisation with the bottom panel which describes the largest circle size depicted at 15 seconds with rupture propagating for about 15 km in the northeast direction (See Figure 4). Thus, it can be mentioned that the northeast area of the earthquake epicenter has a higher energy release rate because of the high stress changes and local fault activity (Hutchings and Mooney, 2021). The total rupture length is approximately 70 km from the southwest to the northeast (35 km from the epicenter) with a total duration of about 18 s. A moderate earthquake has lower energy than a large earthquake, so the rupture extent is not too long and has a relatively short duration. Furthermore, the rupture velocity of this earthquake is 1.5 km/s which is obtained from spatiotemporal variations of rupture kinematics through a linear regression approach (Meng et al., 2011; Bao et al., 2019). This result are consistent with previous studies which stated that the rupture velocity for moderate earthquakes was 0.5-0.9 of the shear wave (Seekins and Boatwright, 2010).

The lower region of the Seram earthquake has a complex tectonic setting and there are active minor faults in the region that have not been identified. The kinematic rupture processes in this study indicate that the source mechanism of the earthquake has an SSW-NNE orientation direction and has a low dip angle of the focal mechanism. Based on Cummins et al. (2020) stated that if an earthquake has a low dip angle value, then the earthquake can trigger a tsunami. However, according to Heidarzadeh et al. (2022), using numerical tsunami modeling, the tsunami in this event was not directly caused by this earthquake but by a submarine landslide. Referring to the rupture parameters in this study, the rupture duration and rupture length indicate that this earthquake has no potential to cause a tsunami (Lomax and Michelini, 2011). Even though this earthquake did not directly generate a tsunami, the direction of the tsunami propagation towards the SSW-NNE was in the same direction as the orientation of the earthquake fault. Thus, it can be assumed that the earthquake that occurred could cause a landslide in the sea, so this submarine landslide was the primary source of the tsunami. This finding implies that if an earthquake occurs with a large magnitude, it is possible to cause a massive submarine landslide and also a devastating tsunami in the bottom area of Seram Island. Further work needs to be carried out to understand better the modeling of tsunami mechanisms and the direction of tsunami propagation in the region.

4. CONCLUSIONS

The 2021 Mw 5.9 Seram earthquake occurred along the Banda Arc near Seram Island. We have used the Multiple Signal Classification Back-Projection (MUSIC-BP) method to image the kinematic rupture processes of this earthquake. A High-frequency P-seismic waveform is processed to obtain rupture directivity, rupture duration, rupture length, and rupture speed. The rupture imaging shows that the rupture moves bilaterally to the southwest and northeast with a speed of 2.4 km/s. The total rupture length is ~70 km from southwest to northeast (~35 km from epicenter) and has a total duration of about 18 s. The maximum amplitude energy of this earthquake released is estimated to be ~15 km from the epicenter. The observed main path of the rupture propagation is consistent with the position of the aftershock location distribution data. Based on the result of the rupture kinematics parameter, the tsunami was not caused directly by the earthquake. However, the direction of tsunami propagation is the same as that of earthquake rupture propagation. Thus, it can be assumed that the earthquake could cause a landslide in the sea, so this submarine landslide was the primary source of the tsunami. Furthermore, this study has revealed that the tectonic setting at the bottom of Seram Island has an SSW-NNE fault orientation

ACKNOWLEDGEMENTS

We thank Incorporated Research Institutions for Seismology (IRIS) for providing freely teleseismic earthquake seismogram data at https://ds.iris.edu/wilber3/find_event and the United States Geological Survey (USGS) for providing distribution aftershocks data accessed at https://earthquake.usgs.gov/earthquakes/search. We also thank Global Centroid-Moment-Tensor (GCMT) for information on earthquake focal mechanism data.

REFERENCES

Bao, H. et al. (2019). Early and persistent super shear rupture of the 2018 magnitude 7.5 Palu earthquake. *Nat. Geosci.*, vol. 12, pp. 200–205. https://doi.org/10.1038/s41561-018-0297-z

Cummins, P. R., Pranantyo, I. R., Pownall, J. M., Griffin, J. D., Meilano, I., & Zhao, S. (2020). Earthquakes and tsunamis caused by low-angle normal faulting in the Banda Sea, Indonesia. *Nat. Geosci.*, vol. 13, pp. 312–318. https://doi.org/10.1038/s41561-020-0545-x

Douglas, A. (1997). Bandpass filtering to reduce noise on seismograms: Is there a better way?. *Bull. Seismol. Soc. Am.*, vol. 87, no. 3, pp. 770–777. https://doi.org/10.1785/BSSA0870030770

Ekström, G., Nettles, M., & Dziewoński, A. M. (2012). The global CMT project 2004–2010: centroid-moment tensors for 13,017 earthquakes. *Phys. Earth Planet. Inter.*, vol. 200, pp. 1–9. https://doi.org/10.1016/j.pepi.2012.04.002

Fan, W & Shearer, P. M. (2015). Detailed rupture imaging of the 25 April 2015 Nepal earthquake using teleseismic *P* waves. *Geophys. Res. Lett.*, vol. 42, no. 144, pp. 5744–5752. https://doi.org/10.1002/2015GL064587

Global CMT, https://www.globalcmt.org/, acessed online on 2022.

Goldstein, P. & Archuleta, R. J. (1987). Array analysis of seismic signals. *Geophys. Res. Lett.*, vol. 14, no. 1, pp. 13–16. https://doi.org/10.1029/GL014i001p00013

Hamilton, W. B. (1979). *Tectonic of Indonesia Region, Geological Survey Professional Paper,* United States Government Printing Office. https://doi.org/10.3133/pp1078

Heidarzadeh, M., Gusman, A. R., Patria, A., & Widyantoro, B. T. (2022). Potential Landslide Origin of the Seram Island Tsunami in Eastern Indonesia on 16 June 2021 Following an Mw 5.9 Earthquake. *Bull. Seismol. Soc. Am.*, vol. 112 no. 5, pp. 2487–2498. https://doi.org/10.1785/0120210274

Hutchings, S. J. & Mooney, W. D. (2021). The Seismicity of Indonesia and Tectonic Implications. *Geochemistry, Geophys. Geosystems*, vol. 22, no. 9. https://doi.org/10.1029/2021GC009812

Irsyam, M. et al. (2020). Development of the 2017 national seismic hazard maps of Indonesia. *Earthq. Spectra*, vol. 36, no. S1, pp. 112–136. https://doi.org/10.1177%2F8755293020951206

Ishii, M., Shearer, P. M., Houston, H., & Vidale, J. E. (2005). Extent, duration and speed of the 2004 Sumatra-Andaman earthquake imaged by the Hi-Net array. *Nature*, vol. 435, pp. 933–936. https://doi.org/10.1038/nature03675

Ishii, M., Shearer, P. M., Houston, H., & Vidale, J. E. (2007). Teleseismic P wave imaging of the 26 December 2004 Sumatra–Andaman and 28 March 2005 Sumatra earthquake ruptures using the Hi-net array. *J. Geophys. Res., Solid Earth*, vol. 112, no. B11307. https://doi.org/10.1029/2006JB004700

Jian, P. R. (2021). The 2010 Jiashian and 2016 Meinong Earthquakes: Doublet Ruptures Interact Across Two Strong Asperities. In: AutoBATS and 3D MUSIC: New Approaches to Imaging Earthquake Rupture Behaviors. *Springer Theses*, Springer, Singapore. https://doi.org/10.1007/978-981-16-5584-5_5

Kehoe, H. L. & Kiser, E. D. (2020). Evidence of a supershear transition across a fault stepover. *Geophys. Res. Lett.*, vol. 47, no. 10. https://doi.org/10.1029/2020GL087400

Kennett, B. L. N. & Engdahl, E. R. (1991). Traveltimes for global earthquake location and phase identification. *Geophys J Int.*, vol. 105, no. 2, pp. 429–465. https://doi.org/10.1111/j.1365-246X.1991.tb06724.x

Kiser, E. D. & Kehoe, H. L. (2021). The hazard of coseismic gaps: the 2021 Fukushima earthquake," *Geophys J Int.*, vol. 227, no. 1, pp. 54–57. https://doi.org/10.1093/gji/ggab208

Kiser, E., Ishii, M., Langmuir, C. H., Shearer, P. M., & Hirose, H. (2011). Insights into the mechanism of intermediate-depth earthquakes from source properties as imaged by back projection of multiple seismic phases. *J. geophys. Res*., vol. 116, no. B06310. https://doi.org/10.1029/2010JB007831

Krüger., F. & Ohrnberger, M. (2005). Tracking the rupture of the Mw = 9.3 Sumatra earthquake over 1,150 km at teleseismic distance. *Nature*, vol. 435, pp. 937–939. https://doi.org/10.1038/nature03696

Liu, Z., Song, C., Meng, L., Ge, Z., Huang, Q., & Wu, Q. (2017). Utilizing a 3D global P-wave tomography model to improve backprojection imaging: a case study of the 2015 Nepal earthquake. *Bull. Seismol. Soc. Am.*, vol. 107, no. 5, pp. 2459–24667. https://doi.org/10.1785/0120170091

Lomax, A. & Michelini, A. (2011). Tsunami early warning using earthquake rupture duration and *P*-wave dominant period: the importance of length and depth of faulting. *Geophys. J. Int.*, vol. 185 no. 1, pp. 283–291. https://doi.org/10.1111/j.1365-246X.2010.04916.x

Madlazim, Fahmi, M. N., Realita, A., & Sari, D. P. (2021). Rupture Imaging For The 30 October Tsunamigenic Earthquake In The Eastern Aegean Sea. Science of Tsunami. *Sci. Tsu. Hazard.*, vol. 40, no. 4, pp. 228–237. http://www.tsunamisociety.org/STHVol40N4Y2021.pdf

Meng , L., Bao, H., Huang, H., Zhang, A., Bloore, A., & Liu, Z. (2018). Double pincer movement: Encircling rupture splitting during the 2015 Mw 8.3 Illapel earthquake. *Earth Planet Sci Lett.*, vol. 495, pp. 164–173. https://doi.org/10.1016/j.epsl.2018.04.057

Meng, H., McGuire, J. J., & Ben-Zion, Y. (2020). Semiautomated Estimates of Directivity and Related Source Properties of Small to Moderate Southern California Earthquakes Using Second Seismic Moments. *J. Geophys. Res., Solid Earth*, vol. 125, no. 4. https://doi.org/10.1029/2019JB018566

Meng, L., Ampuero, J-P., Sladen, A., & Rendon, H. (2012). High-resolution backprojection at regional distance: application to the Haiti M7.0 earthquake and comparisons with finite source studies. *J. Geophys. Res., Solid Earth*, vol. 117, no. B4. https://doi.org/10.1029/2011JB008702

Meng, L., Inbal, A., & Ampuero, J-P. (2011). A window into the complexity of the dynamic rupture of the 2011 *Mw* 9 Tohoku‐Oki earthquake. *Geophys. Res. Lett*., vol. 38, no. 7. https://doi.org/10.1029/2011GL048118

Meng, L., Zhang, A., & Yagi, Y. (2016). Improving back-projection imaging with a novel physics-based aftershock calibration approach: a case study of the 2015 Gorkha earthquake. *Geophys. Res. Lett.*, vol. 43, no. 2, pp. 628–636. https://doi.org/10.1002/2015GL067034

Neo, J. C., Huang, Y., Yao, D., & Wei, S. (2021). Is the Aftershock Zone Area a Good Proxy for the Mainshock Rupture Area?. *Bull. Seismol. Soc. Am.*, vol. 111, no. 1, pp. 424–438. https://doi.org/10.1785/0120190200

Noda, H., Lapusta, N., & Kanamori, H. (2011). Relation between energy radiation ratio and rupture speed in numerically simulated earthquakes. *AGU Fall Meeting*. https://ui.adsabs.harvard.edu/abs/2011AGUFM.S54C..03N/abstract

Rost, S. & Thomas, C. (2002). Array seismology: Methods and applications,. *Rev. Geophys.*, vol. 40, no. 3. https://doi.org/10.1029/2000RG000100

Schmidt, R. (1986). Multiple emitter location and signal parameter estimation. *IEEE Trans. Antennas Propag.*, vol. 34, no. 3, pp. 276–280. http://dx.doi.org/10.1109/TAP.1986.1143830

Seekins, L. C. & Boatwright, J. (2010). Rupture directivity of moderate earthquakes in northern California. *Bull. Seismol. Soc. Am.*, vol. 100 no. 3, pp. 1107–1119. https://doi.org/10.1785/0120090161

Segou, M. & Parsons, T. A new technique to calculate earthquake stress transfer and to probe the physics of aftershocks. (2020). *Bull. Seismol. Soc. Am.*, vol. 110, no. 2, pp. 863–873. https://doi.org/10.1785/0120190033

Spakman, W. & Hall, R. (2010). Surface deformation and slab–mantle interaction during Banda arc subduction rollback. *Nature Geosci.*, vol. 3, no. 8, pp. 562–566. https://doi.org/10.1038/ngeo917

Sultan, M. et al. (2022). Imaging of rupture process of 2005 Mw 7.6 Kashmir earthquake using back projection techniques. *Arab J Geosci.*, vol. 15, no. 871. https://doi.org/10.1007/s12517-022-10095-5

Wang, D., Chen, Y., Wang, Qi., & Mori, J. (2018). Complex rupture of the 13 November 2016 M w 7.8 Kaikoura, New Zealand earthquake: Comparison of high-frequency and low-frequency observations. *Tectonophysics*, vol. 733, pp. 100–107. https://doi.org/10.1016/j.tecto.2018.02.004

Weng, H., & Ampuero, J-P. (2020). Continuum of earthquake rupture speeds enabled by oblique slip. *Nat. Geosci.*, vol. 13, pp. 817–821. https://doi.org/10.1038/s41561-020-00654-4

Xie, Y & Meng, L. (2020). A multi-array back-projection approach for tsunami warning. *Geophys. Res. Lett.*, vol. 47, no. 14. https://doi.org/10.1029/2019GL085763

Yao, H., Shearer, P. M., & Gersoft, P. (2012). Subevent location and rupture imaging using iterative back projection for the 2011 Tohoku M_w 9.0 earthquake," *Geophys J Int.*, vol. 190, no. 2, pp. 1152–1168. https://doi.org/10.1111/j.1365-246X.2012.05541.x

Yukutake, Y. & Iio, Y. (2017). Why do aftershocks occur? Relationship between mainshock rupture and aftershock sequence based on highly resolved hypocenter and focal mechanism distributions. *Earth, Planets Space,* vol. 69, no. 68. https://doi.org/10.1186/s40623-017-0650-2

Zeng, H., Wei, S., & Wu, W. (2019). Sources of uncertainties and artefacts in back-projection results. *Geophys J Int.*, vol. 220, no. 2, pp. 876–1891. https://doi.org/10.1093/gji/ggz482

ISSN 8755-6839

SCIENCE OF TSUNAMI HAZARDS

Journal of Tsunami Society International

Volume 41 Number 4 2022

ESTIMATES OF WAVE HEIGHTS ON THE COAST OF CHILE FROM A TSUNAMI GENERATED BY AN EARTHQUAKE July 8, 1730

R.Kh. Mazova[1], A.A Kurkin[1]., N.A Baranova[2], I.A. Smirnov[1]

[1] Nizhny Novgorod State Technical University n.a. R.E. Alekseev, 24, Minin str., 603095 Nizhny Novgorod, Russia. e-mail address: raissamazova@yandex.ru
[2]Auriga, 6/6 Nartova st., office 829, 603104 Nizhny Novgorod, Russia.
e-mail address: Natalia.baranova@inbox.ru

ABSTRACT

The historical earthquake and tsunami occurred almost 300 years ago on July 8, 1730 in the region of Valparaiso, Chile is studied. The earthquake and tsunami of 1730 were considered to be the largest occurred in Chile since the beginning of recorded history. The earthquake destroyed buildings along more than 1000 km coastline and generated a large tsunami. Estimates of the magnitude of the earthquake lie in the range of $M \sim 9$–9.3. The data given in historical documents on the tsunami, caused by this catastrophic earthquake, supports and documents the strong destruction on the Chilean coast, especially in the coastal cities of Concepcion and Valparaiso, where waves, according to historical records on the coasts, reached 9m and 11m, respectively. The parameters of the earthquake source are poorly understood, but, according to estimates from various sources, the earthquake source was about 600-1000 km long along the Chilean coast. In the work, more than 15 scenarios for numerical simulation of the generation and propagation of tsunami waves up to a 5-meter isobath is carried out, depending on the magnitude of the earthquake and, accordingly, on the size of the earthquake source. The numerical simulation was performed within the keyboard model of the earthquake source; the number of blocks in the computations corresponds to the number of faults in the earthquake source and varied from 2 to 12.

Keywords: *tsunamigenic catastrophic earthquakes, tsunami waves, numerical simulation, Chilean coast.*

1. INTRODUCTION

The earthquake of July 8, 1730 with a magnitude close to $M \sim 9$ has an ambiguous treatment, because in various documents describing the event almost 300 years ago, the earthquake and the tsunami that followed it are described in different ways. In this paper, the authors tried to bring a lot of disparate facts to a logical uniformity and propose a model of a possible seismic source that generates tsunami waves corresponding to the few data recorded in historical documents.

In works [1-10] it is shown that the most affected area is located between the cities of La Serena and Santo Domingo. An earthquake in 1730 with a magnitude close to $M = 9$ (some estimates 9.1–9.3) affected a large region stretching over 900 km from Copiapo in the north to Concepción in the south, causing strong destructions in the capital Santiago. It was followed by a strong tsunami that particularly affected the two coastal towns of Valparaiso and Concepción.

However, historical analysis (see, e.g., [1,2]) has suggested the extraordinary idea of two main seismic events and, as a consequence, three separately generated tsunamis of significantly different intensity. Historical records demonstrate three strong earthquake shocks with an interval of approximately 4 and 7 hours. The first shock occurred at 1.30 am, the second main shock between 3 and 5 am, and the third event between 12 and 1 pm. According to the descriptions, the center of Ilhapel at about 1.30 AM the city was attacked by four or five large tsunami waves, of which the third was the largest. The city of Concepción was also hit by 4 or 5 large tsunami waves, of which the second was the largest. The tsunami took about an hour to fill the city with water before it finally receded. Apparently, the tsunami began with the rundown of water from the coast, because on the night of the earthquake, the fishermen noticed that the water was receding from the bay [1-5]. In the city of Valparaiso, a wall of water has formed 3.5 meters above the usual high tide level.

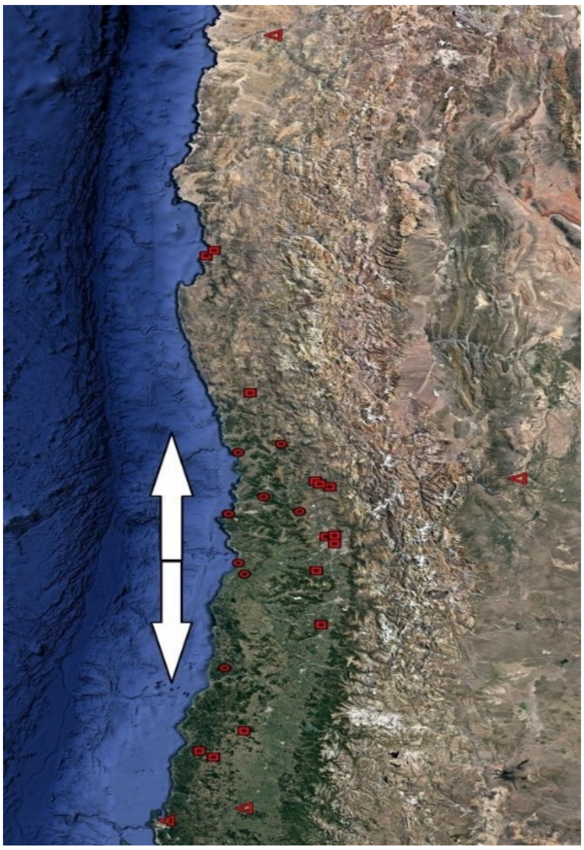

Figure 1. Damage zones of the 1730 earthquake [2].

Available damage reports and eyewitness accounts support that a tsunami on July 8th 1730 caused extensive destructions in the ports of La Serena, Valparaiso and Concepción. The reports describe that tsunami waves damaged coastal areas of the cities of Concepción and Valparaiso at relatively the same time. Also it was also reported that they caused destructions of agricultural land on the coast of Colchagua. Waves have also been seen in Callao in Peru and along the coast of Japan [2-10]. In works [1,2], some generalization of information from sources [3-10] is given, according to which it can be assumed that the picture of the earthquake and the subsequent tsunami looked as follows [1,2]:

- The first shock: occurred between 1 and 2 o'clock in the morning on July 8, 1730. It was prolonged, but not strong throughout the territory.
- The second shock: occurred between 3 and 5 o'clock in the morning on July 8, 1730. I was the most significant in strength and causing strong destructions of buildings. The main force of the second earthquake fell on the area of modern San Antonio, south of Valparaiso, in Concepción and Santiago, the intensity was much lower, but compared to Concepción, the intensity in Santiago was higher. This shock in Santiago caused a tsunami that propagates from Santiago north towards La Serena and Callao and south to Concepción.
- The third shock: occurred between 12 and 13 o'clock in the afternoon on July 8, 1730. Some sources attribute it to aftershocks that lasted a month after the event, 5 or 6 of which were significant. The third shock likely occurred north of Valparaiso and closer to La Serena, which explains both the damage from the earthquake in the area and the reduced intensity in Concepción. Figure 1 shows a map of the intensity of the earthquake with the zones of the greatest damage to coastal structures from the earthquake.

2. STATEMENT OF THE PROBLEM

The appearance of catastrophic tsunamis can be caused by a complex mechanism of movements in the earthquake source. Usually, for numerical simulation of a tsunami generation, seismic data are used to determine the displacement of the bottom in the earthquake source [11]. The keyboard model of the earthquake source is used in the work, which makes it possible to simulate the complex distribution of wave heights along the coast, obtained during a particular earthquake [12, 13].

Preliminary estimates in this work were made when considering 6 scenarios of the generation of the earthquake source in 1730 by analogy with [2]. The earthquake sources were chosen according to the historical description of the processes in the zones of active faults in the Earth's crust for this earthquake. These scenarios of possible earthquakes were considered, with different kinematics of key blocks into which the seismic source was divided. The magnitudes of the considered earthquakes are: $M = 8.7$ for the first scenario, $M = 8.8$ for the second, $M = 9.0$ for the third, $M = 9.1$ for the fourth, $M = 9.2$ for the fifth, and $M = 9.3$ for the sixth ones. The kinematics of key blocks in the earthquake source was determined by a few data on the manifestations of tsunami waves on the coast during this earthquake, given in [1-10].

To determine the approximate sizes of sources for 6 scenarios, to calculate the length and width of the rupture of the Earth's crust for a given earthquake, Wells formulas were used [14]. The displacement of the wave surface above the seismic source during the formation of the tsunami source was estimated using the Iida formula [15]. Table 1 shows data on the length and width of the rupture of the Earth's crust for the earthquake magnitudes considered in this paper.

Figure 2 shows a map of the computation water area with the points along the coast that were most affected by the tsunami generated by the earthquake considered.

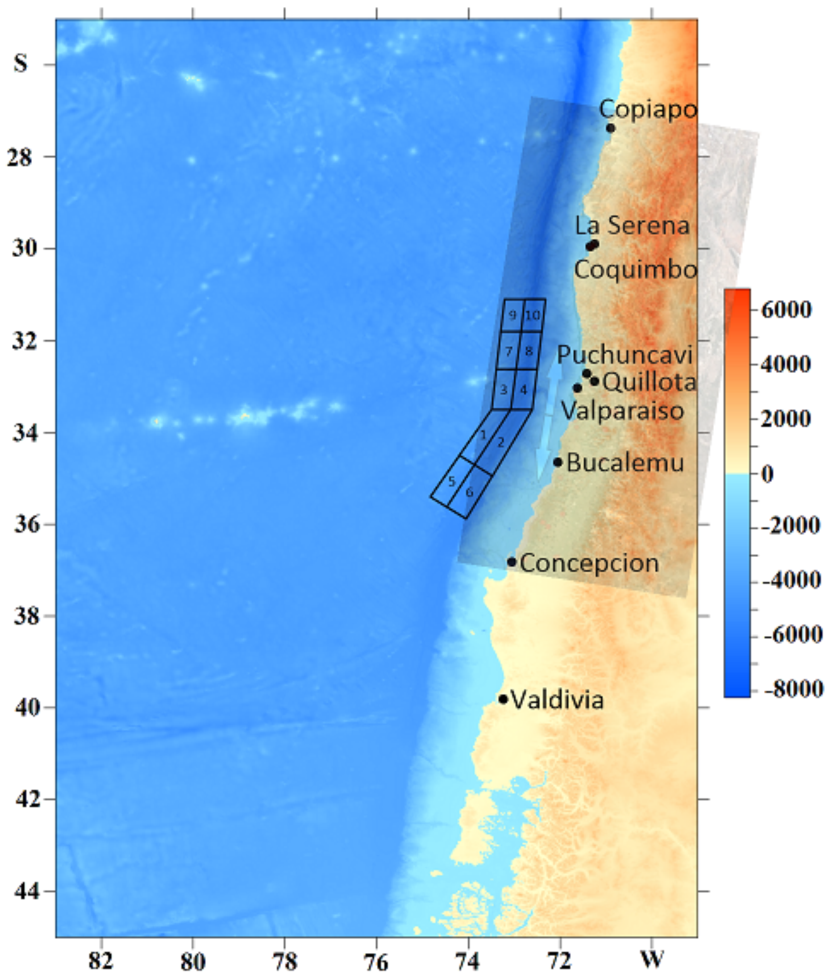

Figure 2. Scheme of the computation water area; blue arrow and dark square indicate zones of the highest intensity of the earthquake and tsunami [1,2]; the dark line marks the contour of the approximate localization of the seismic source taken as the base one in the computations

Table 1. Approximate dimensions of the source and displacement of the wave surface above the source

№ Scenario	Magnitude, M	Rupture length, L, km	Rupture width, W, km	Shift of wave surface, H, m
1	8.7	450	60	10-15
2	8.8	500	65	12-16
3	9.0	650	75	12-20
4	9.1	700	85	15-20
5	9.2	800	90	18-22
6	9.3	850	100	20-25

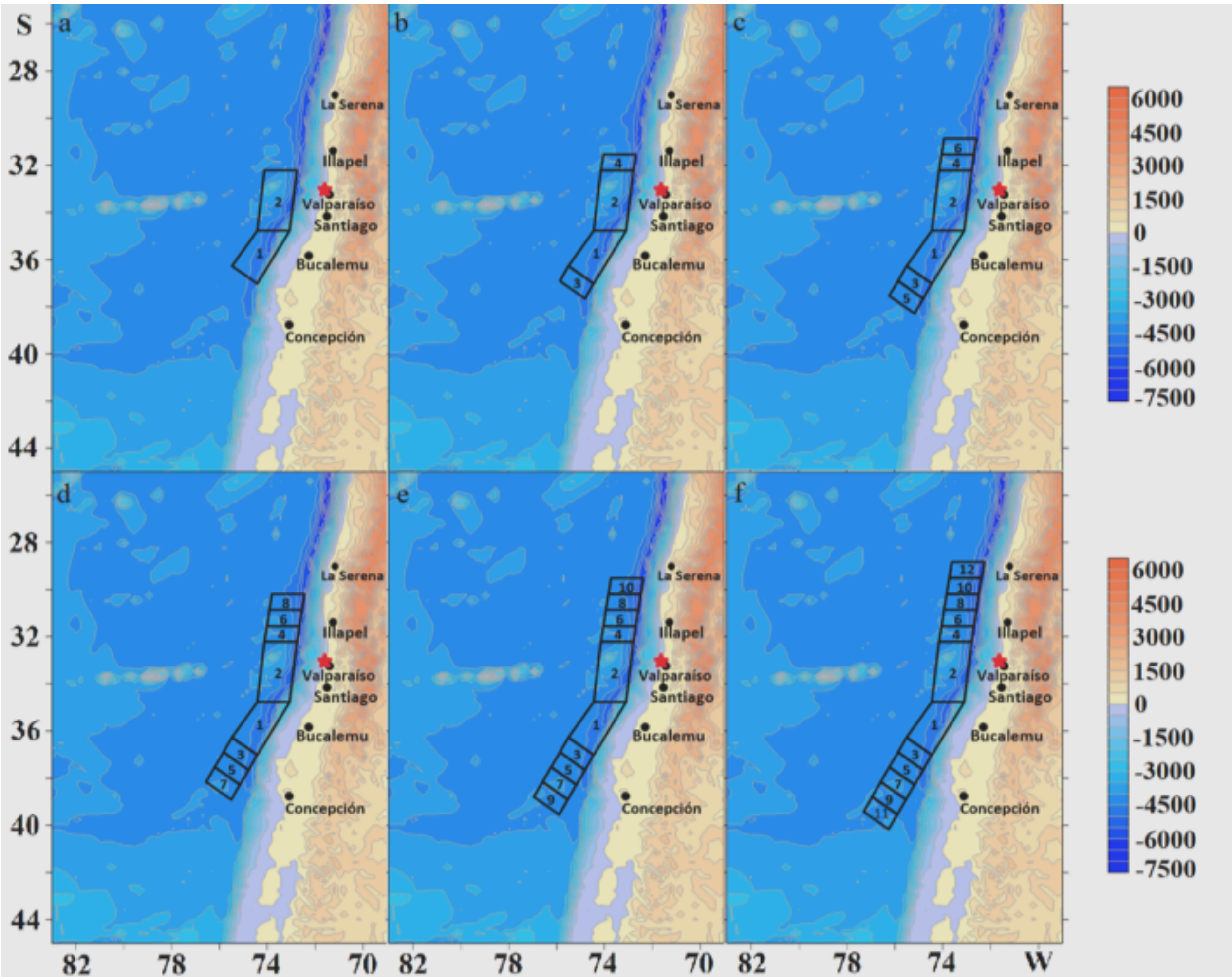

Figure 3. Schematic representation of the source of the earthquake of 1730: a) two-block source; b) four-block source; c) six-block source; d) eight-block source; e) ten-block source; f) twelve-block source

3. NUMERICAL SIMULATION

To describe the modeling of tsunami generation and propagation, a system of nonlinear shallow water equations is used [15,16]. Numerical simulation was carried out using a modified software package built on the basis of a scheme with high algorithmic universality proposed in [12, 13] and built on the basis of the Sielecki-Wurtele scheme [17]. For numerical modeling, the water area of the Pacific Ocean along the coast of Chile from 25° to 45° S and 79°-81° W was considered. For numerical simulations in the Pacific Ocean, a bathymetric map with a half-minute (~ 1.0 km) isobaths section was used.

To simulate the generation of the tsunami source, various displacements of blocks in the earthquake source are considered (see Tables 2-7), which presents the kinematics of the key blocks in the earthquake sources for Scenarios 1-6.

Table 2. The key block kinematics in the earthquake source (Scenario 1)

Block number	1		2	
Height (m)	-6	9	-5	10
Motion start time (sec)	60	90	0	30
Motion end time (sec)	90	120	30	60

Table 3. The key block kinematics in the earthquake source (Scenario 2)

Block number	1		2		3	4
Height (m)	-6	16	-7	15	10	-5
Motion start time (sec)	100	130	40	70	160	0
Motion end time (sec)	130	160	70	100	180	40

Table 4. The key block kinematics in the earthquake source (Scenario 3)

Block number	1		2		3	4	5	6
Height (m)	-6	7	-7	5	5	9	3	5
Motion start time (sec)	100	130	40	70	160	0	180	200
Motion end time (sec)	130	160	70	100	180	40	200	220

Table 5. The key block kinematics in the earthquake source (Scenario 4)

Block number	1		2		3	4	5	6	7	8
Height (m)	-6	7	-7	5	5	9	3	7	4	5
Motion start time (sec)	100	130	40	70	160	0	180	200	220	240
Motion finish time (sec)	130	160	70	100	180	40	200	220	240	260

Table 6. The key block kinematics in the earthquake source (Scenario 5)

Block number	1		2		3	4	5	6	7	8	9	10
Height (m)	-6	7	-7	15	5	9	3	7	4	5	-3	-2
Motion start time (sec)	100	130	40	70	160	0	180	200	220	240	260	280
Motion end time (sec)	130	160	70	100	180	40	200	220	240	260	280	300

Table 7. The key blocks kinematics in the earthquake source (Scenario 6)

Block number	1		2		3	4	5	6	7	8	9	10	11	12
Height (m)	-6	5	-7	10	5	10	3	7	4	5	-3	-2	7	3
Motion start time (sec)	100	130	40	70	160	0	180	200	220	240	260	280	300	320
Motion end time (sec)	130	160	70	100	180	40	200	220	240	260	280	300	320	340

When blocks move in the earthquake source, a tsunami source begins to form on the water surface above the seismic source. There is a displacement of the wave surface and the formation of a wave front, which begins to propagate both to the Chilean coast and to the open water of the Pacific Ocean.

Since the longest block displacement time in the earthquake source, 340 s, falls on the 12-block source (Scenario 6), the formation of the tsunami source takes the same time. The paper considers the propagation of the wave front up to a 5-meter isobath, where the condition of total reflection is set. Figure 4 shows 2D histograms of the distribution of maximum tsunami wave heights on the 5-m isobath along the central part of the Chilean coast.

2-block earthquake source

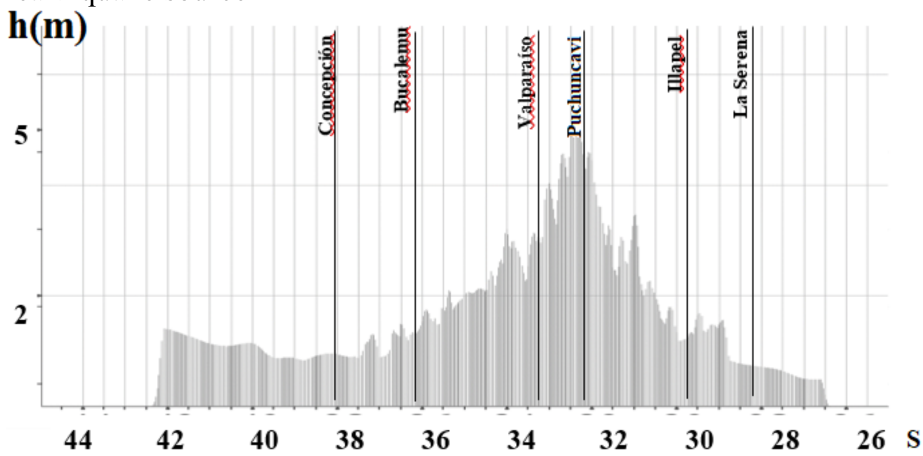

4-block earthquake source

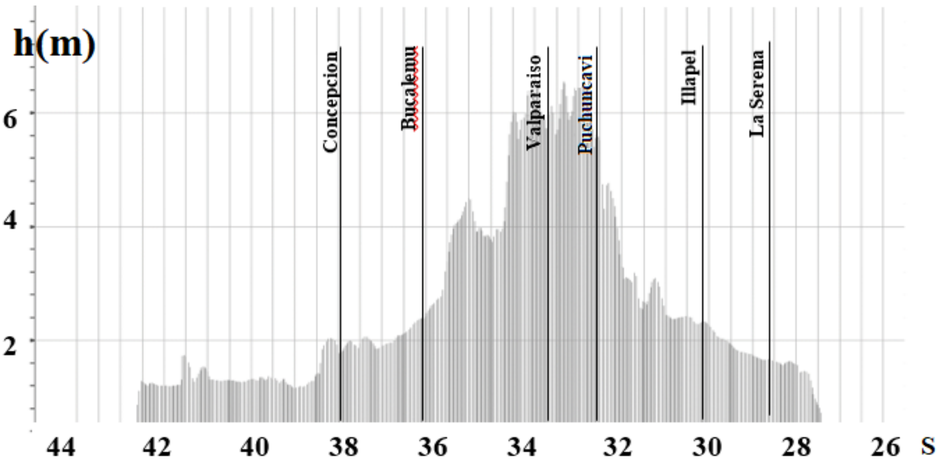

6-block earthquake source

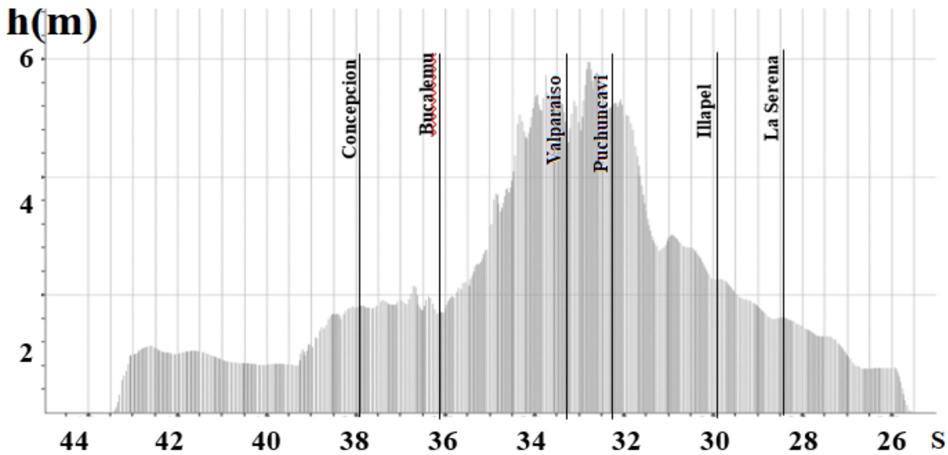

8-block earthquake source

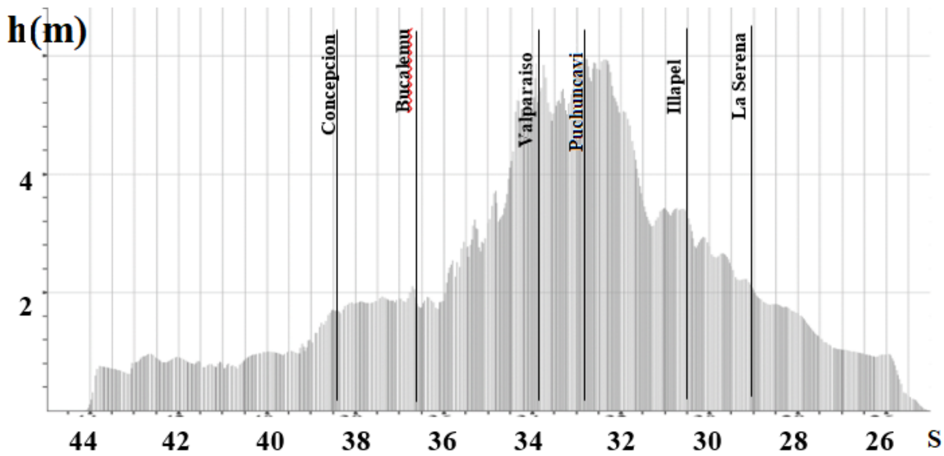

10-block earthquake source

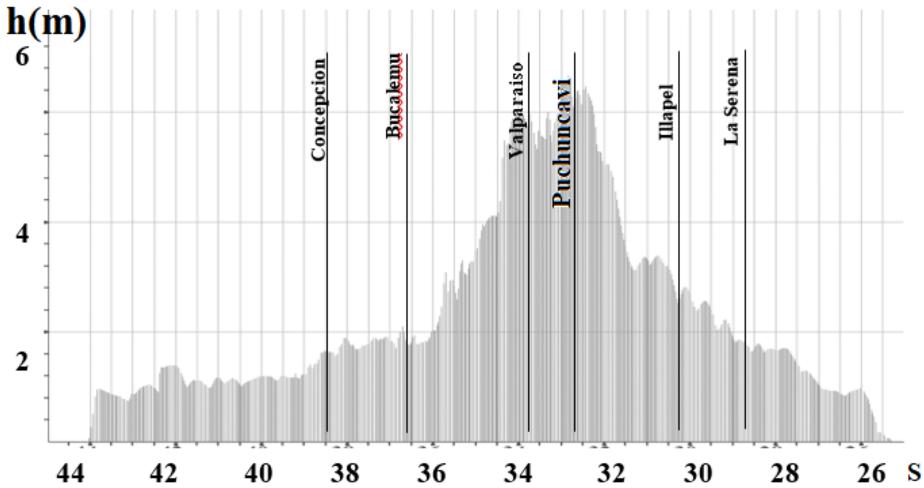

12-block earthquake source

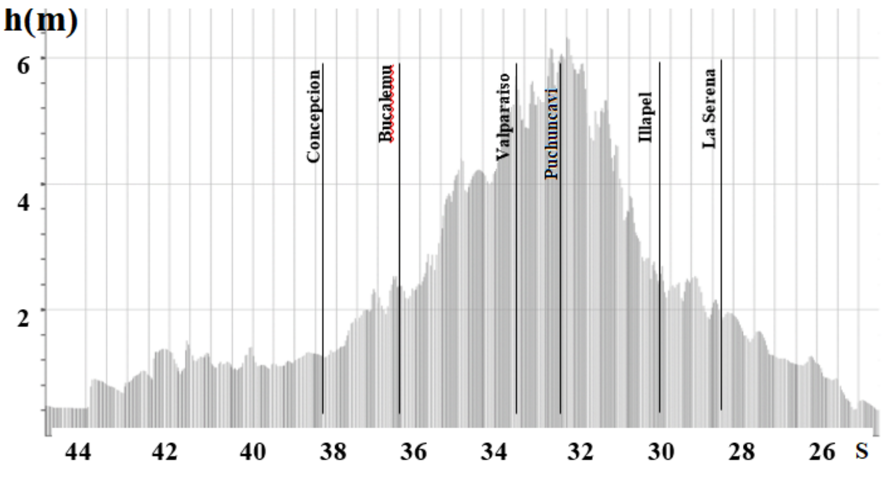

Figure 4. 2D histograms of the maximum wave height distribution along the coast of Chile.

The figures clearly show that the largest wave heights occur in the region of the city of Valparaiso and reach 5 meters. However, according to historical descriptions, there were also large wave heights in the cities of Concepcion and Coquimbo. Based on the estimated results of computations, the following Table of maximum wave heights distribution for a given event can be compile

Table 8. The results of numerical simulation

Wave heights in points on the Chilean coast (m)						
Scenario	**La-Serena**	**Illiapel**	**Valparaiso**	**Puchuncavi**	**Bucalemu**	**Concepcion**
1	1	1,5	5	3	1,7	1,5
2	1,8	2,4	6,2	6	2,2	2
3	1,8	2,4	6	5,8	2	1,8
4	2	3,2	6	6	2	1,8
5	1,8	2,4	6,4	6	2	1,6
6	2	2,4	6,4	5,6	2,4	2

Analyzing the obtained results, it can be noted that the maximum wave height distribution in this setting does not reflect well enough the few historical evidence given in [1-10]. However, the computation details show that the eight-block variant is the most adequate. Based on this scenario, the seismic source was modified by increasing the number of partitions and changing the shape of the source. Figure 5 shows a modified seismic source, for which further studies will be carried out.

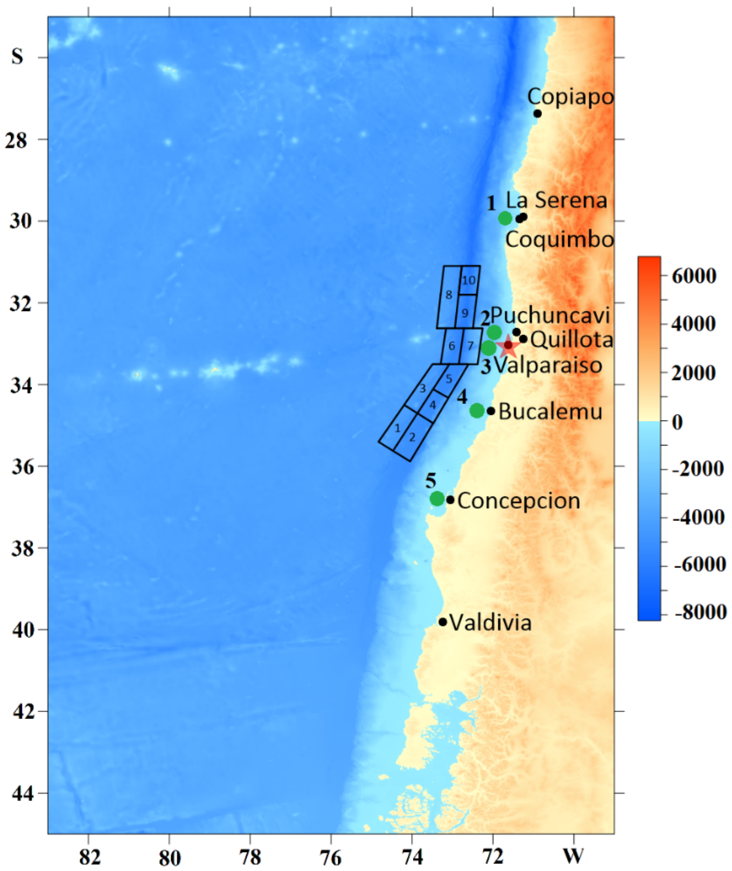

Figure 5. Schematic representation of the seismic source for the 1730 earthquake.

In further scenarios, the kinematics of blocks in the earthquake source is also significantly more complicated. The paper presents a scenario that most closely describes the nature of the manifestation of tsunami waves on the Chilean coast. The Table 9 gives the kinematics of the blocks in the source. The movement starts from block 7 (located close to the earthquake epicenter) for 3 minutes, then, simultaneously with the movements of these blocks, blocks 3-4-5 begin to move south from the epicenter. Blocks 2,5,7,9 and 10 move twice, moving up or down, according to Table 9.

Table 9. Key block kinematics in the earthquake source for Scenario 7

Block number	1	2	3	4	5	6	7	8	9	10
Distance (m)	4	- 4	6	- 5	-6	7	-4	5	-3	5
Start time of first movement (sec)	275	215	155	185	155	60	0	185	90	105
End time of first movement (sec)	305	275	185	215	185	90	60	215	120	155
Distance (m)		6			4		5		-5	4
Start time of second movement (sec)		305			185		305		335	365
End time of second movement (sec)		335			215		335		365	400

Figure 6 shows the generation of the tsunami source when the key blocks move in the earthquake source during the implementation of given scenario (Scenario 7). It is clearly seen that a surface source (tsunami source) is formed in 400 s, and the displacement of the wave surface is clearly visible when moving at the bottom of the corresponding block.

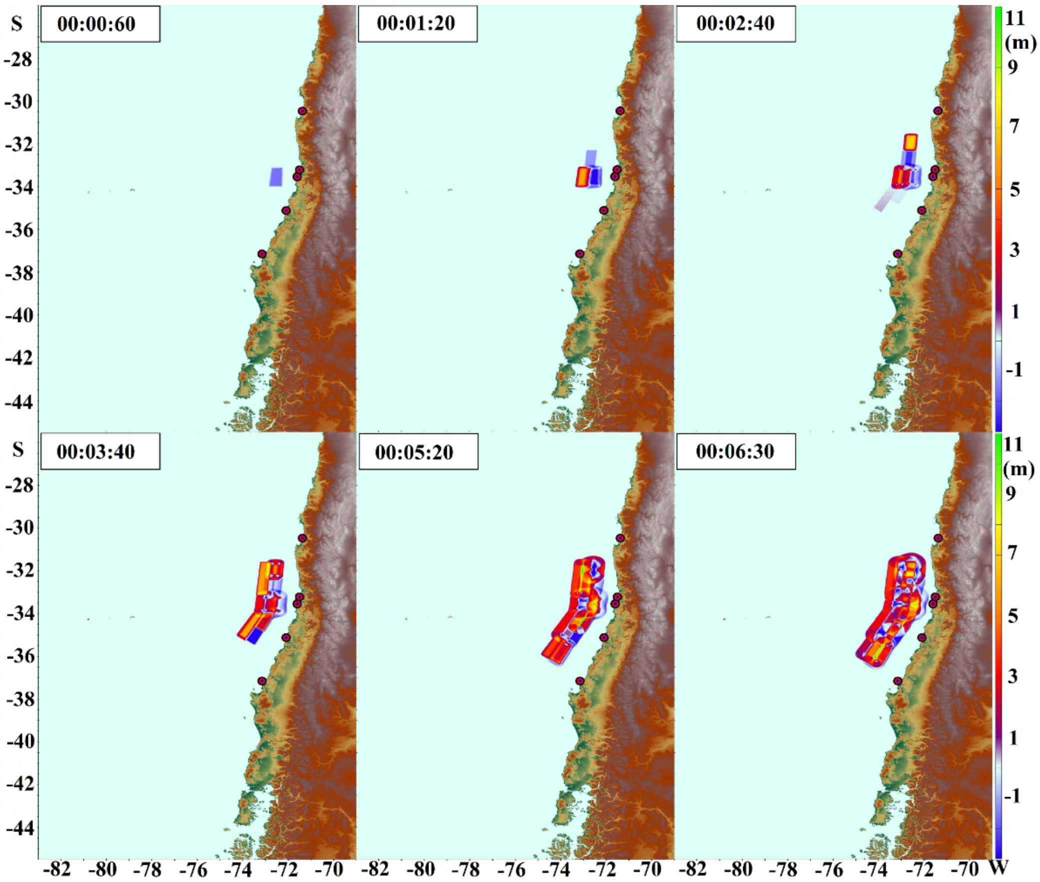

Figure 6. Generation of a tsunami source for 6 time moments during the implementation of a seismic process in an earthquake source (Scenario 7)

Figure 7 shows 6 time moments of the propagation of tsunami waves over the computed water area. It is clearly seen those moments when the wave reaches the corresponding tide gauge. Since the tide gauges are set on a 5-meter isobath, the data shown in Fig. 8 reflect precisely those heights with which the wave approaches a particular point.

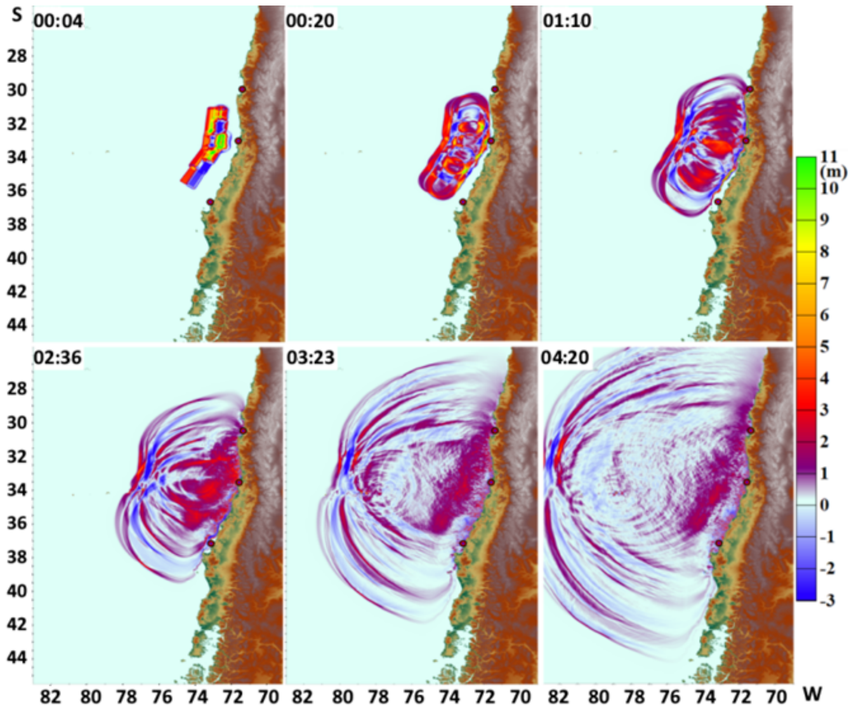

Figure 7. Propagation of tsunami waves over the computation water area (Scenario 7)

A more detailed analysis can be done by analyzing the records from the virtual tide gauge shown in Fig.8.

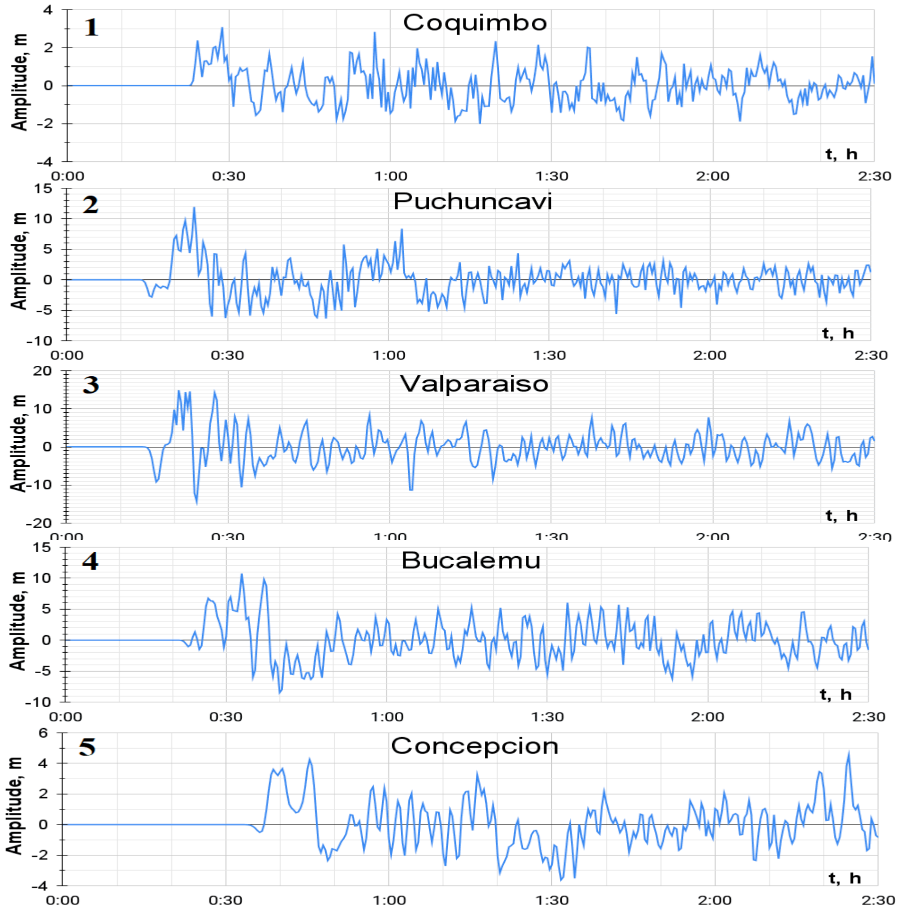

Figure 8. Records from virtual tide gauges for points Coquimbo, Puchuncavi, Valparaiso, Buqcalemu, Concepcion (Scenario 7).

It is clearly seen that in the points located opposite the epicenter of the earthquake, the heights of the waves are quite large: 11-15m. And in the points located to the southwest and northwest of the epicenter, the wave heights are not more than 4m. It should be noted that in almost every point the first wave was not the largest, and the second wave is the largest. The third wave is again smaller in height than the second. Given the description in historical documents, in cities affected by the tsunami, the second wave posed the greatest danger.

According to the 2D histogram of maximum wave heights along the coast in the computation area, shown in Fig. 9, one can see that the largest wave heights are localized opposite the earthquake epicenter, decreasing in height to the northwest and southwest to the cities of Coquimbo and Concepcion.

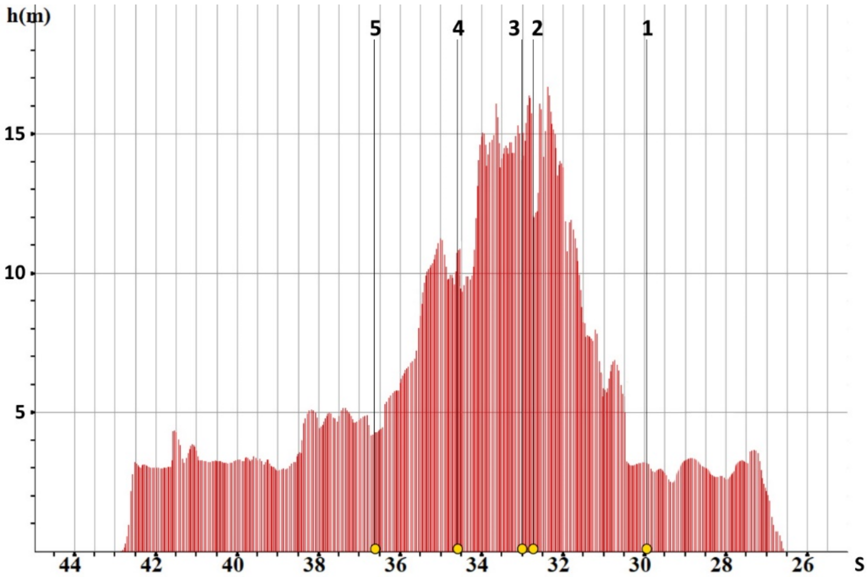

Figure 9. 2D histogram of maximum wave height distribution along the 5 m isobath (Scenario 7). The numbers 1-5 indicate the numbers of virtual tide gauges (Fig. 5).

CONCLUSION

The paper considers a historical event: an earthquake and tsunami on July 08, 1730 with a source located off the western coast of Chile near the city of Valparaiso coast and even, essentially different assumptions about seismic tremors. According to the results of historical data, some authors put forward various hypotheses about the number of earthquakes that occurred in a day from July 8 to July 9, 1730. Also, various works provide contradictory data on the localization of the epicenter of the earthquake. Numerical simulations were carried out for 16 different scenarios with concrete dynamics of the seismic source, within the framework of the keyboard block model of the earthquake source. The mechanism of movement of the keyblocks into which the seismic source was virtually divided is determined by the few data that are given in historical records. The lack of accurate historical data on the heights of tsunami waves on the coast seriously complicated the analysis of the possible implementation of the dynamics in the earthquake source. The results obtained in this work most closely reflect the descriptions of the manifestation of tsunami waves in various parts of the coast. It was found that the average wave height on the selected isobath is about 6m, while the maximum heights in the area of the earthquake epicenter reach 16m. It can be concluded that the smallest-scale division into blocks of a seismic source will allow to specify in more detail the area of wave run-up on the coast in the area of the earthquake epicenter.

ACKNOWLEDGEMENTS

The reported study was funded by the Nizhny Novgorod State Technical University n.a. R.E. Alekseev (project No. 22/2 “Disturbance”) and the Council of the grants of the President of the Russian Federation for the state support of Leading Scientific Schools of the Russian Federation (Grant No. NSH-70.2022.1.5).

REFERENCES

1. Daniel M. Stewart. Recalibrating the July 8th, 1730 Valparaiso, Chile earthquake: giving historical context to primary sources // URL: https://www.academia.edu/44751468/Recalibrating_the_July_8th_1730_Valparaiso_Chile_earthquake_giving_historical_context_to_primary_sources.
2. Carvajal M., Cisternas M., Catalán P.A., Source of the 1730 Chilean earthquake from historical records: Implications for the future tsunami hazard on the coast of Metropolitan Chile // J. Geophys. Res. Solid Earth/ V. 122. P. 3648–3660. DOI: 10.1002/2017JB014063.
3. Lomnitz C. Major earthquakes and tsunamis in Chile during the period 1535 to 1955 // Geologishe Rundschau International. 1970. V. 59. No. 3. P. 938-960.
4. Berninghausen W.H. Tsunamis reported from the west coast of South America, 1562-1960 // Bulletin of the Seismilogical Society of America. 1962. V. 52. P. 915-921.
5. Cox D.C. Pacific tsunami historic file, U.S. Department of Commerce, National Oceanic and Atmospheric Administration, Boulder, Colorado, unpublished manuscript.
6. Instituto Hidrografico de la Armada. Maramotos en la costa de Chile. Valparaiso, Chile, 1982. 48 p.
7. Cox D.C., Iida K., Pararas-Carayannis G. Preliminary Catalog of tsunamis occurring in the Pacific Ocean. – Honolulu: University of Hawaii, 1967. 274 p.
8. Solov'ev S.L., Go Ch.N. A catalog of tsunamis of the eastern shore of the Pacific Ocean. – M.: Nauka Publishing House, 1975/ 202 p.
9. USGS [Electronic resource]. https://earthquake.usgs.gov/learn/glossary/?termID=150
10. Electronic bathymetry Gebco Digital Atlas [Electronic resource]. – http://www.gebco.net
11. Lobkovsky L.I., Baranov B.V. Keyboard block model of strong earthquakes in island arcs and active continental margins // Doklady AN SSSR. 1984. T. 275. No. 4. P. 843-847.
12. Lobkovsky L.I., Mazova R.Kh., Kataeva L.Yu., Baranov B.V. Generation and propagation of catastrophic tsunamis in the Sea of Okhotsk Basin: Possible scenarios // Doklady Earth Sciences. 2006. V. 410(1). P. 1156–1159. DOI: 10.1134/S1028334X0607035X.
13. Mazova R.Kh., Moiseenko T., Kurkin A.A., Jorge Van Den Bosch F., Gustavo Oses A. Numerical Simulation of a Catastrophic Earthquake and Strong Tsunami of April 1, 2014 near the Northwestern Part of the Chilian Coast // Science of Tsunami Hazards. 2021. V. 40. No. 2. P. 83-100.
14. Wells D.L., Coppersmith K.J. New empirical relationships among magnitude, rupture length, rupture width, rupture area, and surface displacement // Bulletin of the Seismological Society of America. 1994. V. 84. P. 974-1002.
15. Pelinovsky E.N. Nonlinear dynamics of tsunami waves. – Gorky: IAP USSR Academy of Sciences, 1982. 226 p
16. Voltsinger N.E., Klevanny K.A., Pelinovsky E.N. Long-wave dynamics of the coastal zone. – Leningrad: Gidrometeoizdat, USSR. 1989. 272 p.
17. Sielecki A., Wurtele M. The numerical integration of the nonlinear shallow water equations with sloping boundaries // J. Comput. Phys. 1970. V. 6. P. 219. DOI:10.1016/0021-9991(70)90022-7.

ISSN 8755-6839

SCIENCE OF TSUNAMI HAZARDS

Journal of Tsunami Society International

Volume 41 Number 4 2022

CONTRIBUTION OF SDGS IN TSUNAMI DISASTER PREPAREDNESS EDUCATION IN INDONESIA

Eko Hariyono[*1], Madlazim[1], Setyo Admoko[1], and Khoirun Nisa'[1]

[1]*Universitas Negeri Surabaya, Surabaya 60231, INDONESIA*

Email: ekohariyono@unesa.ac.id

ABSTRACT

Indonesia is an area with three different volcanic arcs. Almost every year, there are disasters in Indonesia, particularly tsunamis. On the other side, Indonesia has SDGs 2030 focused on disaster management or risk reduction. Based on Structural Equation Modelling (SEM) analysis, this study will look at the part that SDGs education plays in disaster readiness. To attain the research orientation, the researchers developed a tsunami education program and assessed its validity and reliability to find a suitable model. The research approach included a cross-sectional survey to gather quantitative data on the students' replies. The data are valid and expected based on the normal tests. Two of the five indicators from the model influence analysis have been verified, making the model just partially acceptable. However, it is known that only a small number of factors have an impact on other variables based on total effect, direct effect, and indirect effect analyses. Five variables were identified as not significant in the final analysis. Therefore, not all of the model's hypothetical variables can be accepted entirely. The scope of research can be expanded in the future by using more focused variables, a larger sample size, and more respondents.

Keywords: *Disaster, Education, Indonesia, Preparedness, SDGS, Tsunami.*

1. INTRODUCTION

Because of the volcanic paths in Indonesia, which extend from Sumatera to Papua, Indonesia is ranked as the 35th largest country that is often hit by tsunamis (Prahani et al., 2021; Rahsetyo et al., 2021). Indonesia is where the Indo-Australian, Pacific, and Eurasian plates converge (Hariyono et al., 2016; Suryadi et al., 2021; Prasetyo and Sriutami, 2022). Terrible earthquakes and tsunamis may result from this plate. Almost every year, there is a higher chance that Indonesia will experience a tsunami disaster (Li et al., 2016; Hariyono and Liliasari, 2018; Deta et al., 2020; Anggrayni et al., 2020). Tsunami disasters have negative impacts on humans, disruption of life, damage to housing, and loss (Ophiyandri et al., 2020; Al-Habsi et al., 2022). Along with earthquakes, less frequent events like the impacts of falling asteroids, enormous coastal and submarine landslides, and volcanic activity can all result in tsunami waves with a high amplitude (Aksa, 2020; Toulkeridis et al., 2022).

Indonesia has experienced numerous tsunamis over the past ten years, including those in Aceh, Mentawai, and Yogyakarta. Several tsunami disasters have occurred; the biggest disaster is Tsunami generated by a powerful underwater earthquake off the coast of Aceh (Kartika and Madlazim, 2022; Suprapto et al., 2022). The worst tsunami disaster even struck Aceh, a national disaster that led to the collapse of the nation's government, economy, and public infrastructure (Amri and Giyarsih, 2022). However, the tsunami disaster can be anticipated rather than prevented, so the effects were minimal. One factor that causes many disaster victims is knowledge of preparedness for disaster. However, the tsunami warning system that has Indonesia was still traditional and unable to share warnings to communities. Not only equipment warning systems but also evacuation times and community understanding about mitigation was still down (Kim et al., 2022; Suprapto et al., 2022).

Figure 1. Risk Management Strands (Civil Protection and Humanitarian Aid, 2021)

There are many important lessons to be learned from the various disasters in Indonesia, especially for the scientific community and society to improve their disaster preparedness.

In terms of disaster management, disaster preparedness is a crucial aspect that all spheres of society must address (Suryadi et al., 2022). Their level of disaster preparedness will directly impact one's attitude toward responding to disasters. The community, as a stakeholder, is crucial in lessening the effects of disasters. Their level of preparedness will affect people's ability to deal with disasters. As a result, the community must be able to raise awareness of disaster preparedness as a risk factor and a direct influence on community behaviour (Suryadi et al., 2021). The goal of disaster preparedness is to increase resilience to unforeseen disasters. Moreover, Indonesia has SDGs 2030 objectives related to four notions of disaster management. First, education for Sustainable Development (ESD) believes in ensuring all people obtain knowledge for a better life to build community resilience in the face of disaster (Hariyono et al., 2018; Jauhariyah et al., 2019; Pradipta et al., 2021). As a crucial national policy framework, disaster management must encompass all facets of prevention, mitigation, emergency preparedness, and reconstruction.

2. RESEARCH OBJECTIVE

This research will examine SDG education's role in disaster preparedness based on SEM analysis. The researchers created a tsunami education program and evaluated its validity and reliability to identify a fit model to achieve the research orientation. According to the justification given above, the hypothetical model proposed by researchers is shown in figure 1. This model will be investigated.

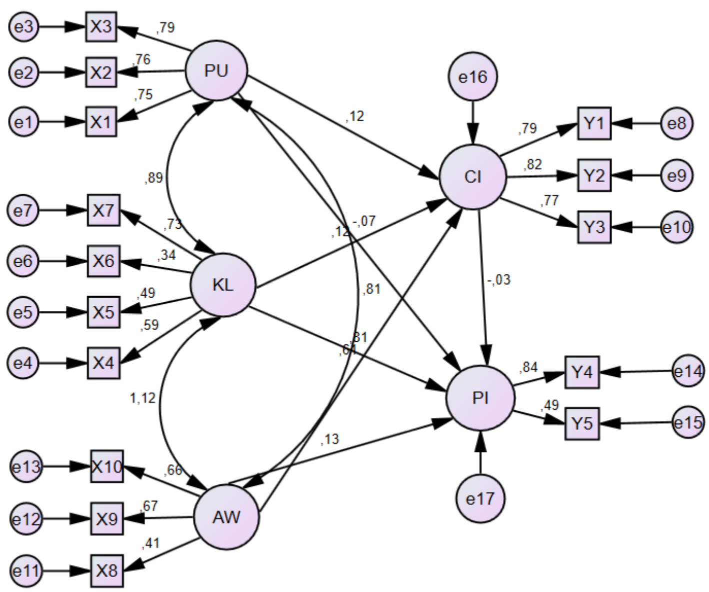

Figure 1. Hypothetical model

Note variable:

- PU : Perceived Usefulness
- KL : Knowledge
- AW : Awareness
- CI : Community Interest
- PI : Program Importance

Note model:

- All PU indicators can explain PU
- There are two KL indicators that can explain KL: X4 and X7
- There are two AW indicators that can explain AW: X9 and X10
- All CI indicators can explain CI
- There is one PI indicator that can explain PI: Y4

(Indicator is said to be able to explain the constructed variable if it has a loading factor value of more than 0.5)

Researchers then conducted empirical research with the following research questions in order to determine the fit model in relation to tsunami disaster preparedness:

a. What is the validity and reliability of tsunami disaster preparedness?
b. How does the fit model for tsunami disaster preparedness?

3. METHODS

A cross-sectional survey was used in the research design to collect quantitative data on the student's responses. The popularity of survey design stems from the strength of the Indonesian demographic (Suprapto, 2018). Then, a survey or questionnaire is a research tool that is adaptable and simple to use. The survey contains a number of concise and well-structured statements that prevent participants from providing another response. The initial data was gathered in August 2022.

The research subjects were chosen at random from a group of participants. The study concentrated on students in Indonesia because the country has many population centres there and is seismically active. The respondents' criteria included active students and alumni from Indonesian universities with a focus on the social and natural sciences. Then, Indonesia is located directly across from the Indian Ocean, where the Eurasian and Indo-Australian plates converge (Fauzi et al., 2022).

The research tool used to gather the quantitative data on educational readiness for tsunami disasters was called a questionnaire. The data was gathered by the researchers. Ten statements about disaster education, society knowledge, curricula, tsunami disasters, disaster awareness, and disaster preparedness were presented to the respondents with the option of agreeing or disagreeing. The statements offered four levels of disagreement: strongly disagree, disagree, agree, and strongly agree. They were written in straightforward language. Following the gathering of data, the student's responses were graded. The student's response was evaluated using a Likert scale with four levels. It provides their responses to queries.

Questionnaire items explored participants' views regarding general preparedness (e.g., how important disaster education is, especially Tsunami) and their perspective and knowledge relating to the tsunami disaster and its effects, regarding how useful the strategies were in preparing them for tsunami disaster and implementing disaster education curriculum. Then a questionnaire was a form of Google Forms and distributed via WhatsApp.

Participants' answers to closed questions were exported to SPSS and AMOS for data cleaning and analysis. Participant's answered multiple questions and indicated their level of agreement with a range of statements on a scale of 1 (strongly disagree) to 4 (strongly agree). "Agree" and "strongly agree" responses were combined for each item and considered agreement when reporting the findings.

The author conducted a quantitative treatment of items selected through CFA (Confirmatory Factor Analysis). CFA was used to check the validity and reliability of the questionnaire. CFA can show the trend in participants' responses and check the relationship between two variables using AMOS program (Abraham and Barker, 2015; Brown, 2015; Eaton and Willoughby, 2018). There are several indicators such as CMIN/DF (Chi-Square Fit Statistics/Degree of Freedom), RMR (Root Mean Square Residual), GFI (Goodness of Fit Index), AGFI (Adjusted Goodness of Fit Index), NFI (Normed Fit Index), RFI (Relative Fit Index), IFI (Incremental Fit Index), TLI (Tucker-Lewis Index), CFI (Comparative Fix Index), RMSEA (Root Mean Square Error of Approximation), PGFI (Parsimonious Goodness Fit Index), and PNFI (Parsimonious Normed Fit Index) (Jöreskog and Sörbom, 1996; Hair et al., 2010; Ogbeibu et al., 2021; Oktasari et al., 2019). The author followed moderate criteria shown in Table 1.

Table 1. Criteria of goodness fit indices

Parameter	Acceptable Fit Indices	Goodness Fit Indices
CMIN/DF	2-3	2
RMR	.05	
GFI	.85	
AGFI	.80	
NFI	.80	
RFI	.80	
IFI	.90	
TLI	.90	
CFI	.90	
RMSEA	.05	
PGFI		
PNFI		

(Byrne, 2016; Hu and Bentler, 1999; Hooperet al., 2008; Lee et al., 2021)

4. RESULTS AND DISCUSSION

4A. Validity and Reliability

Table 2. Residual Statistics

	Minimum	Maximum	Mean	Std. Deviation	N
Predicted Value	42.00	60.00	51,29	5.329	180
Std. Predicted Value	-1.773	1.663	.000	1.000	180
Standard Error of Predicted Value	.000	.000	.000	.000	180
Adjusted Predicted Value	42.00	60.00	51.29	5.239	180
Residual	.000	.000	.000	.000	180
Std. Residual	.000	.000	.000	.000	180
Stud. Residual	.000	.000	.000	.000	180
Deleted Residual	.000	.000	.000	.000	180

Stud. Deleted Residual	.000	.000	.000	.000	180
Mahal. Distance	3.479	37.378	14.917	8.851	180
Cook's Distance	.000	.000	.000	.000	180
Centered Leverage Value	.019	.209	.083	.049	180

In order to answer the research questions. There are outlier tests to check the validity of students' responses. Outlier test showed in AMOS output. Parametric analysis shows that the data is valid and not an outlier. It's shown from Mahalanobis distance. We know that $\chi(0,001;15)$ = 37,6973, then minimum and maximum scores smaller than $\chi(0,001;15)$ score. That means the data is valid without an outlier. The next step is the multivariate normality test shown in figure 2. More than 50% of the points form a straight line, meaning it has a multivariate normal distribution. The normality test results in this study show that the points are scattered around the diagonal line on the normal probability plot graph.

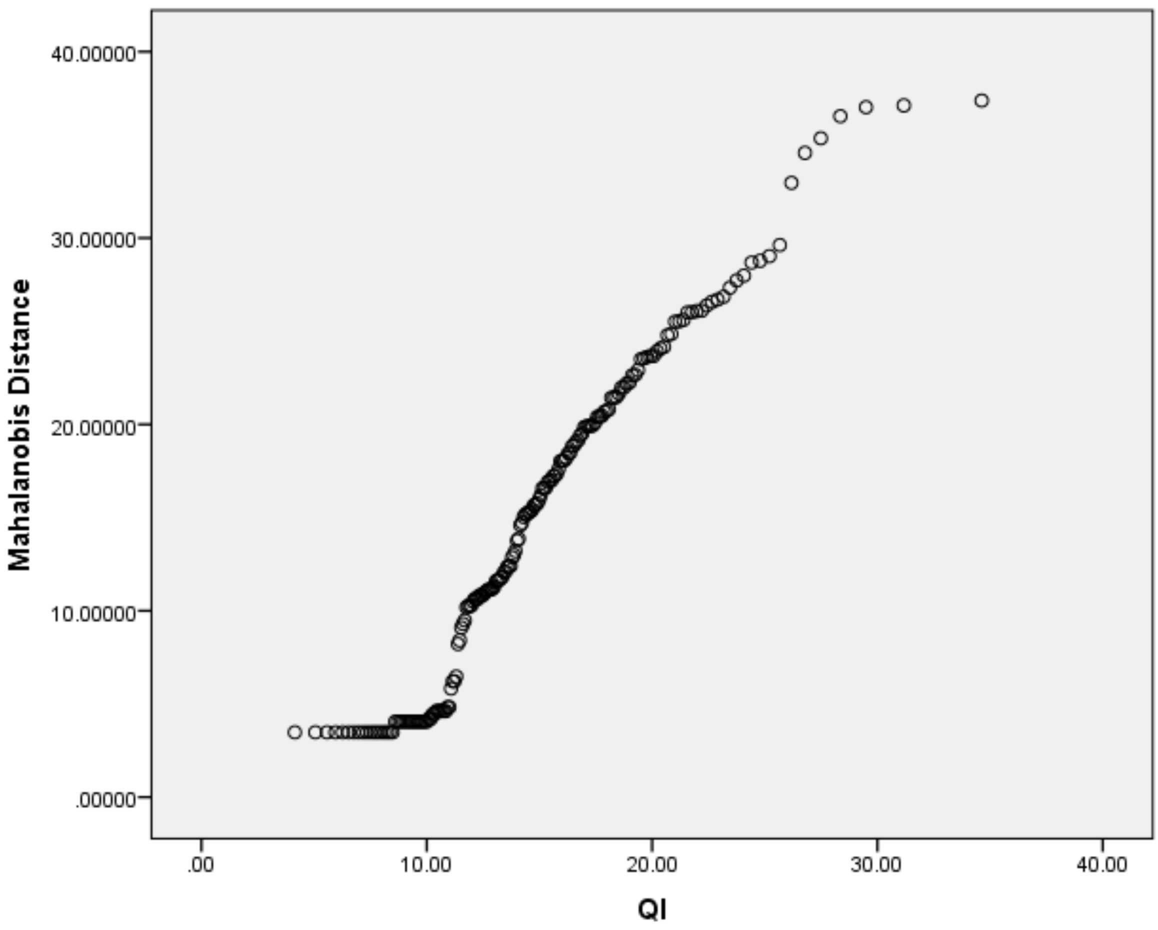

Figure 2. Multivariat normality data

Table 3. Correlations data

		Mahalanobis Distance	QI
Mahalanobis Distance	Pearson Correlation	1	.981**
	Sig. (2-tailed)		.000
	N	180	180
QI	Pearson Correlation	.981**	1
	Sig. (2-tailed)	.000	
	N	180	180
**. Correlation is significant at the 0.01 level (2-tailed)			

Table 3 shows the correlations test using a two-tailed test. Pearson correlation is 0,981 more than r table = 0,1463 (Johnson and Wichern, 2007). The results of the correlation coefficient obtained 0,981, which indicated a high correlation coefficient. The scatterplot and table 3 show that the data comes from a multivariate, normally distributed sample. After the normality test, CFA with SEM was processed, assisted by AMOS software.

The model chi-square, CMIN/DF, RMSEA, and CFI must report in SEM analysis (Kline, 2015). The chi-square represents a fundamental measure of overall fit. CMIN/DF shows a difference between the covariance matrix studied and the estimated one. RMSEA corrects if there is a chi-square tendency to reject models with large samples or measures the deviation of the parameter values of a model with its population covariance matrix.

Meanwhile, GFI shows a non-statistical measure by calculating a weighted comparison of the variances in the covariance matrix of the sample data and explained by the population covariance matrix. TLI (Tucker Lewis Index) is a measure that combines the size of parsimony into the index of comparison between the tested model and the baseline model. Accordingly, five out of all parameters indicated a non-goodness fit index. The five parameters are Chi-square, probability, AGFI, TLI, and CFI.

4B. Model Influence Analysis

Table 4. Model Fit Test

Criteria	Cut-Off	Result	Conclusion
Chi-square	Small (< = 37,6973)	148,820	Not Good
RMSEA	<0,08	0,069	Good
CMIN/DF	<2,00	1,860	Good
Probability	>0,05	0,000	Not Good
GFI	>0,90	0,903	Good
AGFI	>0,90	0,854	Not Good
TLI	>0,95	0,919	Not Good
CFI	>0,95	0,938	Not Good

Table 4 explains that 62,5% indicated not good, which means the suitability between the covariance matrix and the resulting population covariance matrix estimate. This is because the diversity in the sample is appropriate or representative of the diversity in the population.

The chi-square obtained is 148,820 or not good, so the model is not a good model. A high GFI value in this index indicates a better fit. RMSEA shows the model is acceptable. AGFI shows the hypothetical model can be accepted. TLI and CFI have values that are close to one. This shows that the model is an almost good fit with a value of less than 0,02.

According to Hooper et al. (2008), the model is good if at least one of the feasibility test methods is met, including Chi-Square, GFI, AGFI, RMSEA, and CFI. Some of these criteria were chosen because they are least sensitive to sample size, model specification errors, and parameter estimates (Boomsma, 2000). However, based on table 4, two of the five indicators have been met so the model is not fully acceptable.

Table 5. Total Effect Analysis

	AW	KL	PU	CI	PI
CI	,610	,121	,119	,000	,000
PI	,109	,803	-,069	-,028	,000

SEM analysis is used to describe the total effects among variables. The total effects between the two latent variables are the sum of the direct and indirect effects contained in the research model. The variables CI to CI, CI to PI, and PI to PI show a significant total effect. The Community Interest (CI) variable has relationship with PI (Program Importance) variable. While other variables do not show the total effect on the variables in the model. Further details are presented in Tables 6 and 7.

Table 6. Direct Effect Analysis

	AW	KL	PU	CI	PI
CI	,610	,121	,119	,000	,000
PI	,127	,806	-,066	-,028	,000

Direct effects between two variables occur when an arrow connects the two variables. The estimated value measures this effect among variables. For example, table 6 shows that only the CI to CI, CI to PI, and PI to PI show a significant direct effect. Other variables do not directly impact the variables in the model.

Table 7. Indirect Effect Analysis

	AW	KL	PU	CI	PI
CI	,000	,000	,000	,000	,000
PI	-,017	-,003	-,003	,000	,000

Indirect effects among variables can occur when a variable affects another variable by going through one or more latent variables according to the trajectory contained in the research model. For example, table 7 shows that CI (Community Interest) has a significant indirect effect on AW (Awareness) variable. This also occurs between CI-KL, CI-PU, CI-CI, PI-CI, CI-PI, and PI-PI. So, Community Interest (CI) variable has a role important in Awareness (AW), Knowledge (KL), Perceived Usefulness (PU), and Program Important (PI).

Protection and respect from the community are integral to all education preparedness. Humanitarian Aid (BNPB) aims to support people in addressing their needs and managing the risks they face. The knowledge of society about Tsunamis can improve from their beliefs, social interaction, and local knowledge of disasters and the environment (Hariyono et al., 2020). So, knowledge (KL) is essential to understanding the occurrence of tsunami disasters (Hariyono et al., 2016; Suryani & Hariyono, 2021; Madlazim et al., 2022). The increase in the population of coastal communities around the coastal area (CI) and the lack of awareness (AW) create some problems in dealing with the Tsunami (Hariyono & Liliasari, 2017). One of the programs important to dealing with the tsunami disaster is preventing fatalities, protecting the community, and accelerating the resumption of normal operations. There is an indicator of perceived usefulness (PU).

Table 8. Hypothetical Analysis

			Estimate	S.E.	C.R.	P	Meaning
CI	<---	PU	,125	,205	,610	,542	Not Significant
CI	<---	KL	,180	,455	,395	,693	Not Significant
CI	<---	AW	,847	,360	2,356	,018	Significant
PI	<---	PU	-,073	,221	-,331	,740	Not Significant
PI	<---	KL	1,267	,549	2,305	,021	Significant
PI	<---	AW	,186	,492	,379	,705	Not Significant
PI	<---	CI	-,030	,226	-,132	,895	Not Significant

Further analysis showed that there were five variables indicated as not significant. There are CI-PU, CI-KL, PI-PU, PI-AW, and PI-CI. Therefore, variables AW (Awareness) to CI (Community Interest) and KL (Knowledge) to PI (Program Importance) got significant. So not all variables in the hypothetical model can not be accepted completely.

5. CONCLUSIONS

The data from the outlier test are reliable. The normality test results reveal that the points on the normal probability plot graph are dispersed all around the diagonal line. Two of the five indicators from the model influence analysis have been satisfied, making the model just partially acceptable. It is known that only a small number of factors have an impact on other variables based on total effect, direct effect, and indirect effect analyses. Five variables were identified as not significant in the final analysis. There are PI-PU, PI-AW, CI-PU, CI-KL, CI-CI, and PI-PU. Variables AW to CI and KL to PI become prominent as a result. Therefore, not all of the model's hypothetical variables can be accepted entirely.

There are still a lot of factors that have an impact on disaster education, but this research is still generic in nature. The authors advise future researchers to employ more focused variables in order to expand the depth of their research future. Additionally, researchers can expand their audience and recruit more participants. The study must include extensive, random surveys of multiethnic people throughout Indonesia.

ACKNOWLEDGEMENTS

Thanks to Unesa for providing support in conducting this research.

REFERENCES

Abraham, J., & Barker, K. (2015). Exploring Gender Difference in Motivation, Engagement and Enrolment Behaviour of Senior Secondary Physics Students in New South Wales. *Res Sci Educ*, *45*, 59-73.

Aksa, F. I. (2020). Wisdom of Indigenous and Tacit Knowledge for Disaster Risk Reduction. *Indonesian Journal of Geography*, *52*(3), 418-426.

Al-Habsi, Z., Hereher, M., El-Hussain, I., Omira, R., Baptista, M. A., Deif, A., Al-Awadhi, T., & Al-Nasiri, N. (2022). Tsunami hazard and risk zoning for Qurayyat in northeast Oman coast: Worst-case credible scenarios along the Makran Subduction Zone, Western Asia. *Journal of Asian Earth Sciences: X,* 8, 100103

Amri, I., and Giyarsih, S. R. (2021). Monitoring Urban Physical Growth in Tsunami-Affected Areas: A Case Study of Banda Aceh City, Indonesia, *Geojurnal, 87*, 1929-1944.

Anggrayni, S., Hariyono, E., & Madlazim. (2020). The Students' Voice of Volcanology in Education for Sustainable Development Context. *IOP Conf. Series: Journal of Physics: Conf. Series,* 1491 012032

Boomsma, A. (2000). Reporting Analyses of Covariance Structures. *Structural Equation Modeling, 7*(3), 461-483.

Brown, T.A. (2015). *Confirmatory Factor Analysis for Applied Research, 2nd ed*. Guilford Press: A Division of Guilford Publications, Inc., New York.

Byrne, B. M. (2016). *Structural equation modeling with AMOS: Basic concepts, applications, and programming, (3rd edition*). New York: Routledge.

Civil Protection and Humanitarian Aid. (2021). DG ECHO Guidance Note Disaster Preparedness. Uni Eropa: Civil Protection Humanitarian Preparedness. https://civil-protection-humanitarian-aid.ec.europa.eu/system/files/2022-02/dg_echo_guidance_note_-_disaster_preparedness_en.pdf

Deta, U. A., Fadilah, R. N., Agustina, P. Z. R., Prakoso, I., Nurlailiyah, A., Saregar, A., Misbah, & Lestari, N. A. (2020). The Scientific Argumentation Profile of Earthquake Mitigation of Non-Science Undergraduate Student in Universitas Negeri Surabaya. *Journal of Physics: Conference Series,* 1467, 1-5.

Eaton, P., & Willoughby, S. D. (2018). Confirmatory Factor Analysis Applied to the Force Concept Inventory. *Physical Review Physics Education Research, 14*, 1-11.

Fauzi, Y., Hardiansyah, Mayasari, Z. M., & Susanto, A. (2020). Spatial Modeling of Tsunamis and Tsunami Inundation Analysis of "Panjang" Beach in Bengkulu City, Indonesia. *Journal of Tsunami Society Internasional, 41*(1), 95-108.

Ghozali, I. (2017). *Model Persamaan Struktural Konsep dan Aplikasi Program AMOS 24*. Semarang: Badan Penerbit Universitas Diponegoro.

Hair, J. F., Black, W. C., Babin, B. J., & Anderson, R. E. (2010). *Multivariate Data Analysis 7th Ed.* New Jersey: Prentice Hall.

Hariyono, E., & Liliasari, S. (2018). Disaster Mitigation Model of Eruption Based on Local Wisdom in Indonesia. In (Ed.), Natural Hazards - Risk Assessment and Vulnerability Reduction. IntechOpen. https://doi.org/10.5772/intechopen.79217

Hariyono, E., & S, L. (2017). The Characteristics of Volcanic Eruption in Indonesia. In (Ed.), Volcanoes - Geological and Geophysical Setting, Theoretical Aspects and Numerical Modeling, Applications to Industry and Their Impact on the Human Health. IntechOpen. https://doi.org/10.5772/intechopen.71449

Hariyono, E., Abadi, Liliasari, Wijaya, A. F. C. & Fujii, H. (2018). Designing Geoscience Learning for Sustainable Development: A Professional Competency Assessment for Postgraduate Students in Science Education Program. *Jurnal Penelitian Fisika dan Aplikasinya, 8*(2), 61-70.

Hariyono, E., Liliasari, B., Tjasyono, & Madazim. (2016). Volcanic eruption crisis and the challenges of geoscience education in Indonesia. AIP Conference Proceedings 1708, 080004; https://doi.org/10.1063/1.4941190

Hariyono, E., Prahani, B., & Mardiyanti, M. (2020). Volcano Project Design: Innovation In Geoscience Learning. *Prisma Sains: Jurnal Pengkajian Ilmu dan Pembelajaran Matematika dan IPA IKIP Mataram, 8*(2), 139-149.

Hooper, D., Coughlan, J., & Mullen, M. R. (2008). Structural equation modelling: Guidelines for determining model fit. *The Electronic Journal of Business Research Methods, 6*(1), 53-60.

Hu, L. T, & Bentler, P. M. (1999). Cut off criteria for fit indices in covariance structure analysis: conventional criteria versus new alternatives. *Structural Equation Modeling: A Multidisciplinary Journal, 6*(1), 1–55.

Jauhariyah, M. N. R., Hariyono, E., Abidin, E. N., & Prahani, B. K. (2019). Fostering Prospective Physics Teachers' Creativity in Analysing Education for Sustainable Development Based Curricula. *Journal of Physics: Conference Series*. 1417 012086

Johnson, R. A., & Wichern, D. W. (2007). *Applied Multivariate Statistical Analysis*. New Jersey: Prentice Hall.

Jöreskog, K. G., & Sörbom, D. (1996). *LISREL 8: Structural Equation Modelling with the SIMPLIS Command Language.* Chicago: Scientific Software International.

Kartika, D., & Madlazim. (2022). Pencitraan Rupture Gempa Bumi Sumatra 10 Januari 2012 Mw 7.2 Menggunakan Metode Multiple Signal Classification Back Projection (MUSICBP). *Jurnal Inovasi Fisika Indonesia (IFI), 11*(3), 73-80

Kline, R. B. (2005). *Principles and Practice of Structural Equation Modeling (2nd Edition ed.).* New York, NY: The Guilford Press.

Lee, T.-Y., Hsing, S.-C., & Li, C.C. (2021). An improved stress-scale specifically designed to measure stress of women with newly diagnosed breast cancer. International Journal of Environmental Research and Public Health, 18, 2346.

Li, L., Cheung, K. F., Yue, H., Lay, T., & Bai, Y. (2016). Effects od Dispersion in Tsunami Green's Functions and Implications for Joint Inversion with Seismic and Geodetic Data: A Case Study of the 2010 Mentawai Mw 7,8 Earthquake. *Geophysical Research Letters, 43*(21), 11182-11191.

Madlazim, Prastowo, T., Fahmi, M. N., Melianda, E., & Kusuma, S. (2022). Effective tsunami early warning using the product of P-Wave dominant period and source rupture duration of more than 50 seconds. *Science of Tsunami Hazards: Journal of Tsunami Society International, 41*(1), 39-53.

Ogbeibu, S., Jabbour, C. J. C., Gaskin, J., Senadjki, A., & Hughes, M. (2021). Leveraging STARA Competencies and Green Creativity to Boost Green Organisational Innovative Evidence: A Praxis for Sustainable Development Bus. Strateg. *Environ*, 1-20.

Oktasari, D., Ismet., & Siahaan, S. M. (2019). Validation Construct: Confirmatory Factor Analysis (CFA) Instruments Scientific Communication Skills Students in Learning Physics, *Journal of Physics: Conference Series,* 1567, 1-6.

Ophiyandri, T., Hidayat, B., & Ghiffari, C. (2020). Community Satisfaction Levels on the Housing Reconstruction Project After Mentawai Tsunami in 2010 – A Case Study at Sipora Island. *IOP Conference Series: Materials Science and Engineering, 933*(1), 012041.

Pradipta, D. D., Madlazim, & Hariyono, E. (2021). The Effectiveness of Science Learning Tools Based on Education Sustainable Development (ESD) to Improve Problem-Solving Skills. *IJORER: International Journal of Recent Educational Research, 2*(3): 342-353

Prahani, B. K., Nisa', K., Amiruddin, M. Z. B., Suprapto, N., Madlazim, & Mahtari, S. (2022). Analysis of the Top 100 Cited Publications in Earthquake Research During 1991 to 2021. *Journal of Tsunami Society Internasional, 41*(1), 77-94.

Rahsetyo, P.P., Sahara, D.P., Nugraha, A.D., Syahbana, D. K., Zulfakriza, Ardianto, Martanto, Afif, H., Baskara, A. W., Hermawan, I.B., & Sasongko, A.D. (2021). Hypocenter Determination of Volcano-Tectonic (VT) Earthquake around Agung Volcano in Period October-December 2017 Using a Non-Linear Location Method: A Preliminary Result. *IOP Conference Series: Earth and Environmental Science, 873*(1), 012098.

Suprapto, N. (2018). Demographic sources as a local wisdom: Potency of Indonesian physics education researchers in conducting survey research. *Journal of Physics: Conference Series*, 1171(1), 012003

Suryadi, T., Zulfan, Z., & Kulsum, K. (2021). The Relationship between Knowloedge and Attitudes about Community Disaster Preparedness in Lambung Village, Banda Aceh. *International Journal of Disaster Management*, 4(1), 1-10.

Suryani, D., & Hariyono, E. (2021). Geoscience Literacy Profile of Junior High School Students. *IJORER: International Journal of Recent Educational Research, 2*(3), 305-315

Toulkeridis, T., Martinez, N., Barrantes, G., Renteria, W., Barragan-Aroca, G., Simon-Baile, D., Palaciosm I., Salazar, R., de Jesus, Salcedo-Hurtado, E. J., & Pararas-Carayannis, G. (2022). Impact and Response in Central and South America due to the Tsunami Generated by the Submarine Eruption of Hunga Tonga-Hunga Ha'Apai Volcano. *Journal of Tsunami Society Internasional, 41*(1), 4-38.

ISSN 8755-6839

SCIENCE OF **TSUNAMI HAZARDS**

Journal of Tsunami Society International

Volume 41 Number 4 2022

THE 326 BC EARTHQUAKE AND TSUNAMI IN THE NORTHERN ARABIAN SEA - IMPACT ON THE FLEET OF ALEXANDER THE GREAT

George Pararas-Carayannis

Tsunami Society International

ABSTRACT

Ancient Greek and Indian texts support that destructive sea waves along the Makran coast in the northern Arabian Sea were responsible for the partial destruction of Alexander the Great's fleet in 326 BC. At that time, and after the conclusion of all its operations along the Indus River and its tributaries, the Greek fleet had reached the Indian Ocean and was waiting in an estuary of River Hab, north of the Indus River delta, for calmer seas and for the seasonal monsoon winds to subside, before beginning the long journey from India to Babylon, in what is presently known as the Persian Gulf. Since the Greek fleet had spent considerable time in the fall of that year in protective bays of the Indus delta/Kutch and the Makran regions (India in ancient times), it is very possible that the reported sustained damage to the fleet was caused from a tsunami rather than storm waves. After repairs were completed, the fleet under the command of admiral Nearchus of Crete began its long and arduous journey west in the North Indian Ocean, towards Babylon in what is now known as city of Hillah of Iraq in the Persian Gulf. In all probability, the tsunami originated along the Makran Subduction Zone – the same source area that historically has produced several earthquakes and tsunamis, the best known in recent times being one in 1945. Based on reviews of ancient Greek accounts such as those of Plutarch, Nearchus but mainly of Arrian's of Nicomedia "Indice" and to a lesser extent on Sri Lanka and Indian records, the present study reconstructed the chronology of the impact on the fleet based on the ancient Athenian

lunar calendar. By using current geophysical knowledge of recent events in this region, and the present study concluded that the 326 BC earthquake occurred in late October or early November of 326 BC (known as Pyanepsion, "Πυανεψιών" in Ancient Greek). As mentioned, at that time the Greek fleet was either at anchor at the estuary near the delta of River Hab, or had just set out to sea on its way to Babylon. The Hab River estuary is located in the easternmost end of the Makran Subduction Zone (MSZ) in the Northern segment of the Arabian Sea - a source region of large earthquakes and tsunamis, recently and in the past. The delay in the departure of the Greek fleet from this estuary caused by opposing monsoon winds, limited the possibility of its total destruction if it had begun earlier its long journey to Babylon.

Earlier in August of that same year, Alexander the Great with about a third of the Greek land forces had already taken a long and difficult march back to Babylon, via a southern land route, which included the harsh Gedrosian desert, a journey which resulted in the death from starvation for most of the soldiers. The present study is an evaluation of these events as deduced, from the historical records, but also from current geophysical understanding of the seism-tectonics of the Makran Subduction Zone - a source region of large earthquakes and tsunamis, recently and in the past. The best-known recent earthquake and tsunami in the same eastern region of the Makran Subduction Zone was the Moment Magnitude 8.1 earthquake of 19 November 1945.

Keywords: *disaster archaeology; seismo-tectonics; Makran Subduction Zone; Alexander the Great's India Campaign; Arrian's "Indice"; Plutarch's "Alexander"; Plutarch's "Parallel Lives".*

1. INTRODUCTION

Major earthquakes and destructive tsunami waves have occurred frequently in the past along the Makran Subduction Zone (MSZ) in the northern Arabian Sea. Ancient Greek and India accounts indicate that in late 326 BC a major earthquake on the MSZ generated a tsunami, which impacted and caused some damage to the fleet of Alexander the Great. At that time the Greek fleet was near an estuary of River Hab, just north of the Indus River delta, while waiting for calmer seas and for the seasonal monsoon winds to subside, before beginning the long journey from India to Babylon, in what is presently known as Persian Gulf.

The MSZ is an extensive and complex tectonic plate margin in South-Central Asia along the Makran coasts of Iran, of the since 1947 Pakistan, and of India. This is a region that historically has produced several earthquakes and tsunamis. The best known of such events in recent times, was the great Makran earthquake and tsunami of 1945, but there were many other destructive events before it, particularly along the eastern segment of the MSZ (Pararas-Carayannis. 2001b; 2005b, 2006a).

Most of the earthquakes in this region of Southeast Asia occur mainly on land along the boundaries of the Indian tectonic plate and of the Iranian and Afghan micro-plates. At least 28 earthquakes with magnitudes close to 7 or more have occurred since 1668 to the present time (Ambrasseys and Bilham, 2003). According to historical records, an earthquake in 893-894 AD with an estimated moment magnitude of 7.5, occurred in the Debal (lower Sindh) region of what is now Pakistan, killing 150,000 people and destroying several towns. However, there is no data on whether this earthquake or subsequent similar events in the distant past generated tsunamis, since no one was aware back then of the association of earthquake-induced sea floor displacements and the resulting tsunami wave generative mechanisms. However, based on reviews of ancient Greek accounts of Plutarch, Nearchus but mainly of Arrian's of Nicomedia "Indice" historical account — and to a lesser extent on Indian historical records — the present study reconstructed the chronology of events based on the ancient Athenian lunar calendar and, by using current geophysical knowledge of recent events in this same region, concluded that a major tsunamigenic earthquake occurred in late October or early November of 326 BC (a period known as Pyanepsion - "Πυανεψιών" in the ancient Athenian lunar calendar), when the Greek fleet was in the easternmost region of the MSZ.

The historical ancient accounts by Nearchus of Crete, Plutarch and Arrian are not clear as to whether an earthquake occurred which generated a tsunami, as such events were not well understood and were simply attributed to acts of Olympian gods — mainly Poseidon ("Ποσειδών" - Neptune). Probably many other hardships and losses which occurred during the arduous journey of the fleet down the Indus River and the battles fought on both river sides, overshadowed the damages caused by waves which were experienced later, after the fleet reached the delta of the Indus River in the North Arabian Sea. Furthermore, the accounts by Nearchus and Plutarch are not clear as to the occurrence of earthquakes and resulting sea waves. However based on the historical narrative in Arrian's "Indice", it can be reasonably concluded that the degree of reported damage which occurred to Alexander the Great's fleet — which was located in the vicinity of the River Cab estuary at the time — was not caused by storm waves of monsoon winds, but from tsunami waves similar to those generated by the 1945 earthquake or by other previous earthquakes in the eastern MSZ region of the North Arabian Sea. The present study is based on the chronology of reported events, which indicates that there were no monsoon winds in late October or early November of 326 BC. Based on the well-known high frequency of major earthquakes in this region and elsewhere in the Indian Ocean, as well as on Arrian's account, it can be reasonably concluded that a tsunami was responsible for the partial damage to the Greek ships. Fortunately the fleet was in the estuary of River Hab, in the relatively safe eastern region of MSZ, which limited the size of the tsunami waves and their destructive impact.

2. HISTORIC RECORDS

Prior to discussing in some detail the impact of the 326 BC earthquake and tsunami on the fleet of Alexander the Great and the geotectonic nature of the MSZ and the past disaster events in this region of the North Arabian Sea, it seems appropriate to present first a brief summary of historical events and accounts relating to ancient disasters and of perceptions about them, as well as of Alexander's early life, of his Asian and India campaign, and of the return journeys of his armies by land and by sea to Babylon.

The following is a brief review of his early life, based primarily on the accounts by Nearchus, Plutarch and Arrian. Unfortunately, Nearchus' book "Indike" — which described the journey back to Babylonia - was lost. However, some of its contents are known from another book — also named "Indice" — written by Arrian of Nicomedia. The account of Alexander's voyage of the fleet is based primarily on Arrian's writings. These early historical accounts are not clear as to the occurrence of earthquakes or of resulting sea waves because such phenomena were not understood and were simply attributed to acts of gods. However, Arrian's narrative in "Indice," can be regarded as a book of naval expedition and discovery of the unknown until then North Arabian Sea and Persian Gulf. Following, in the form of an introduction is a brief summary of Alexander's early life, and of Plutarch's account entitled "Alexander". A brief description is also included of Indian records for historical disasters in the North Arabian Sea, as well as of Sri Lanka (Ceylon) accounts and legends pertaining to sea wave disasters along the Southeast coasts of India.

2.1 Tsunami Occurrence Elsewhere in Alexander's Empire

There is also additional mention of a tsunami elsewhere in Alexander's Empire. However, an allegorical account below by the ancient historian, Diodorus Siculus (Diodorus of Sicily) includes a description of a sea-monster creating a huge wave flooding the harbor of Alexandria in Egypt. Of course, the event was attributed to god Poseidon who was believed to be the originator of earthquakes and tsunamis.

Although there is no specific accounting in ancient texts of tsunami along the Makran region, it is interesting to note that besides Alexander the Great's fleet, Julius Caesar's Roman fleet also sustained damage from unusual wave conditions (not a tsunami) and tidal phenomena in 55 AD. Caesar was forced to retreat from the shores of England after suffering damage to his fleet while anchoring in areas that had extensive tidal ranges and unusually large waves. The following account of a tsunami is given by the ancient historian, Diodorus Siculus (Diodorus of Sicily). Diodorus in his rather allegorical narrative below includes a sea-monster in his account of the tsunami wave that flooded Egypt's harbor of Alexandria.

Fig. 1. Depiction of Diodorus Siculus sea-monster creating a tsunami.

"As the Macedonian construction came within range of their missiles, portents were sent by the gods to them in their danger. Out of the sea a tidal wave tossed a sea-monster of incredible size into the midst of the Macedonian operations. It crashed into the mole but did it no harm, remained resting. A portion of its body against it for a long time and then swam off into the sea again. This strange event threw both sides into superstition, each imagining that the portent signified that Poseidon would come to their aid, for they were swayed by their own interest in the matter".

2.2 Alexander the Great's Early Life 349-340 BC

Briefly, Alexander was the son of Macedonia's king Phillip II and of the 19-year old Olympias, the daughter of Neoptolemus I king of Epirus - a fiery woman who took part in secret rites of worship of Dionysus and Orpheus, and had been initiated in the Kaverian Mysteries held yearly on cape of Chloi, exactly opposite the famous Kabeirion of Samothrace. Phillip II was the king of the ancient kingdom of Macedonia from 359 BC until his assassination in 336 BC. He was an accomplished military commander who set the stage for Alexander's victory over Darius III and the conquest of Persia.

Between the ages of 7-16, Alexander displayed arrogant intelligence and clashes with his father. However, despite his violent and nervous character, he was characterized by great self-control and self-discipline. His ambition was always accompanied by magnanimity, unlike Philip who was somewhat vain.

Philip's career made Alexander's conquests possible, by saving Macedonia from the verge of extinction, beating off powerful neighbors before expanding, until he dominated the rest of Greece and the Balkans. In the process, he created a uniquely effective army, combining many different types of troops into one formidable, fast moving team. This was the army Alexander led against the Persian Empire, composed of Philip's men, fighting in the same way they had done for more than 20 years. It was Phillip's career that made Alexander's subsequent conquests possible. However, whenever it was known that Philip had either taken possession of a glorious city or had been victorious in some important battle, Alexander the Great did not hear it with much pleasure, but said to his peers, "children, my father will see to it all, and will not leave no work, great and brilliant, to achieve it with you (*which in Ancient Greek is stated «ὤ῀ παιδες, πάντα προλήψεται ὁ πατήρ, ἐμ οί δ΄ οὐδέν ἀπολείψει μεθ΄ ὑμῶν ἔργον ἀποδείξασθαι μέγα καί λαμπρόν)».*

Because Alexander desired neither pleasure nor wealth but virtue and glory, he thought that the more he got from his father, the less he would achieve himself". However, his views were changed and improved when Aristotle - one of history's greatest philosophers — became his teacher when Alexander was 13 years old, and taught him about medicine, philosophy, morals, religion, logic and art. Also, under Aristotle's three-year tutelage, Alexander developed a passion for the works of Homer, for which Aristotle gave him an annotated copy, which later he carried in his campaigns.

Philip's own assessment of the abilities of his son changed drastically after Alexander managed to tame "Bucephala", a wild horse that no one else had managed to do. The taming of Bucephala made his father recognize that his son would be greater than him. It was then that Phillip the king of Macedonia wept for joy and exclaimed: *"My child, ask for a kingdom equal to yours, because Macedonia is not enough for you (ὦ˜ παῖ, ζήτει σεαυτῷ βασιλείαν ἴσην· Μακεδονία γάρ σ΄ οὐ χωρεῖ)".*

Alexander's leadership qualities were further recognized by a delegation of Persians, which Alexander received in the absence of his father. The Persians left impressed, as what they had heard of Philip was nothing compared to what they heard of his son. Of course Aristotle's teachings had turned Alexander much wiser and diplomatic.

In brief, Alexander's leadership qualities became more evident during his subsequent campaigns in Asia, where he focused on the unification of conquered regions by taking the Hellenistic culture to a completely different level by introducing ideas of freedom, equality, philosophy, drama, and scientific categorization and study - based on Aristotle's teachings - and spreading them across Asia Minor and the Middle East all the way to the Indian subcontinent.

2.3 Plutarch's Account in "Parallel Lives"

A good historical account of Alexander the Great can be found in the works of Plutarch (79 AD) entitled "Alexander". This account provides good information on the conquest in Asia and India, but very little information about the Greek fleet's journey in the Northern Arabian Sea and in the Persian Gulf. Furthermore, he does not mention anything about earthquakes or catastrophic sea waves.

In his historical account "Parallel Lives," Plutarch provides in detail biographies of both Alexander the Great and of Julius Caesar, but also discusses the life, character and actions of forty-four other well-known, Greeks and Romans, describing them with parallelisms and an infinite number of historical and psychological elements. In this account Plutarch paints Alexander the Great with every historical detail and accuracy, down to his smallest psychological fibers indicating his determination.

2.4 Sri Lanka and Indian Records

Also, according ancient texts, large earthquakes and destructive waves occurred east of Sri Lanka (Ceylon), although the dates are somewhat conflicting as to the timing of these events, which may possibly relate to differences in calendars. According to Sri Lanka historical records (Fernando, 2005), in Sri Lanka (known as "Mahawamsa" then) in the time of King Kelanitissaa, a town named "Kalyani Kanika" and several other townships in the Eastern seaboard of Ceylon were inundated or destroyed by what must have been tsunami waves. Also provided in these records is an account that "Viharamahadevi", the daughter of King Kelanitissa, was set afloat at Kalyani Kanika to appease the Gods, but that she was brought back to shore by sea currents, which landed her in Kirinda. However, the dates do not match, since the tsunami in Sri Lanka is purported to have occurred at the time of King Kelanitissa - in the 2nd Century BC, and apparently had a different source of origin.

Ancient Indian legends refer that a port city named Poompuhar, located at the confluence of rivers Kaveri and the Bay of Bengal in the Thanjavur District in the southern Indian State of Tamil Nadu - once known as “Kaveripattinam” — was washed away by a wave around AD 500. According to this legend, goddess “Manimekhalai” was angry with the Chola King and caused the city to be swallowed up by the sea. However, a tsunami in this region of the Bay of Bengal must have had a source near the Andaman Islands and Sumatra - probably in the same source region as that of 26 December 2004, and not in the Makran Subduction Zone of the North Arabian Sea, which would need to refract 180 degrees northward-thus reducing significantly the height and destructive impact of its waves on the very north-eastern region of the Arabian Sea.

As mentioned, Sri Lanka (Ceylon) was struck and devastated by the 2004 tsunami generated by a great earthquake along the coast of the Burma plate, and included the north-west portion of the island of Sumatra as well as the Andaman and Nicobar Islands, which separate the Andaman Sea from the Indian Ocean. Sri Lanka’s south and east coasts were hardest hit by this particular tsunami and more than 50,000 people lost their lives, and about more than 1,200 in the eastern district of known as Batticaloa (Pararas-Carayannis, 2005, 2006 a & b). This disaster was a very similar recurrence of the events reported in the above-cited ancient records. Included in a subsequent section of this report are analyses by the present author based on the documented impacts of the 26 December 2004 and of the 28 November 1945 earthquakes in the Makran region of the North Arabian Sea.

2.5 Brief Summary of Alexander’s Indian Campaign and Return to Babylon

According to Plutarch (79 AD), after defeating the Persians, Alexander continued his conquest of Asia by turning south into Arachosia (southeast Persia) and then continuing north into Afghanistan where he founded cities to serve as army garrisons and centers of his administration. Still inhabiting to the present time in a northern region of Afghanistan is a group of native people who racially differ from the rest of the country’s population, have Greek characteristics, and use words of Greek origin in their language. These people appear to be surviving descendants of s garrison left behind by Alexander’s Macedonian general Craterus or Krateros (in Greek: Κρατερός; c. 370 BC – 321 BC), on his northern land route of return to Babylon with more than a third of the Greek forces. Craterus, who claimed succession of Alexander, was killed subsequently in 321 BC at the Battle of the Hellespont (Fig. 2).

Fig. 2. Battle of the Hellespont

2.6 Construction of Fleet – Journey on River Indus

The following is an account of Alexander's earlier campaign, after entering Bactria and Sogdiana, and marching of his armies as far as the Jaxartes River. After two years in this region, during 327-326 BC, Alexander's army crossed the Hindu Kush mountain region (present Pakistan) and begun the conquest of India. There were several battles fought during the India campaign. Although victorious, after the May 326 BC battle of Hydaspes - near the northernmost of the five great tributaries of the Indus River, and as already stated, Alexander was pressured by his generals to end his Asian conquest and for the troops to return to Babylonia. Reluctantly he agreed and in June of that year, he sent a third of his army under the command of general Craterus, back to Carmania over a northern land route. The size of this army is estimated at 75,000 men. Subsequently, Alexander ordered that 30 oared galleys (Athenian type of triremes as shown in Fig. 3 below)) and other tow boats and rafts to be built, and sail down the Indus River in support of the ongoing Indian campaign and, subsequently, to transport part of the army with these back to Babylonia (Mesopotamia).

Fig. 3. The Athenian type of trireme that served as Alexander's flagship, "Olympias," named after his mother.

In command of the newly constructed fleet and other support vessels, Alexander appointed Nearchus of Crete, who previously had been the satrap of Lycia and Pamphylia (in Asia Minor), after the Sogdian campaign, and one of his two commanders of the Shield bearers, a heavy infantry unit, before the battle of Hydaspes.

Apparently the 30 triremes could not have been sufficient to carry Alexander's army, even with a third of the army already gone back to Carmania by a land route. Based on Plutarch's account, Alexander's army in India at that time amounted to about 140,000 foot soldiers and 15,000 cavalrymen. In all probability, many more barges and tow ships were used to transport some of the soldiers, while the bulk of the army marched along both banks of the Indus. Overall, the India Campaign and the fleet's journey down the Indus River took approximately seven months, during which Alexander conquered of what is now the Punjab State in northwestern India.

The map below (Fig. 4) shows the Indus River and its tributaries leading to the delta of the North Arabian Sea, which was named as the Port of Alexander, which no longer exists since subsequent extensive sedimentation changed the shoreline.

Fig. 4. Alexander's India Campaign along the Indus River Valley (map of livius.org), and of Port of Alexander at the delta of Indus River

2.7 Sea and Land Routes of Alexander's Army and Fleet

Finally, the fleet and the bulk of the army reached Patala, the present city of Bahmanabad, about 75 km northeast of Hyderabad (Fig. 5). A portion of the army continued on land southeast of the Indus River and fought several squirmishes before regrouping in August of 326 BC at Patala for the journey back to Carmania. According to Plutarch's account below, Alexander must have traveled further down the Indus River on a single ship to the ocean, because he describes such a voyage and the appointment of Nearchus as commander of Alexander's fleet, as follows:

"His (Alexander's) voyage down the rivers took up seven months' time, and when he came to the sea, he sailed to an island which he himself called Scillustis, others Psiltucis, where going ashore, he sacrificed, and made what observations he could as to the nature of the sea and the sea-coast. Then having besought the gods that no other man might ever go beyond the bounds of this expedition, he ordered his fleet, of which he made Nearchus admiral and Onesicritus pilot, to sail round about, keeping the Indian shore on the right hand, **…_"**

The island of Scillustis or Psiltucis mentioned by Plutarch must have been a sand island near the mouth of the Indus River, which no longer exists.

Fig. 5. Alexander's Sea and Land Routes

2.8 The Greek Fleet's Journey to the Indus River Delta/Kutch Region

Overall, the India Campaign and the fleet's journey down the Indus River took approximately seven months, during which Alexander conquered of what is now the Punjab State in northwestern India.

On 15 September 326 BC, following the departure of the bulk of army via the southern land route, the Greek fleet, under Nearchus' command, set out to sea for Carmania and Babylonia with the remaining army which had dwindled to about 17,000 - 20,000 men. There is no information on the size of the fleet at his time in the ancient texts. It is possible that many more local ships were added since 30 triremes would not have been sufficient to carry so many men and their supplies for the long sea voyage.

September was too early in the season for the journey west as the monsoon winds blow in this region from a southwest direction from May through October. It is possible that Nearchus received false information from the natives who were anxious to see Alexander's ships leave. Almost immediately after leaving Patala, the ships encountered adverse winds. It took almost a week to reach the Erythraean Sea (the Indian Ocean). Subsequently, the fleet headed north, through the lagoon between the mouths of the rivers Indus and Hab (south of present Karachi which was then part of India).

2.9 Alexander's Army Return Via the Southern Land Route

In August 326 BC, Alexander with about 135,000 foot soldiers and cavalry men left Patala towards Carmania, for the long and difficult march back homeward, through the harsh Gedrosian desert (Arrian, 135-37 AD) — which was part of the ancient Achaemenid empire (present region of Baluchistan region in Iran). Fig. 6 below is another map showing Alexander's armies return to Babylon by sea and land routes and the extent of the empire between 334 to 323 BC. Apparently, only one-fourth of the army survived the march back on the southern land route through the harsh Gedrosian desert (Fig. 7). Plutarch describes Alexander's difficult journey via the southern land route and the hardships the army endured as follows:

" ……and (Alexander) returned himself by land through the country of the Orites, where he was reduced to great straits for want of provisions, and lost a vast number of his men, so that of an army of one hundred and twenty thousand foot and fifteen thousand horse, he scarcely brought back above a fourth part out of India, they were so diminished by disease, ill diet, and the scorching heats, but most by famine. For their march was through an uncultivated country whose inhabitants fared hardly, possessing only a few sheep, and those of a wretched kind, whose flesh was rank and unsavory,…."

Fig. 6. The empire established by Alexander the Great between 334 to 323 BC - Routes of the land Armies and of the Greek fleet down the Indus River, its tributaries and the open sea return to Babylon

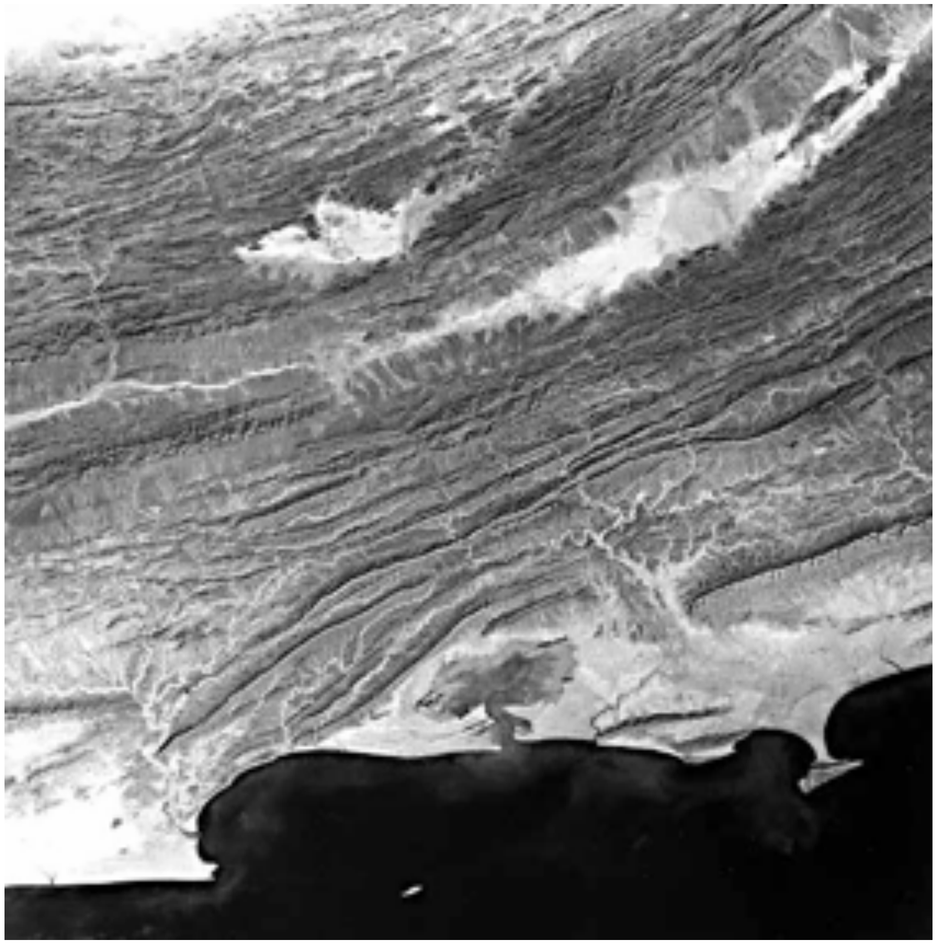

Fig. 7. NASA Satellite photo of a section of the Makran rugged and tectonic coastline showing uplifted terraces, headlands, sandy beaches, mud flats, rocky cliffs, bays and deltas. Numerous mud volcanoes along the shores. Alexander with about 135,000 foot soldiers and cavalry men marched through this harsh Gedrosian desert and only one-fourth of the army survived.

3. EVALUATION OF THE TSUNAMI OF 326 BC THAT IMPACTED THE GREEK FLEET IN 326 BC

There is no specific information in the afore-mentioned historical records about the occurrence of an earthquake or tsunami in 326 BC in the North Arabian Sea. The intensity of such event could not have been felt or estimated in the vicinity of the estuary of River Hab where the Greek fleet was at that time. However for an earthquake along the Makran subduction zone (MSZ) to generate a significant tsunami, its epicenter must have been near the coast further west, its focal depth must have been relatively shallow, its Richter magnitude greater than 7.0, and must have included some sizable degree of vertical crustal displacements of the sea floor.

In all probability, and again based on the historic accounts about the damage to the Greek fleet which was south of present Karachi near the estuary of River Hab at that time at the easternmost and relatively safer eastern region of MSZ, which limited the size of the tsunami waves and their impact. However, based on these considerations and the relative historic recurrence frequency of such earthquakes along the East-West trending seismogenic MSZ coast (of present southern Pakistan and Iran) in terms of geologic time, the present study can reasonably conclude that a significant tsunamigenic earthquake indeed occurred in 326 BC. Such an earthquake on the MSZ could have generated a significant tsunami with greater wave heights to the North and the South, and to a lesser heights along the Western and Eastern ends of the great fault. Such earthquake could have been very similar to the Makran earthquake of 1945, which generated a very destructive tsunami along coastal areas of India, Pakistan, Iran and Oman. Although infrequently, both the East and West segments of the Makran Subduction Zone in the Northern Arabian Sea, are capable of generating tsunamigenic earthquakes that can have an upper limit of moment magnitude of as much as 8, and such events have occurred with relatively high degree of frequency in terms of geologic time. (Pararas-Carayannis, 2005 b, 2006 a; b; Shah-hosseini EtAl. 2011)

Although not as frequent, there is also evidence that major earthquakes along the West segment of the MSZ coast have also generated tsunami waves on the south coast of Iran Shah-hosseini EtAl., 2011). Coastal boulder deposits found along the rocky coasts from Chabahar to Lipar, indicate the formation of Quaternary marine terraces, tectonic uplift, and coastal boulder deposits. Some of the boulders weighing up to 18 tons were found up to 6 m above the present mean sea level and up to 40 meters inland from the present shoreline. (Reyss EtAl, 1998). Based on such determinations of paleo-tsunami events, it may be possible that an earthquake along this Eastern MSZ zone in 326 BC could have generated a tsunami that partially damaged the Greek fleet when it was still in the estuary of River Hab.

Additionally there are other historical accounts of tsunami generation along the eastern and western coasts of India, purportedly causing destruction as far away as Sri Lanka and elsewhere. The best known of the most recent historical events was that of 1945. Other major or great recent and past earthquakes have generated significant tsunamis that impacted different coastlines of the northern Arabian Sea and of the Indian Ocean.

Another possibility is that the 326 BC earthquake occurred in the Gujarat region, where large events are also known to occur — particularly along the Kutch Graben region or even near the Bombay Graben. However, none of the recent earthquakes that have occurred along the Kutch Graben region have generated destructive tsunamis (Pararas-Carayannis, 2001). It is possible that an earthquake in the Guajarat region could have triggered an underwater landslide and a local tsunami, but such an event would not have the azimuthal concentration of energy to cause destruction on the East coast of Sri Lanka. More than likely, the large earthquake reported in the ancient texts originated along the Makran subduction zone — a region capable of generating destructive tsunamis (Pararas-Carayannis, 2005a,b 2006). However other possible tsunamigenic seismic sources in the Indian Ocean are examined to evaluate if a previous earthquake in the 326 BC could have generated waves which damaged the Greek fleet.

3.1 Partial Destruction of the Greek Fleet by a 326 BC Tsunami

Renewed southwest monsoons and dwindling food and water supplies slowed the fleet's progress, forced Admiral Nearchus to seek safe anchorage for the Greek fleet and to establish a fortified shore camp for about 24 days, while waiting for better weather conditions and for the seasonal monsoon winds to subside. From Plutarch's description and timing it can be concluded that the fleet had sailed north of the Indus River delta, and a new camp was established just south of the Hab River (south of present Karachi). Upon establishing this camp, the soldiers were forced to hunt and fish for food and to drink briny water. Fig. 8 below is a map indicating the location of the Greek fleet. It was probably at this time and at this location — in early November 326 BC - that the large earthquake and tsunami occurred probably near the region where the fleet had taken refuge. Fig. -- shows a probable tsunami generation area along the Eastern Makran subduction zone and the location of the Greek fleet at the time of November 326 BC where tsunami waves caused damage. As stated, this date was estimated based on a period known as Pyanepsion - "Πυανεψιών" of the ancient Athenian lunar calendar).

Fig. 8. Most likely location of the Greek fleet at the time of the November 326 BC tsunami.

According to Lietzin (1974), this earthquake had large magnitude and massive tsunami waves which destroyed a good part of Alexander's fleet. Also, according to Sri Lankan texts, a destructive tsunami struck the East side of the island of Ceylon, but the location and the given date of this tsunami's occurrence does not agree with the 326 BC event near the Hab river estuary in the Northwest Arabian Sea.

3.2 More Probable Location and Magnitude of the 326 BC Tsunamigenic Earthquake

In all probability and as stated, the earthquake of 326 BC occurred along the Makran coast (present southern Pakistan and Iran) and generated destructive tsunami waves. This earthquake could have been very similar to the Makran earthquake of 1945, which also generated a destructive tsunami along the coastal areas of India, Pakistan, Iran and Oman. Although infrequently, and as already stated, the Eastern Makran subduction zone in the Northern Arabian Sea is capable of generating tsunamigenic earthquakes that can have an upper limit of moment magnitude (Mw) of as much as 8 (Pararas-Carayannis, 2005; 2006).

There is no information in the historical records about the intensity of such an earthquake in 326 BC earthquake from which a magnitude can be estimated, or to determine that unusual sea waves from such event could have an impact as far away as eastern Sri Lanka (Ceylon) along the East side of India. Thus, it cannot be affirmed with any certainty whether the destructive sea waves in Sri Lanka which were reported in ancient texts, were generated by the same earthquake source in the Northern Arabian Sea as those of the 1945 event, or by any underwater landslide parallel to the NW trending Kutch graben, or even near the Bombay graben (See Fig. 9 below) in the Guajarat region of India - similar to one perhaps caused by a 25 January 2001 event. However, it should be also mentioned that none of the recent earthquakes that have occurred along the Kutch Graben region are known to have generated destructive tsunamis (Pararas-Carayannis, 2001a – see: "The Earthquake of 25 January 2001 in India” http://drgeorgepc.com/Earthquake2001India.html).

Fig. 9. The Indus delta/Kutch region in the Guajarat region of India – east of the Makran Subduction Zone - is a region that has produced numerous destructive earthquakes in recent times, including a devastating earthquake in 2001 (after Pararas-Carayannis, 2001a).

However, it is possible that an earthquake further South in the Guajarat region could have triggered an underwater landslide and a local tsunami, which perhaps could have affected the Greek fleet in 326 BC, although such an event would not have the azimuthal concentration of energy to cause destruction on the East coast of Sri Lanka (Pararas-Carayannis, 2005c, 2006).

3.3 Probable Scenario of the 326 BC Tsunami

It is not known with any certainty if the tsunami of 326 BC struck the Greek fleet while at anchor, or while out at sea. None of the examined ancient texts provide information about losses or extent of the damage. However, based on Plutarch's and other historical accounts, and from current knowledge of the seismo-tectonics of the region, the chronology of the journey of Alexander's fleet and the possible impact of the 326 BC tsunami can be evaluated.

The timing of the large earthquake was critical to the fate of the fleet. What saved the Greek fleet from more extensive destruction was its location at that time when the tsunamigenic earthquake occurred. Such an earthquake probably occurred along the Makran Subduction Zone in late October or early November of 326 BC, when the ships were still in the Indus delta/Kutch region — near the delta of River Hab (just south of present Karachi). According to Plutarch, and the aforementioned Athenian lunar calendar, the Greek ships did not set sail from the estuary between the mouths of rivers Indus and Hab until early November, when the Southwest monsoons subsided (see Fig. 10 below).

Fig. 10. Location of Alexander's Fleet in late October 326 BC before heading for the River Hab estuary

The delay in the fleet's departure due to the adverse winds was a blessing in disguise and probably saved most of the ships from destruction. If the earthquake had occurred later in November after the fleet had left the River Hab estuary and was closer to Morontobara (present day Karachi), or when the fleet was sailing further west along the Makran coast (of southern Pakistan) near Bagisara (of present Ormara), there could have been total destruction of the Greek ships if sailing in shallower waters near the shore.

Not only the timing of the earthquake but the orientation of the tsunami generating area was critical to the fate of the Greek fleet. The tsunami generating area along the Makran Subduction Zone (NSZ) has an east-west orientation. Therefore, the azimuthal propagation of the tsunami energy would have been greater to the North and to the South and much less to the East or West. Thus the tsunami waves would have been very large along the entire Makran region, as well as along the southwestern coasts of India, as the tsunami wave energy refracted in deeper water. Immediately to the East of the MSZ, where the Greek fleet was located, the waves were not as high or as destructive. It is estimated that the tsunami waves at the River Hab estuary did not exceed 2 meters. Apparently, the destruction must have been partial and most of the ships were able to make repairs and continue the journey west.

3.4 The Fleet's Journey after the 326 BC Tsunami

With no opposing winds during the monsoon transitional period in November of 326 BC, the ships made significant progress westward (Fig. 11).

Fig. 11. Greek triremes under sail with favorable westerly winds

According to Arrian (based on Nearchus' account), after leaving the Indus delta/Kutch region, the Greek fleet continued the difficult journey, first to Morontobara or Woman's Harbor (present Karachi) near the mouth of the Hab River, then through the Sonmiani Bay, along the Makran coast. One night, they anchored and camped on the battlefield where Leonatus, one of Alexander's generals, had defeated the native population, the Oreitans ('Mountain people'). Leonatus had left a large food deposit for Nearchus' men — enough for ten days. Thus, with renewed supplies and favorable winds the ships reached the Hingol River and then continued westward to Bagisara (present Ormara), where the 326 BC tsunami probably must have had its maximum impact earlier in November 326 BC.

The fleet made significant progress westward when the Northeast (winter) monsoons picked up in early December, thus reaching rapidly Colta (Ras Sakani), Calima (Kalat) and an island called Carnine (Astola). After provisioning there, the fleet continued and passed Cysa (near Pasni) and Mosarna (near Ras Shahid). Here, a Gedrosian pilot joined them, who led them in two days to modern Gwadar, where they were delighted to see date palms and gardens. Three days later, Nearchus' men surprised Cyisa, a town near modern Châh Bahâr and took away supplies. Next, they anchored near a promontory dedicated to the Sun, called *Bageia* ("dwelling of the gods") by the natives and probably identical to Ra's Kûh Lab. The places that Nearchus mentions in his account of the voyage — as conveyed by Arrian of Nicomedia (Talmena, Canasis, Canate, Taa, Dagaseira) cannot be identified, although it is plausible that the last mentioned town is modern Jâsk.

3.5 Alexander's Army Return Via the Southern Land Route

Apparently 30 triremes could not have been sufficient to carry Alexander's army, even with a third of the army already gone back to Carmania by a land route. In August 326 BC, Alexander with about 135,000 foot soldiers and cavalry men left Patala towards Carmania, for the long and difficult march back homeward, through the harsh Gedrosian desert (Arrian, 135-37 AD) — which was part of the ancient Achaemenid empire (present region of Baluchistan region in Iran). Apparently, only one-fourth of the army survived the march back. Plutarch describes Alexander's difficult journey via the southern land route and the hardships the army endured as follows:

" ……and (Alexander) returned himself by land through the country of the Orites, where he was reduced to great straits for want of provisions, and lost a vast number of his men, so that of an army of one hundred and twenty thousand foot and fifteen thousand horse, he scarcely brought back above a fourth part out of India, they were so diminished by disease, ill diet, and the scorching heats, but most by famine. For their march was through an uncultivated country whose inhabitants fared hardly, possessing only a few sheep, and those of a wretched kind, whose flesh was rank and unsavory,…."

Fig.7 shown previously is a NASA satellite photo of a section of the Makran rugged and tectonic coastline showing uplifted terraces, headlands, sandy beaches, mud flats, rocky cliffs, bays and deltas, as well as numerous mud volcanoes along the shores.

4. EXAMINATION OF RECENT AND PREVIOUS MAJOR EARTHQUAKE AND TSUNAMI GENERATING SOURCES IN THE EASTERN AND WESTERN MAKRAN SUBDUCTION ZONE (MSZ) AND ELSEWHERE IN THE INDIAN OCEAN FOR POSSIBLE IMPACT ON THE GREEK FLEET IN THE YEAR 326 BC

In view of the lack of early historical documentation and understanding of earthquakes, tsunamis or other geophysical phenomena, and in order to narrow down the source of the waves that impacted the Greek fleet in 326 BC while in the Eastern Makran region of the North Arabian Sea, this section of the report reviews briefly the recent development of seismology and of the science of tsunami hazards in the 19th Century, as well as recent and old documented and recurring major earthquakes and tsunamis along the Eastern (Reyss EtAl. 1998), and Western segments of the Makran subduction zone in the North Arabian Sea, as well as elsewhere in the Indian Ocean (Pararas-Carayannis, 1978, 2001, 2005a,b,c,d, 2006a,b.,2007; Mokhtari and Farahbod, 2005; Murty and Bapat, 1999). The Makran accretionary wedge is one of the largest on Earth (Dorostian & Gheitanchi, 2003. A 7-km-thick column of sands and quartzolithic turbidites are incorporated into this wedge in a series of deformed thrust sheets, and has over pressured landward of the deformation front (Fruehn EtAl, 2003).

With the advent of seismology in the 19th century, major destructive tsunamigenic earthquakes begun to be monitored and documented in the Indian, Pacific, Atlantic Oceans and elsewhere around the world. The scientific studies and understanding about tsunamis begun much later, after the moment magnitude 8.6 earthquake of 1 April 1946 struck off the coast of Unimak Island in Alaska's Aleutian Islands. This particular tsunami caused the greatest damage and number of deaths in the Hawaiian Islands. It was an unprecedented disaster which led to the 1960 creation of the United States' first tsunami warning system, and subsequently to the development of extensive international research programs about past tsunami hazards.

These studies were further expanded in the following years to include other previous and subsequent tsunami disasters. Besides the 28 November 1945 earthquake and tsunami in the Northern Arabian Sea, there were more tsunamigenic earthquakes near Karachi in the present Southern Pakistan, near the estuary of River Hab. This is the location where the Greek fleet sustained partial damage from an apparent tsunami in 326 BC. In terms of geologic time such events recur in the same areas, therefore the following is only a cursory review of the impact of the better known recent major tsunamigenic earthquake events, particularly of the 28 November 1945, in the North Arabian Sea. Also reviewed are other historical earthquakes in Northwest India, as well as more recent tsunamigenic earthquakes elsewhere in the Indian Ocean. The following brief review was undertaken in order to evaluate which were the earthquakes elsewhere which may have generated the waves that impacted the Greek fleet in the year 326 BC.

There are several regions where large earthquakes have occurred in the past and destructive tsunamis were generated. Besides the Makran Subduction Zone, the Karachi and deltaic Indus region, the Owens Fault Zone, and the Kutch Grabben region, tectonic subduction and thrust faulting occur also in the Andaman Sea, along a short segment of Sri-Lanka, but also along the great Sunda Arc. Large earthquakes in recent times and in the distant past generated extremely destructive tsunamis along other coastlines of the Indian Ocean. One of the most recent was the one generated by the great earthquake of 26 December 2004 (Pararas-Carayannis 2005 a,b,c) .

As documented by the above referenced study, the on-going and recurring seismo-tectonic processes in the Indian Ocean are mainly the direct result of the Indian and Australian blocks moving northward at a rate of about 40 mm/yr (1.6 inches/yr) and colliding with the Eurasian continent (Fig. 12) (Tapponnier EtAl. 1986).

The main regions that were identified as more critical for past and future tsunami generation are the Andaman Sea Basin, the Northern and Eastern segments of the Great Sunda Tectonic Arc, and the Chagos Archipelago. Therefore the seismicity and potential of tsunami generation of the above-cited tsunamigenic regions are briefly reviewed, for the purpose of evaluating the source of the waves that could have impacted the Greek fleet in the year 326 BC.

Fig. 12. Migration of the India tectonic plate northward in the last 71 nillion tears and its collision with the Eurasian plate and formation of the Himalayan mountain range.

4.1 Evaluation of Possible Impact on the Greek Fleet in 326 BC from an Earthquake and Tsunami Generated along the Makran Subduction Zone (MSZ) in the Northern Arabian Sea, Similar to the 28 November 1945

While in the vicinity of the Hab river estuary on the Northwest coast of India, the Greek fleet could have been partially damaged by a tsunami in 326 BC similar to the one generated by the 28 November 1945 earthquake in the Eastern Makran Subduction Zone (MSZ) in the Northern Arabian Sea. Shown below in figure 13 is the epicenter of the 1945 earthquake, the Makran Accretionary Front, and the tectonic subduction zone in the Northern Arabian Sea, where the Greek fleet sailed later in early November 325 BC on its way to Babylon in the Persian Gulf. In order to evaluate the possibility of impact from a similar tsunami generated in 326 BC, the 1945 earthquake and tsunami were re-examined. Also examined were other major geotectonic features in the Northern Arabian Sea, close to the present day Karachi of Pakistan, the epicenters of historical earthquakes near the Ornach Nal Fault the Makran Accretionary Front, the two major zones of subduction, the Murray Ridge, and the Owen Fracture Zone (Fig. 14), as reported in the literature (Huhn EtAl ,1998; Regard EtAl, 2003; Pararas-Carayannis 2005a,b; 2006). The following is a brief overview of this event.

Fig. 13. The generating area of the 28 November 1945 tsunami off the Makran coast of Pakistan (After Pararas-Carayannis 2006b).

A thorough analysis of historical records reveals that many earthquakes and tsunamis have occurred in the past along the Makran Subduction Zone (MSZ) in the North Arabian Sea throughout geologic history and in recent times (Jacob and Quittmeyer, 1979). An earthquake on the MSZ could have been a most probable source of a tsunami which impacted the Greek fleet in 326 BC when it was in the River Hab estuary. Since earthquakes on the MSZ have occurred frequently in terms of geologic time, such an event could have be very similar to the great earthquake of 28 November 28, 1945 on the MSZ which generated a very destructive tsunami (Pararas-Carayannis, 2006d). According to the literature, the 1945 earthquake was a thrust event that ruptured approximately one-fifth of the entire length of the MSZ, and was estimated to have been 200 – 250 km. (Byrne et al. 1992). However, a revised moment magnitude of Mw 8.1 for this event would suggest a longer rupture - in the order of 300-350 Km. Although infrequent, such large earthquakes occur from time to time mainly on the eastern segment of the MSZ. Nine other smaller earthquakes are known to have occurred also in the eastern Makran with similar thrust tsunamigenic mechanism characteristics (Pararas-Carayannis, 2006b).

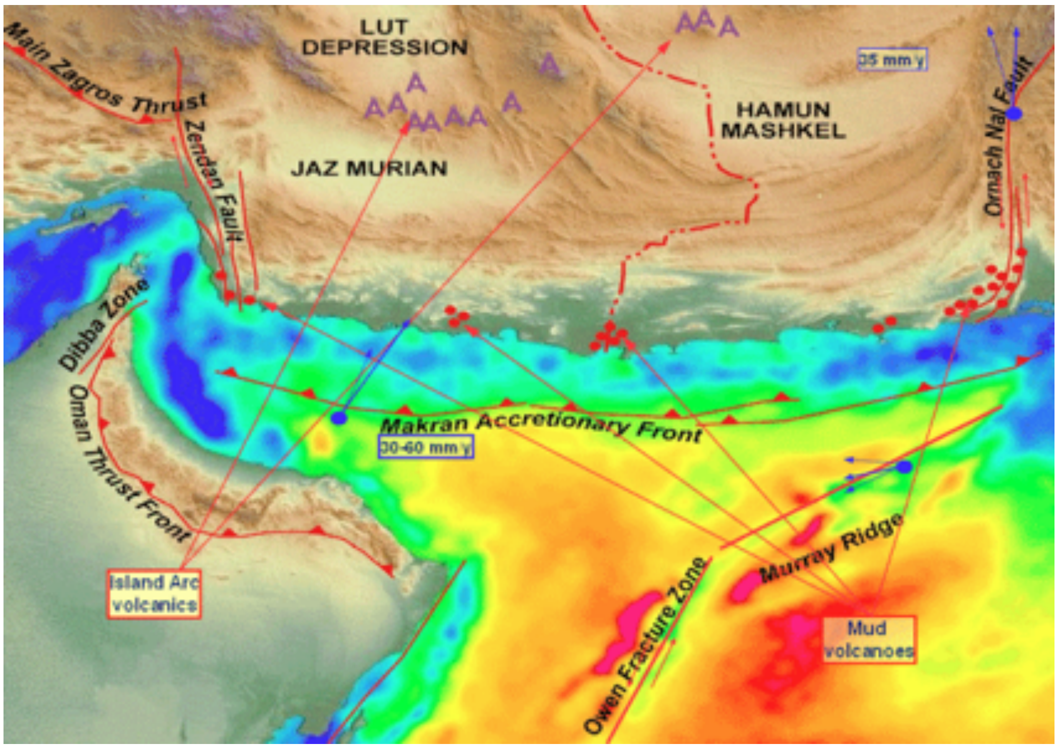

Fig. 14. Map of the Northern Arabian Sea showing the Makran Accretionary Front, two major zones of subduction, the Murray Ridge, the Owen Fracture Zone and the epicenters of historical earthquakes near the Ornach Nal Fault close to the present day Karachi of Pakistan

The great earthquake of 28 November 1945 is an example of the size of earthquakes that subduction along MSZ can produce (Mokhtari and Farahbod, 2005; Pararas-Carayannis 2005a,b.c, 2006). The tsunami was very destructive not only in the Northern Arabian Sea, but caused serious destruction along India's west coast, and great loss of life along the coasts of Pakistan, Iran, India and Oman, where run-up heights varied from 1 to 13 m. Specifically along the Makran coast of Pakistan, the tsunami's maximum run up height of 13 m (40 feet), destroyed fishing villages, caused great damage to port facilities, and resulted in deaths of more than 4,000 people. Waves of about 6.5 feet in height killed all the people of Khudi, a fishing village about 30 miles west of the present city of Karachi. Also Karachi was struck by the 1945 tsunami (Pakistan Meteorological Department, 2005).

Waves as high as 11.0 to 11.5 meters struck the Kutch region of Gujarat causing extensive destruction and loss of life. Eyewitnesses reported that the tsunami came in like a fast rising tide. The tsunami reached as far south as Mumbai, Bombay Harbor, Versova (Andheri), Haji Ali (Mahalaxmi), Juhu (Ville Parle) and Danda (Khar). In Mumbai, the height of the maximum wave was 2 meters, washing away fifteen persons. Five people died at Versova (Andheri, Mumbai), and six more at Haji Ali (Mahalaxmi, Mumbai). Several fishing boats were torn off their moorings at Danda and Juhu (Pararas- Carayannis, 2006b). However to the East of this MSZ zone, the waves were significantly lower. Karachi in present day Pakistan was struck by waves of only about 2 meters (6.5 feet) in height. Therefore, Alexander's fleet - which in 326 BC was located east of the delta of River Hab South of present-day Karachi - when such a similar event may have occurred, must have been inpacted by similar waves of about 2 meters, thus limiting the extent of damage (Pararas-Carayannis, 2006; http://drgeorgepc.com/TsunamiPotentialMakranSZ.html).

In brief, the Makran Subduction Zone always had the potential for very large earthquakes. Fortunately, they are infrequent and are usually preceded by smaller events that signal the occurrence of a larger earthquake. For example, for ten years prior to the 1945 event, there was a concentration of seismic activity in the vicinity of its epicenter. Recent seismic activity indicates a similar pattern and a large earthquake is possible in the region west of the 1945 event (Quittmeyer and Jacob, 1979). Although there are no historical records, it is believed that large earthquakes generated very destructive tsunamis in the distant geologic past.

Finally, a factor that could contribute to the destructiveness of a tsunami generated from this region would be the relatively large astronomical tide, which for the Makran coast is about 10-11 feet. A tsunami arriving during high tide would be significantly more destructive. In addition, the compacted sediments in this zone of subduction could contribute to a greater tsunami by causing a bookshelf type of failure – as that associated with the 1992 Nicaragua earthquake (Pararas-Carayannis, 1992).

The above stated documentation supports a reasonable conclusion that a significant earthquake and tsunami generated along the Makran Subduction Zone (MSZ) in the Northern Arabian Sea in 326 BC may been the event that caused damage to ships of the Greek fleet in the vicinity of the Hab River estuary at that time, in the easternmost end of the Makran Subduction Zone.

4.2 Possible Tsunami Impact on the Greek Fleet from an Earthquake on the Eastern Makran Subduction Zone similar to the 26 January 2001 Guajarat Earthquake

Discussed in section 4.1 of the present report is a brief evaluation of possible tsunami impact on the Greek fleet in 326 BC from similarly repeating earlier historical earthquakes in the Kutch, Bombay, and Cambay and Namacia grabens of Northwestern India. Provided in this section is a brief evaluation of the possible tsunami and earthquake impact on the fleet, from another similar to the more recent earthquake of 26 January 2001, magnitude R7.7, Guajarat earthquake. This recent earthquake also occurred along this same seismically active region of the Northeast trending Kutch and Bombay grabens of Northwest India as shown in Figure, and a previous occurrence in 326 BC could have been responsible in causing some damage to the Greek fleet, when it was still in the vicinity of the Haab river estuary - as reported in Arrian's of Nicomedia "Indice" account. The possibility that an earthquake occurred in the Gujarat region in 326 BC along the Kutch Graben region or even near the Bombay graben was discussed earlier in this report. Although none of the recent earthquakes that have occurred along the Kutch Graben region have generated destructive tsunamis (Pararas-Carayannis, 2001), it is possible that an earthquake could have triggered an underwater landslide and a local tsunami that could have reached the Haab river estuary. Another possibility of tsunami generation could be in the area of present day seismic region of Karachi in Pakistan - the ancient city of Morontobara of India.

4.3 Probable Impact on the Greek Fleet in 326 BC from an Earthquake and Tsunami in the Karachi and Deltaic Indus River Region

This is also a region near present Karachi and the deltaic Indus River where many earthquakes and tsunamis have occurred frequently in the past and could have had an impact on the Greek fleet in 326 BC. Four major faults exist in and around present day Karachi of Pakistan, along the southern coast of Makran, and in other parts of deltaic Indus River (Pararas-Carayannis, 2001, 2005). The first of these is the Allah Bund Fault, which traverses Shahbundar, Jah, Pakistan Steel Mills, and continues to the eastern parts of Karachi - ending near Cape Monze. This fault has produced many large earthquakes in the past in the deltaic river areas along the coast, causing considerable destruction. A major earthquake in the 13th century destroyed Bhanbhor. Another major earthquake in 1896 was responsible for extensive damage in Shahbundar (Pararas-Carayannis, 2001, 2005).

The second major fault near present-day Karachi is an extension of the one that begins near Rann of the Kutch region of India. The third is the Pubb fault which ends into the Arabian Sea near the Makran coast. Finally, the fourth major fault near Karachi is located in the lower Dadu district, near Surajani. A major thrust fault which runs along the southern coast of the Makran coast and parts of deltaic Indus is believed to be of the same character as the West Coast fault along the coast of Maharashtra, where a tsunami may have been generated in 1524, near Dabhol (Pararas-Carayannis, 2001b, 2006). Any earthquake along the Makran subduction zone, but particularly one south of Karachi, in the year 326 BC could have generated a tsunami affecting the Greek fleet. An earthquake in the same area as that of 26 January 2001, magnitude R 7.7 Guajarat earthquake on the Northeast trending Kutch and Bombay grabens of Northwest India – as shown in Figure 15 below - could have generated similar tsunami waves in 326 BC

Also, a recent study of coastal boulder deposition on the Iranian coast of the Makran subduction zone found 58 large boulders weighing up to 18 tons and up to 6 meters above mean sea level and up to 40 meters from the present shoreline (Shah-hosseini, EtAl, 2011). Using hydrological models, this study concluded that only tsunami waves of 4 meters in height were capable of detaching and transporting inland these boulders, and that such tsunami waves have also occurred on the Eastern Makran subduction zone near to the coast of Iran.

Fig. 15 Epicenter of the 26 January 2001, magnitude R 7.7 Guajarat earthquake on the Northeast trending Kutch and Bombay grabens of Northwest India

4.4 Evaluation of Possible Impact on the Greek Fleet in 326 BC from an Earthquake and Tsunami in the Andaman Sea Basin.

The Andaman Sea basin is another seismically active region in the Indian ocean at the southeastern end of the Alpine-Himalayan belt where many earthquakes have occurred recently and in the distant past (Sinvhal et al.1978, Verma et al. 1978). Thus, the seismo-tectonic history of this region was examined for the purpose of evaluating whether a possible tsunamigenic earthquake from this region could have had an impact to the Greek fleet in 326 BC when it was near the estuary of River Hab, in the Arabian Sea near the Makran coast.

Tectonic subduction and thrust faulting occur in the Andaman Sea, the Northern Arabian Sea, along a short segment of Sri-Lanka, and along the great Sunda Arc. Large earthquakes in recent times and in the distant past generated extremely destructive tsunamis along coastlines of the Indian Ocean. One of the most recent was the one generated by the great earthquake of 26 December 2004 (Pararas-Carayannis, 2005). As documented by this referenced study and illustrated earlier in Figure 12 the on-going and recurring seismo-tectonic processes in the Indian Ocean are mainly the direct result of the Indian and Australian blocks moving northward and colliding with the Eurasian continent.

The Andaman Sea basin is characterized by an extensional feature, which developed along a leaky transform segment of the megashear zone - the Andaman fault - between the Indo-Australian domain and the Sunda-Indochina block (Sinvhal EtAl, 1978; Uyeda and Kanamori, 1979; Taylor and Karner, 1983;), Neotectonics and time space seismicity of the Andaman Nicobar). This old shear zone has acted as a western strike slip guide for the extrusion of the Indochina block about 50-20 million years ago, and in response to the indentation of the Indian tectonic plate into Eurasian block as previously shown in Fig. 12.

Subsequently, the Andaman fault system, recently prolonged through the Sumatra zone (the Sumatra fault), reactivated due to the lateral escape of the Sumatra fore-arc sliver plate and as a result of the oblique convergence and subduction with the Indo-Australian plate (Tapponnier et al., 1986).

Although active subduction and sinistral crustal movements in the Andaman Sea Basin have caused many minor and intermediate earthquakes, a few major events and only one known earthquake with magnitude greater than 8. Review of the historical record indicates that in April 1762, an earthquake at the Araken Coast off Myanmar generated the earliest known tsunami in the Bay of Bengal. Also, in October 1847, an earthquake near the Great Nicobar Island generated another tsunami, but no details are available. On 31 December 1881 a magnitude 7.9 earthquake near Car Nicobar, generated another tsunami in the Bay of Bengal. The height of the maximum tsunami wave recorded at Chennai was one meter. During an eighty year period from 1900 to 1980, a total of 348 earthquakes were recorded in the area bounded by 7.0 N to 22.0 N and 88.0 E to 100 E. These earthquakes ranged in magnitude from 3.3 to 8.5 (Bapat, 1982), but only five of these had magnitudes equal to or greater than 7.1 and generated tsunamis (Murty and Bapat, 1999). For the shorter period from 1916 to 1975, only three of the earthquakes had magnitudes greater than 7.2 and generated significant tsunamis (Verma EtAl., 1978).

Until the great earthquake of 26 December 2004, only the earthquake of 26 June 1941 had been the strongest ever recorded in the Andaman and Nicobar Islands, in generating a destructive tsunami. Two other earthquakes on 23 August 1936 and 17 May 1955, with magnitudes 7.3 and 7.25, respectively, did not generate tsunamis of any significance. Based on these statistical information, it can be concluded that most of the earthquakes in the Andaman Sea Basin, even those with magnitudes greater than 7.1, do not usually generate significant tsunamis. The possible reason for the low number of tsunamis is that most of the earthquakes in the Andaman Sea are mainly associated with strike-slip type of faulting that involves lateral crustal movements. The exception was the 26 December 2004 earthquake, which, not only ruptured the Great Sunda Arc along the northern Sumatra region, but also ruptured the same segment in the Andaman Sea as that in 1941 (Pararas-Carayannis, 2006).

A possible explanation for the extreme tsunami generated in the Andaman segment in December 2004 is that this event had a different mechanism and involved both thrust and bookshelf faulting within the compacted sediments of the Andaman Sea segment of the Great Sunda Arc (Pararas-Carayannis, 2005). In brief, and based on the historical record and the tsunami propagation from major and even great tsunamigenic earthquakes as that of 26 December 2004, it can be concluded that no similar event in 326 BC could have caused damage to the Greek fleet which was at that time Northwest of India in the North Arabian Sea.

4.5 Evaluation of Possible Impact on the Greek Fleet in 326 BC from an Earthquake and Tsunami similar to the 19 August 1977 in the Lesser Sunda Islands of Indonesia.

This earthquake occurred in 19 August 1977 just South of the Lesser Sunda Islands (Nusa Tenggara region), West of Sumba Island in Indonesia. The Lesser Sundas include Bali, Lombok, Sumbawa, Sumba, Flores, Timor, Alor and adjacent smaller islands (see Fig. 16).

This was the largest earthquake along the Java Trench in several decades and generated a major destructive tsunami, which was particularly damaging along the coasts of Sumba, Sumbawa, Lombok and Bali. Waves of up to 30 meters in height were reported on the adjacent Indonesian coasts, and as much as 8 meters in Australia. This earthquake's epicenter was at 11.09S; 118.46E about 170 kilometers SSW of Pradapare, Sumba Island (West Nusa Tenggara) and its Moment Magnitude was recalculated (Mw- 8.2, Ms - 8.1, ML - 8.9). The quake's maximum intensity was estimated to be VIII in the immediate area, and Mo - 24*10*20 Nm. (Pararas-Carayannis, 1978;1989).

Fig 16. Flores Island in the Lesser Sunda Islands where a major tsunami was generated on 12 December 1992

With support from UNESCO-IOC and the U.S. National Oceanic and Atmospheric Administration (NOAA), the author participated in a survey of this earthquake and tsunami, in order to determine the tsunami run-up and extent of inundation. The survey was conducted by land where accessible, and by air reconnaissance for inaccessible coastal areas of the islands of Sumba, Sumbawa, Lombok and Bali (Pararas-Carayannis, 1978). Based on these observations and the directionality of the source and the tsunami's main energy propagation towards the Southern Indian Ocean, the present study concludes that no historically previous large tsunami waves from this region, could have reached the Eastern Makran area south of present Karachi where the Greek fleet sustained some damage in 326 BC.

4.6 Evaluation of Possible Impact on the Greek Fleet in 326 BC from an Event Similar to the 12 December 1992 Earthquake and Tsunami near Flores Island in Indonesia.

There was repetition of seismic and tsunami activity in the same region about 25 years later. The deadliest tsunamigenic earthquake in the Lesser Sunda Islands region of Indonesia occurred again near Flores Island on 12 December 1992 (Fig. 16 above). It had an Ms 7.8 magnitude, a maximum Mercalli intensity of VIII (*Severe*) and its generating source was a thrust fault dipping 32 degrees to the south and extending about 110 kilometers from Cape Batumanuk to Cape Bunga. The maximum tsunami waves generated by the earthquake were almost 26 meters in height, reached shore in five minutes, and ran inland as far as 300 meters. The disaster caused at least 2,080 fatalities, including 1,490 in Maurnere, on Flores, and 700 on Babi Island (U.S. Geological Survey). More than 500 people were injured and 90,000 were left homeless by this event. Nineteen people were killed and 130 houses were destroyed on Kalaotoa. Damage was assessed at exceeding US $100 million. Approximately 90% of the buildings were destroyed at Maumere, the hardest hit town, by the earthquake and tsunami while 50% to 80% of the structures on Flores were damaged or destroyed. Damage also occurred on Sumba and Alor (USGS, 1992). However, given the southern orientation of this tsunami's source region in the Indian Ocean, and its confinement by surrounding islands, it can be definitely concluded that an earlier occurrence of such an event could not possibly have reached the Eastern Makran area where the Greek fleet sustained some damage in 326 BC.

Fig. 17. Map of East Java and of the Lesser Sunda Islands

4.7 Evaluation of Possible Tsunami Impact on the Greek Fleet from other Earthquake Sources of Indonesia - the 28 March 2005 Earthquake and Tsunami

Provided in the following section is an overview of other major tsunamis in the Indian Ocean in recent times – such as that of 28 March 2005 East of the Island of Java in Indonesia - which although very destructive locally and elsewhere, did not impact significantly the

Northern Arabian Sea in the vicinity of Karachi. Thus a previous recurrence and impact in the North Arabian Sea of such events causing damage to the Greek fleet in 326 BC would not have been possible because of the tsunami's energy southern directionality. None-the-less, and for the purpose of eliminating this earthquake source as having a significant tsunami impact on the Greek fleet, the following section provides a cursory review of this event, emphasizing the different focusing of the tsunami waves that were generated. Fig. 17 above is a map of Eastern Java and of the Lesser Sunda Islands. The block that was moved by the 28 March 2005 earthquake was relatively small in comparison. Whether this movement will now stress loads another segment of the great Sunda fault to the South and causes another earthquake soon, is not known. However, another great earthquake similar to that of 1833 (magnitude 8.7) along the south coast of the western Sumatra will eventually occur. That particular earthquake generated a great tsunami. The waves may have been as much as 10 to 15 meters on the western coast of Sumatra. Luckily, most of the energy from that tsunami was directed towards the unpopulated regions of the southwest Indian Ocean. When such an event will occur again, is not known. The only thing known with certainty is that it will occur in this region. In conclusion, a tsunami from this region could not have had an impact on the Greek fleet in 326 BC while it was in the vicinity of the estuary of River Hab, in the relatively safe eastern region of MSZ,

4.8 Evaluation of Possible Tsunami Impact on the Greek Fleet from the Great 26 December 2004 Earthquakes and Tsunami in Indonesia and the Indian Ocean.

The great tsunamigenic earthquake of 26 December 2004 was also evaluated as a possible source region of destructive waves which could have affected the Greek fleet in 326 BC when it was located in the vicinity of the Hab River estuary, at the easternmost end of the Makran Subduction Zone in the North Arabian Sea.

This 26 December 2004 tsunamigenic earthquake resulted from a sudden episode of the Indian plate's subduction and of the Burma tectonic movement plate in a northeast direction (Paris EtAl. 2010). As previously stated, this movement caused dynamic transfer and loading of stress to both the Australian and Burma plates, immediately to the south, on the other side of the triple junction point. As a result of this load transfer, the Australian plate moved in relation to the Burma plate and probably rotated somewhat in a counterclockwise direction, causing the subsequent great earthquake of 28 March 2005 as explained in section 4.7 above. Thus, a Coulomb stress transfer analysis, based on rupture parameters and the geometric distribution of aftershocks for both the 26 December 2004 and the 28 March 2005 events, would help establish the space-time evolution of stresses and help determine both static and dynamic modifications that could possibly trigger future events along known faults in the region. In conclusion there was no tsunami damage to the Greek fleet from this region in 326 BC.

5. CONCLUSIONS

Although infrequently, large magnitude earthquakes occur along the Makran Subduction Zone (MSZ) region of Southern Iran and Pakistan, the Indus river delta/Kutch region, the Andaman Sea and elsewhere in the Indian Ocean. Such earthquakes, involving mainly thrust motions are known to generate frequent destructive tsunamis. Also, destructive tsunami waves can be generated by underwater landslides particularly in the North Arabian Sea and the Northern Andaman Sea because of extensive sediment accumulation along the deltas of major rivers. Large earthquakes near the Kutch Graben region can trigger also waves from underwater landslides. Major and great earthquakes elsewhere in the Indian Ocean have also generated destructive tsunami waves.

Ancient Greek and Indian texts support that destructive sea waves along the Makran coast in the northern Arabian Sea were responsible for the partial destruction of Alexander the Great's fleet in 326 BC. At that time the fleet was at an estuary of River Hab, north of the Indus River delta/Kutch of India while waiting for calmer seas and for the seasonal monsoon winds to subside, before beginning the long journey from India to Babylon, in the Persian Gulf. It is very possible that the reported damage to the fleet was caused from a tsunami rather than storm waves. Repairs to the ships were made and the journey continued west towards Babylon in the Persian Gulf. In all probability, the reported waves in the ancient texts originated along the Makran Subduction Zone – the same source area that produced a great earthquake and tsunami in 1945 as well as other extreme disasters in the past. Based on reviews of ancient Greek accounts such as those of Plutarch, Nearchus but mainly of Arrian's of Nicomedia "Indice", the present study reconstructed the chronology of the impact on the fleet based on the ancient Athenian lunar calendar, as occurring in early November of 326 BC. By using also current geophysical knowledge of recent events in this region, and the documentation of the 1945 and of other events, the present study concluded that the reported waves of the 326 BC most probably originated on the MSZ.

The azimuthal propagation of the tsunami energy propagation of the 1945 event was greater to the North and to the South with waves reaching a maximum run up height of 13 m (40 feet), causing extensive destruction and numerous deaths. However, the waves that struck Karachi were only 2 meters (6.5 feet) high. Based on the ancient records and current geophysical knowledge, it is believed that a 326 BC earthquake occurred in late October or early November. At that time Greek fleet was either at anchor at the estuary near the delta of River Hab south of Karachi or had just set out to sea. It is estimated that Greek fleet was struck by waves that were as much as 2 meters in height. The timing of the 326 BC tsunamigenic earthquake and the location of Alexander's fleet were critical. If the earthquake had occurred later in November of 326 BC, after the fleet had left Morontobara (Karachi), or when it was near Bagisara (present Ormara), the outcome could have been disastrous. The delay due to adverse monsoon winds probably saved the Greek fleet from total tsunami destruction. Additionally reviewed and evaluated by the present study are other possible tsunamigenic source areas in the Indian Ocean which may have had an impact on the Greek fleet in 373 BC.

REFERENCES

Ambrasseys, N. and Bilham, R., 2003, *"Earthquakes and Associated Deformation in North Baluchistan 1892-2001"*, Bulletin of the Seismological Society of America, Vol .93, No. 4, p. 1573 - 1605.

Arrian of Nicomedia", 135-137 AD *Indikê,* appendix to *Anabasis*. one of seven books of the history of Alexander's march into Asia – based primarily on the *Indikê* by Alexander's fleet-commander Nearchus. (The first chapters are derived from Megasthenes, a Greek envoy who visited Patna.)

Bapat, A. (1882). *"Tsunamis and earthquakes in the Bay of Bengal"*, Tsunami Newsletter, International Tsunami Information Center, Honolulu, Volume XV, No. 3, 36-37.

Byrne Daniel E., Sykes Lynn R. Davis Dan M., 1992. *"Great thrust earthquakes and aseismic slip along the plate boundary of the Makran subduction zone".* JOURNAL OF GEOPHYSICAL RESEARCH, VOL. 97, NO. B1, PAGES 449–478, 1992

Diodorus Siculus. Diodorus of Sicily in Twelve Volumes with an English Translation by C. H. Oldfather. 1989. Vol. 4-8. Cambridge, Mass.: Harvard University Press; London: William Heinemann, Ltd. 1989)

Dorostian A., Gheitanchi M. R., 2003, *"SEISMICITY OF MAKRAN*" European Geophysical Society 2003. *Tectonics of a Lateral Transition Between Subduction and Collision:The Zagros-Makran Transfer Deformation Zone (SE IRAN)*, Geophysical Research Abstracts, Vol. 5, 01210, 2003

Fernando, A.D.N., 2005. Tsunamis, earthquakes, their intensity and periodicity. Online edition of the Island of Sri Lanka http://servesrilanka.blogspot.com/2005/03/tsunamis-earthquakes-their-intensity.html

Fruehn, J., White, R. S. and Minshull, T. A., 1997. *"Internal deformation and compaction of the Makran accretionary wedge"*, Terra Nova, 9: 101-104. DOI:10.1046/j.1365-3121.1997.d01-13.x

Huhn K. , Kukowski N. , Schillhorn T. and E. Flueh, 1998. Morphotectonics of the Makran accretionary wedge imply new aspects for the plate tectonic situation in the northeast Indian Ocean. http://www.geomar.de/add_info/former_info/abstracts98/agu98abstracts.html

Jacob, K. H. and Quittmeyer, R. L., 1979. The Makran region of Pakistan and Iran: Trench-arc system with active plate subduction. In: Farah, A. and de Jong, K. A. (Editors), Geodynamics of Pakistan: 305-317.

Mokhtari, M., Farahbod, A.M. 2005. Tsunami Occurrence in the Makran Region, Tsunami Seminar, Tehran, 26th February 2005.

Murty. T. and A. Bapat, 1999 "Tsunamis on the coastlines of India", International Tsunami Symposium, May 1999 (Abstract).

Nearchus of Crete, 325 BC. *Indik*e in classical' Greek. Nearchus of Crete. "Indice http://www.livius.org/ne-nn/nearchus/nearchus.html

Pakistan Meteorological Department, 2005 *"History of Tsunamis in Pakistan/Arabian Sea",* Report, January 2005.

Pararas-Carayannis, G., 1977, Indonesian Earthquake and Tsunami of August 19, 1977, Intern. Tsunami Information Center Report, Abstracted article in Tsunami Newsletter, Vol. X, No. 3, September, 1977.

Pararas-Carayannis, G., 1978. *"The Earthquake and Tsunamis of 19 August 1977 in the Lesser Sunda Islands of Indonesia"*. ITIC Progres Reports for 1976-1977 prepared for the 1978 Sixth Session of ITSU, in Manila, Philippines. http://drgeorgepc.com/Tsunami1977Indonesia.html

Pararas-Carayannis, G. 1989. Five-Year Plan for The Development of A Regional Warning System in the Southwest Pacific. A Report prepared to the United Nations Development Program (UNDP), New York, May 1989, 21 p.

Pararas-Carayannis, G., 1992. *"The Earthquake and Tsunami of 2 September 1992 in Nicaragua"* http://drgeorgepc.com/Tsunami1992Nicaragua.html

Pararas-Carayannis, G. 2001a. The Earthquake of 25 January 2001 in Guajarat, India. http://www.drgeorgepc.com/Earthquake2001India.html

Pararas-Carayannis, G., 2001b. The Earthquake and Tsunami of 28 November 1945 in Southern Pakistan. http://drgeorgepc.com/Tsunami1945Pakistan.html

Pararas-Carayannis, G., 2005a. The Great Earthquake and Tsunami of 26 December 2004 in Southeast Asia and the Indian Ocean, http://drgeorgepc.com/Tsunami2004Indonesia.html

Pararas-Carayannis, G., 2005b. The Earthquake and Tsunami of 26 June 1941 in the Andaman Sea. http://drgeorgepc.com/Tsunami1941AndamanSea.html

Pararas-Carayannis, G., 2005c. The Great Earthquake and Tsunami of 1833 off the coast of Central Sumatra in Indonesia http://drgeorgepc.com/Tsunami1833Indonesia.html

Pararas-Carayannis, G., 2005d. The Great Earthquake and Tsunami of 28 March 2005 in Sumatra, Indonesia, http://drgeorgepc.com/Tsunami2005ndonesia.html

Pararas-Carayannis, G., 2006a, Potential of tsunami generation along the Makran Subduction Zone in the Northern Arabian Sea – Case Study: The Earthquake and Tsunami of 28 November 1945, 3rd Tsunami Symposium of the Tsunami Society May 23-25, 2006, East-West Center, Un. of Hawaii, Honolulu, Hawaii,Science of Tsunami Hazards Vol 24(5), 2006 http://drgeorgepc.com/TsunamiPotentialMakranSZ.html

Pararas-Carayannis, G., 2006b. The Earthquake and Tsunami of 17 July 2006 in Southern Java, Indonesia http://drgeorgepc.com/Tsunami2006IndoJava.html

Pararas-Carayannis G., 2006c. Earthquake and Tsunami of June 26, 1941 in the Andaman Sea and the Bay of Bengal. http://www.drgeorgepc.com/Tsunami1941AndamanIslands.html

Pararas-Carayannis G., 2006d. The Earthquake and Tsunami of 28 November 1945 in Southern Pakistan. Science of Tsunami Hazards, January 2006 Science of Tsunami Hazards Vol 24 No 5, pages 358-384 http://drgeorgepc.com/Tsunami1945Pakistan.html https://www.researchgate.net/publication/38106162

Pararas-Carayannis G. 2007a. INDONESIA EARTHQUAKES AND TSUNAMI - Earthquakes and Tsunami of September 12, 2007 in Indonesia http://www.drgeorgepc.com/Tsunami2007Indonesia.html

Pararas-Carayannis, G., 2007b. *"The Earthquake of 31 May 1935, near Quetta (Balochistan), Pakistan"* http://drgeorgepc.com/Earthquake1935PakistanQuetta.html

Pararas-Carayannis G. 2008. Future Tsunami Disasters in the Indian Ocean. World Conference on Earthquake Engineering, October 12-17, 2008. Beijing, China.

Paris, R., Fournier, J., Poizot, E., Etienne, S., Morin, J., Lavigne, F., Wassmer, F., 2010. Boulder and fine sediment transport and deposition by the 2004 tsunami in Lhok Nga (western Banda Aceh, Sumatra, Indonesia): a coupled offshore–onshore model. Marine Geology268, 43–54.

Plutarch of Chaeronea, 79 AD. Life of Alexander, 356-323, translated by John Dryden Also in "The Fortune and Virtue of Alexander"

Quittmeyer, R.C., and Jacob, K.H., 1979, *"Historical and Modern Seismicity of Pakistan, Afghanistan, N.W. India and S.E. Iran",* Bulletin of the Seismological Society of America, 69/3, pp. 773-823, 1979

Regard V. Bellier O., Thomas J.-C., Abbassi M.R., Mercier J. L., Shabanian E., Feghhi Kh., Soleymani Sh., Bonnet S., Bourlès D. L., Braucher R., and J. Martinod, 2003. Tectonics of a Lateral Transition Between Subduction and Collision: The Zagros-Makran Transfer Deformation Zone (SE IRAN) European Geophysical Society 2003. Geophysical Research Abstracts, Vol. 5, 01210, 2003

Shah-hosseini Majid, Morhange Christophe, Naderi Beni Abdolmajid, Marriner Nick, Lahijani Hamid, Hamzeh Mohammadali, Sabatier François, 2011. Coastal boulders as evidence for high-energy waves on the Iranian coast of Makran. Marine Geology 290 (2011) 17–28

Reyss J.L , Pirazzoli P.A, Hangipour C., Hatte C. and Fontugne M., 1998. Quaternary marine terraces and tectonic uplift rates on the south coast of Iran. January 1998 Geological Society London Special Publications 146(1) DOI: 10.1144/GSL.SP.1999.146.01.13

Sinvhal, H., Khattri, K.N., Rai, K. and V.K. Gaur. (1978), *"Neotectonics and time-space seismicity of the Andaman Nicobar region"*, Bulletin of the Seismological Society of America, Volume 68, No. 2, 399-409.

Tapponnier, P., Peltzkr, G. and R. Armijo, 1986, "On the mechanism of collison between India and Asia". In: COWARD, M.P. & RIES, A.C. (eds) Collision Tectonics. Geological Society, London, Special Publications, 19, 115-157.

USGS, 1992. Significant Earthquakes of the World in 1992, Archived 2009-09-12 at the Wayback Machine United States Geological Survey

Verma, R.K., Mukhopadhyay, M. and N.C. Bhuin. (1978), *"Seismicity, gravity and tectonics in the Andaman Sea"*, in *"Geodynamics of the Western Pacific"*, Proceedings of the International Conference on Geodynamics of the Western Pacific - Indonesian Region, March 1978, Tokyo, Advances 'in Earth and Planetary Science 6, Supplement Issue of Journal of Physics of the Earth, edited by S. Uyeda,

Murphy R.W. and K. Kobayashi, Center for Academic Publications, Japan Scientific Societies Press, Tokyo, 233-248.

ISSN 8755-6839

SCIENCE OF **TSUNAMI HAZARDS**

Journal of Tsunami Society International

Volume 41 Number 4 2022

WWW.TSUNAMISOCIETY.ORG

TSUNAMI SOCIETY INTERNATIONAL, 1325 South 33rd Avenue, Hollywood, Florida 33021, USA.

WWW.TSUNAMISOCIETY.ORG